2004

THE TRANSPORT AND MODULATION OF HIV PROTEASE INHIBITORS INTO THE RAT CENTRAL NERVOUS SYSTEM AND MILK

Jeffrey Earl Edwards
University of Kentucky, geoff523@excite.com

ABSTRACT OF DISSERTATION

Jeffrey Earl Edwards

The Graduate School

University of Kentucky

2004

THE TRANSPORT AND MODULATION OF HIV PROTEASE INHIBITORS INTO THE RAT CENTRAL NERVOUS SYSTEM AND MILK

ABSTRACT OF DISSERTATION

A dissertation submitted in partial fulfillment of the requirements of the degree of Doctor of Philosophy in The Graduate School at the University of Kentucky

By

Jeffrey Earl Edwards

Lexington, Kentucky

Director: Patrick J. McNamara, Professor, Pharmaceutical Sciences

2004

ABSTRACT OF DISSERTATION

THE TRANSPORT AND MODULATION OF HIV PROTEASE INHIBITORS INTO THE RAT CENTRAL NERVOUS SYSTEM AND MILK

The objective of this dissertation is to study the mechanism by which HIV protease inhibitors enter into the central nervous system (CNS) and breast milk of rats, and what effects MDR modulators have on the distribution and metabolism of HIV protease inhibitors. The transporter P-glycoprotein (P-gp) has been shown to limit the distribution of HIV protease inhibitors into the CNS of rodents. This thesis examined the effects of GF120918, an MDR modulator, on the CNS distribution of amprenavir, an HIV protease inhibitor, in rats. GF120918 significantly increased the unbound CNS concentrations of amprenavir without altering the unbound blood concentrations of amprenavir. The results of these studies show that GF120918 can inhibit P-gp at the blood brain barrier (BBB) to increase the unbound CNS concentration of amprenavir and potentially other HIV protease inhibitors. Many first generation MDR modulators inhibited both P-gp transport and CYP3A metabolism. Therefore, a principal goal of this thesis was to determine if GF120918 could selectively inhibit P-gp transport without inhibiting CYP3A metabolism. Using in vitro (human) and in vivo (rat) studies, GF120918 selectively inhibited P-gp at the BBB without inhibiting CYP3A metabolism. The transporter MRP1 has been shown to both transport HIV protease inhibitors and expressed in the CNS. Studies contained in the thesis have shown that mrp1 is not localized to the BBB of rats, therefore, mrp1 is unlikely to play a significant role in the distribution of HIV protease inhibitors into the CNS of rats. The distribution of nelfinavir, an HIV protease inhibitor, into rat breast milk was studied in the thesis as a first approach in understanding the extent to which HIV protease inhibitors can accumulate into milk. The concentration of nelfinavir in rat milk was

approximately half that of plasma. P-gp protein expression was detected in lactating rat mammary tissue. However, GF120918 showed no effect on the distribution of nelfinavir into rat milk suggesting that P-gp does not play a significant role in the distribution of HIV protease inhibitors into milk.

Keywords: HIV Protease Inhibitors, P-glycoprotein, MRP1, Lactating Rat Model, MDR Modulation

Jeffrey Earl Edwards

January, 2004

THE TRANSPORT AND MODULATION OF HIV PROTEASE INHIBITORS INTO THE RAT CENTRAL NERVOUS SYSTEM AND MILK

By

Jeffrey Earl Edwards

Director of Dissertation
Patrick J. McNamara
Director of Graduate Studies
Dr. Todd D. Porter
January, 2004

RULES FOR THE USE OF DISSERTATIONS

Unpublished dissertations submitted for the Doctor's degree and deposited in the University of Kentucky Library are as a rule open for inspection, but are to be used only with due regard to the rights of the authors. Bibliographical references may be noted, but quotations or summaries of parts may be published only with the permission of the author, and with the usual scholarly acknowledgments. Extensive copying or publication of the dissertation in whole or in part also requires the consent of the Dean of the Graduate School of the University of Kentucky.

DISSERTATION

Jeffrey E. Edwards

The Graduate School

University of Kentucky

2004

THE TRANSPORT AND MODULATION OF HIV PROTEASE INHIBITORS INTO THE RAT CENTRAL NERVOUS SYSTEM AND MILK

DISSERTATION

A dissertation submitted in partial fulfillment of the
requirements of the degree of Doctor of Philosophy in
The Graduate School
at the University of Kentucky

By
Jeffrey Earl Edwards
Lexington, Kentucky
Director: Patrick J. McNamara, Professor, Pharmaceutical Sciences
2004

ACKNOWLEDGEMENT

I would like to thank Dr. Patrick J. McNamara for giving me the opportunity to develop myself as a scientist under his direction. I will always admire his breadth of knowledge and his critical thinking skills. I would also like to thank my committee members Drs. Mary Vore, Jeffrey Moscow, Bradley Anderson, Robert Yokel, and Val Adams for there input and guidance. I would also likely to thank the Graduate Center for Toxicology. Finally I would like to thank my family and friends for all there support during my time at the University of Kentucky.

TABLE OF CONTENTS

LIST OF TABLES

LIST OF FIGURES

LIST OF FILES

JEDWARDS.PDF	2.39 MB

CHAPTER I. INTRODUCTION

The viral load of the human immunodeficiency virus (HIV) in plasma can be reduced to levels below the limit of detection using a combination of nucleoside reverse transcriptase inhibitors, non-nucleoside reverse transcriptase inhibitors, and HIV protease inhibitors (Rana and Dudley, 1999). This combination of antiretroviral drugs has reduced the mortality of individuals infected with HIV (Lambotte et al., 2003). Unfortunately, discontinuation of the antiretroviral therapy will cause the plasma viral load to return to pretherapeutic levels (Lambotte et al., 2003). One explanation for the rebound of HIV in the plasma is the existence of HIV reservoirs, where the viron is able to survive in the body even during antiretroviral therapy. One of the proposed HIV reservoirs is the central nervous system (CNS)(Pierson et al., 2000). An indicator of HIV survival in the CNS is the prevalence of HIV-associated dementia, a cognitive and motor impairment observed in HIV positive patients (Swindells et al., 1999).

P-glycoprotein (P-gp), the product of the ABCB1 (formerly MDR1) gene, reduces the distribution of the HIV protease inhibitors indinavir, saquinavir, ritonavir, nelfinavir, and amprenavir into the CNS (Bellamy, 1996; Asperen et al., 1997; Kim et al., 1998; Lee et al., 1998; Polli et al., 1999). P-gp is located on the apical membrane of capillary endothelial cells that make up the blood-brain barrier (BBB). The distribution of HIV protease inhibitors into the CNS is significantly greater in mdr1a -/- knockout mice (Kim et al., 1998) and in mice treated with the MDR modulators valspodar (PSC-833), LY-335979 (Choo et al., 2000), and GF120918 (Polli et al., 1999) compared to mdr1a +/+ and control mice, respectively. The hypothesized clinical significance of P-gp efflux of HIV protease inhibitors at the BBB is sub-therapeutic concentrations of HIV protease inhibitors in the CNS. The use of MDR modulators with HIV protease inhibitors could potentially increase the distribution of HIV protease inhibitors into the CNS to levels that would reduce the prevalence of HIV-associated dementia.

One obstacle in MDR modulation, the use of MDR modulators to inhibit P-gp, is the inadvertent effects of the MDR modulators on drug metabolism. Many substrates/inhibitors of P-gp are also substrates/inhibitors of the metabolizing enzyme cytochrome P4503A4 (Kim et al., 1999; Wandel et al., 1999; Yasuda et al., 2002). For example, there is an increase in the plasma concentration of doxorubicin, a P-gp and CYP3A4 substrate, when cyclosporine is co-administered (Bartlett et al., 1994). Cyclosporine inhibits both P-gp and CYP3A4, and therefore

cyclosporine not only increases the distribution of doxorubicin by inhibiting P-gp, but also inhibits CYP3A4 metabolism of doxorubicin (Wandel et al., 1999). It would be advantageous to identify MDR modulators that selectively inhibit P-gp over CYP3A4 in order to avoid toxicities due to metabolism inhibition.

HIV protease inhibitors are also transported by the multidrug-resistant associated protein (MRP1) the product of the ABCC1 gene (Srinivas et al., 1998; van der Sandt et al., 2001). There are conflicting reports on the expression of MRP1 at the BBB (Regina et al., 1998; Seetharaman et al., 1998a; Sugiyama et al., 1999; Decleves et al., 2000). If MRP1 is expressed at the BBB it could have a significant effect on the distribution of PIs into the CNS. Clarifying its expression would help in identifying the potential mechanisms by which HIV protease inhibitors distribute into the CNS.

Just as the BBB regulates transport into the CNS (De Boer et al., 1998), the mammary-epithelial barrier regulates transport into breast milk (Shennan, 1998). It has also been shown that specific carrier mediated transporters are located at the mammary epithelial barrier and can cause elevated milk concentrations of xenobiotics, including the HIV reverse transcriptase inhibitor zidovudine (Oo et al., 1995; Gerk et al., 2001; Alcorn and McNamara, 2002). It has been observed that there is an increase in the risk of HIV transmission through breast feeding, with increased HIV viral load in milk (Rousseau et al., 2003). HIV reverse transcriptase inhibitors have been used to prevent the transmission of HIV from mother to child through breast milk (Nolan et al., 2002), and therefore it is hypothesized that HIV protease inhibitors will also prevent the transmission of HIV through milk.

There is little information concerning the distribution and transport of HIV protease inhibitors into breast milk. This lack of information makes it difficult to determine if HIV protease inhibitors can be used to prevent the transmission of HIV through milk. Preliminary studies have shown mRNA expression of mdr1b (P-gp) in rat mammary tissue. Therefore, P-gp could potentially play a significant role in the distribution of HIV protease inhibitors into milk. In addition to understanding the transport of HIV protease inhibitors into milk, determining the protein expression and transport function of P-gp at the mammary epithelial barrier would help in identifying potential distribution pathways of other P-gp substrates into milk.

CHAPTER II. BACKGROUND

A. HIV Protease Inhibitors

The HIV protease is responsible for the cleavage of the HIV *gag-pol* polyprotein into its functional subunits, including the integrase and reverse transcriptase enzymes (Flexner, 1998). Three of the cleavage sites for the HIV protease contain a phenylalanine-proline or tyrosine-proline bond. A relatively new class of drugs, called HIV protease inhibitors, prevents the HIV protease from cleaving the *gag-pol* polyprotein into its functional subunits (Flexner, 1998). An immature viron is produced that can not infect other cells with the HIV genome. HIV protease inhibitors prevent HIV infected cells from infecting new cells, but do not affect previously infected cells.

There are currently 6 FDA approved HIV protease inhibitors; amprenavir, indinavir, lopinavir, nelfinavir, ritonavir, and saquinavir (Pomerantz and Horn, 2003). Figure 1 shows the structures of indinavir, nelfinavir, ritonavir, saquinavir, and amprenavir. Most of the HIV protease inhibitors are designed as synthetic analogs of the phenylalanine-proline sequence (Flexner, 1998). It has been shown that HIV protease inhibitors in combination with nucleoside and non-nucleoside reverse transcriptase inhibitors can reduce the HIV viral load in plasma below detectable levels (Rana and Dudley, 1999). In addition to lowering the plasma viral load, HIV protease inhibitors also reduce the viral load in lymphoid tissue, a known reservoir for HIV (Ruiz et al., 1999).

The greater lipophilicity of the HIV protease inhibitors compared to HIV reverse transcriptase inhibitors may explain the differences in antiviral activity in the lymphoid tissue. For example, the predicted octanol to water coefficients (log P, mean ± S.D.) for the neutral form of amprenavir, indinavir, lopinavir, nelfinavir, ritonavir, and saquinavir are 4.20, 2.88, 6.26, 6.98, 5.28, and 4.44, respectively, estimated using chemical properties prediction software (ACD Labs 6.0). These values are greater than the predicted log P for the HIV reverse transcriptase inhibitors zidovudine (-0.53) and didanosine (-1.33). However, HIV protease inhibitors are extensively bound to plasma proteins, especially to α-1-acid glycoprotein, which limits their tissue distribution (Acosta, 2002). The human plasma protein binding values for amprenavir, indinavir, nelfinavir, ritonavir, and saquinavir are 90%, 60%, ≥ 98%, ≥ 99%, and 97% ,

respectively (Acosta et al., 2000). In contrast, the HIV reverse transcriptase inhibitors zidovudine and didanosine are minimally bound to human plasma proteins (Acosta et al., 1996) (Product Sheet, Videx).

It was predicted that antiretroviral drugs, including HIV reverse transcriptase and protease inhibitors, would completely eradicate HIV from the body (Perelson et al., 1997). Although the HIV virus can be reduced to undetectable levels in the plasma for an extended period of time, the virus is able to persist (Finzi et al., 1997; Wong et al., 1997). The failure of the antiretroviral therapy can be explained by the existence of reservoirs in the body where HIV is able to survive (Pierson et al., 2000; Sonza and Crowe, 2001; Lambotte et al., 2003). One proposed reservoir is the CNS, which is a result of subtherapeutic concentrations of the antiretroviral drugs (Chun and Fauci, 1999; Ruiz et al., 1999; Pierson et al., 2000; Sonza and Crowe, 2001). As mentioned previously, P-gp transports HIV protease inhibitors out of the BBB, and away from the CNS (Kim et al., 1998). It is hypothesized that P-gp causes subtherapeutic concentrations of the HIV protease inhibitors in the CNS. Therefore, increasing the distribution of HIV protease inhibitors into the CNS could potentially reduce the HIV viral load in the CNS and ameliorate the effects of HIV-associated dementia. One method to increase the distribution of the HIV protease inhibitors into the CNS is to inhibit P-gp at the BBB.

Figure 1: Structure of indinavir, nelfinavir, ritonavir, saquinavir, and amprenavir.

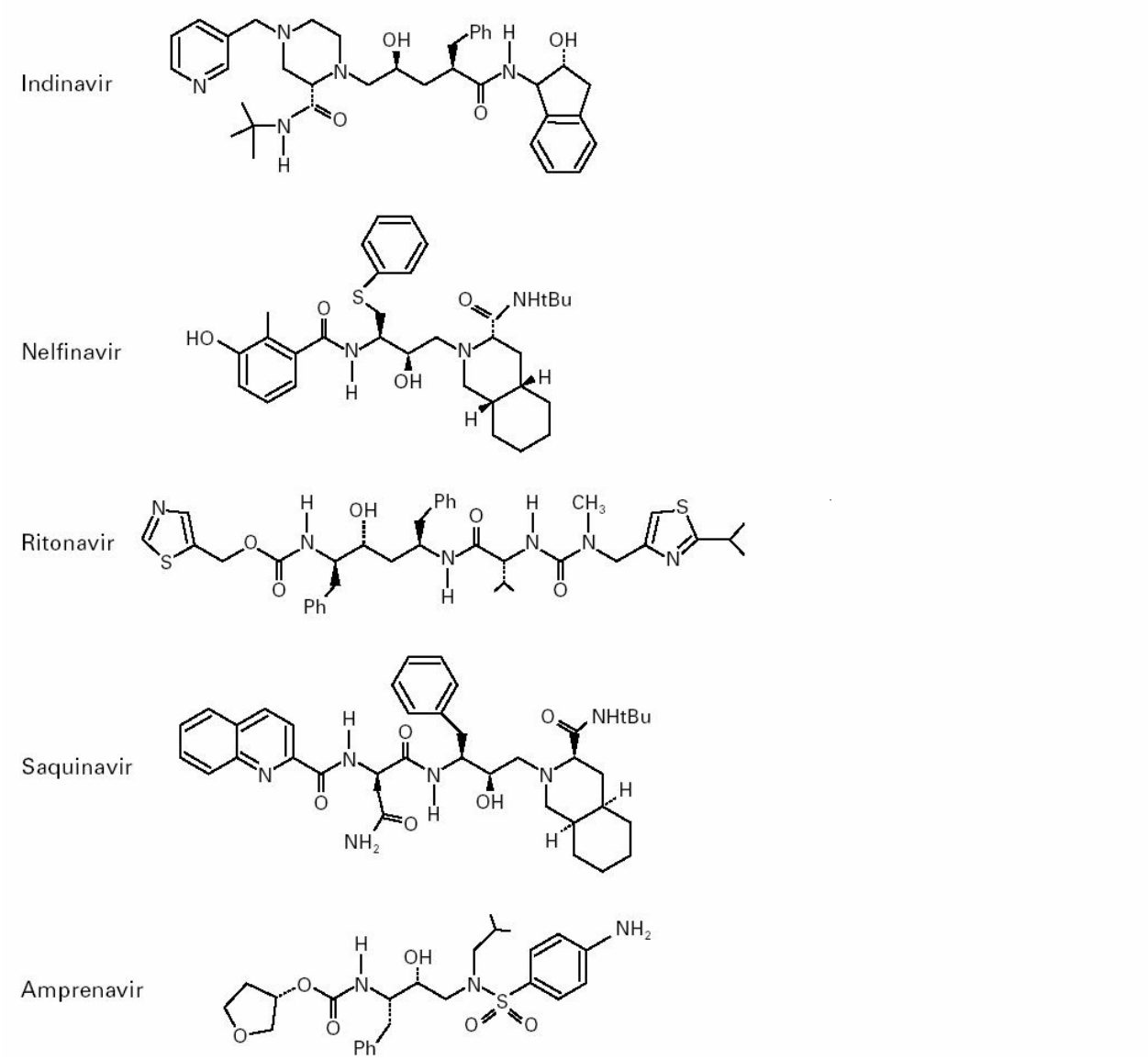

Flexner. N Engl J Med, 1998.

B. ATP-Binding Cassette (ABC) Transporters

P-gp is part of the ATP-binding cassette (ABC) family of transporters (Dean et al., 2001b). ABC transporters use ATP hydrolysis to transport molecules across a cell membrane (Dean et al., 2001a). A functional ABC transporter contains 2 ATP binding sites and contains 1 or more transmembrane domain. Each transmembrane domain can contain 6 to 11 transmembrane helices. The ATP-binding sites are located in the intracellular compartment and contain a Walker A, Walker B, and a signature motif (Dean et al., 2001b). The signature motif differentiates the ABC transporters from other proteins containing ATP binding sites (Dean et al., 2001a). Human ABC transporters have been categorized into 7 subfamilies (ABC A through G) based on the gene structure, domains, and sequence homology of the ATP-binding cassette and transmembrane domains (Dean and Allikmets, 2001). ABC transporters are responsible for transporting both endogenous (e.g. bile-acids) and exogenous (e.g. doxorubicin) molecules (Dean et al., 2001b).

P-gp, the product of the ABCB1 gene, is known to transport the HIV protease inhibitors amprenavir, indinavir, nelfinavir, ritonavir, and saquinavir (Kim et al., 1998; van der Sandt et al., 2001; Williams et al., 2002) and has a significant effect on the distribution of HIV protease inhibitors into the CNS of rodents (Polli et al., 1999; Choo et al., 2000). MRP1, another ABC transporter and the product of ABCC1 gene, has been reported to transport the HIV protease inhibitors saquinavir, ritonavir, and indinavir but not amprenavir (Jones et al., 2001a; Jones et al., 2001b; van der Sandt et al., 2001; Williams et al., 2002). There is also a report that shows an inverse relationship in the intracellular accumulation of saquinavir and ritonavir with the level of MRP1 expression in human lymphocytes (Meaden et al., 2002), further suggesting that saquinavir and ritonavir are substrates of MRP1. However, one report shows that indinavir, saquinavir, and ritonavir are not substrates of MRP1 (Huisman et al., 2002). The discrepancy has not been resolved between these reports on the transport of indinavir, saquinavir, and ritonavir using MRP1 transfected cell lines.

MRP2, the product of the ABCC2 gene, has been shown to transport the HIV protease inhibitors saquinavir, ritonavir, and indinavir (Huisman et al., 2002; Williams et al., 2002). MRP3 and MRP5, the products of the ABCC3 and ABCC5 genes respectively, have been shown not to transport the HIV protease inhibitors saquinavir, ritonavir, and indinavir (Huisman et al.,

2002). The murine breast cancer resistance protein 1 (Bcrp1), another ABC transporter, has also been reported to not transport saquinavir, ritonavir, and indinavir (Huisman et al., 2002). The focus of this dissertation will be on the ABC transporters ABCB1 (P-gp) and ABCC1 (MRP1).

ABCB1 (P-gp)

P-gp is a 170 kDa protein consisting of 1280 amino acids (Figure 2) (Fardel et al., 1996; Ambudkar et al., 1999; Borst and Elferink, 2002). P-gp consists of two homologous halves containing 2 transmembrane domains and 2 ATP binding sites. Each transmembrane domain consists of 6 transmembrane helices for a total of 12 transmembrane helices. P-gp is glycosylated and phosphorylated, but only phosphorylation appears to affect transport activity (Fardel et al., 1996).

P-gp was initially discovered in cancer cells resistant to traditional chemotherapeutic agents (Gottesman and Pastan, 1993). P-gp actively transports xenobiotics out of cells causing sub-therapeutic intracellular concentrations. This is one mechanism which can result in multidrug resistance. P-gp is also located on the apical membrane of non-cancer cells, including intestinal cells, hepatocytes, kidney cells, and brain capillary endothelial cells (Ambudkar et al., 1999). Because P-gp is located on excretory organs, like the kidney and liver, it has been suggested that it plays a role in the excretion of xenobiotics. However, the presence of P-gp in non-secretory organs (i.e. brain and testis) would suggest that it plays a role in the distribution of xenobiotics as well.

Mice and rats possess two functionally equivalent proteins for human P-gp, called mdr1a and mdr1b (Deuchars et al., 1992; Gottesman and Pastan, 1993). The tissue distribution and cellular orientation of mdr1a and mdr1b are similar to that of MDR1, which makes the rodent a convenient and relevant model for P-gp function in vivo (Schinkel, 1998). A knockout mouse lacking the mdr1a and/or mdr1b genes has been developed and used to determine the effects of P-gp in vivo (Schinkel, 1998). For example, the distribution of nelfinavir into the CNS is over 27 times higher in mdr1a knockout mice than in wild-type mice (Choo et al., 2000). This would be further evidence that P-gp can play a significant role in the distribution of xenobiotics into the CNS. Interestingly, knockout mice deficient in P-gp do not show any physiological abnormalities. This would suggest that either P-gp does not play a significant role in the

distribution and elimination of endogenous compounds and/or other redundant systems take the place of P-gp.

P-gp transports an array of structurally diverse compounds including anthracyclines, vinca alkaloids, steroids, and HIV protease inhibitors (Sharom, 1997; Lee et al., 1998; Ambudkar et al., 1999; Borst and Elferink, 2002). In general, most of the substrates for P-gp are lipophilic molecules. The binding site(s) of P-gp have yet to be definitively identified. There are numerous studies that would argue for multiple binding sites for P-gp substrates (Martin et al., 2000; Wang et al., 2000; Garrigues et al., 2002). Although multiple binding sites have been suggested, it also has been shown that substrate binding to one site can cause changes in other binding sites (Wang et al., 2000). This complex relationship makes it difficult to accurately describe the mechanism by which P-gp substrates are transported and may also explain why P-gp can transport such a diverse array of molecules. In addition to substrate binding sites, another binding site for the MDR modulators GF120918 and nicardipine has been proposed (Martin et al., 2000). In the model proposed by Martin et al. (Martin et al., 2000), GF120918 and nicardipine caused allosteric changes to the other binding sites, and thus showed noncompetitive inhibition of P-gp transport. However, GF120918 has been shown to competitively inhibit daunorubicin transport, a model P-gp substrate, using rat liver membrane vesicles (Wallstab et al., 1999). This illustrates the complex nature of substrate/inhibitor binding to P-gp. An "induced-fit mechanism" has been proposed to explain how P-gp is able to transport a wide variety of structurally different molecules (Loo and Clarke, 2001; Loo et al., 2003). In their proposed model, the transmembrane helices change their orientation to accommodate the binding of structurally different substrates. Thus, the three dimensional structure of P-gp would be different for structurally different substrates. Unfortunately, there is no all inclusive model to explain P-gp transport and inhibition, but it is clear that the substrate binding site(s) allow P-gp to transport a wide variety of molecules.

Figure 2: Structure of P-glycoprotein.

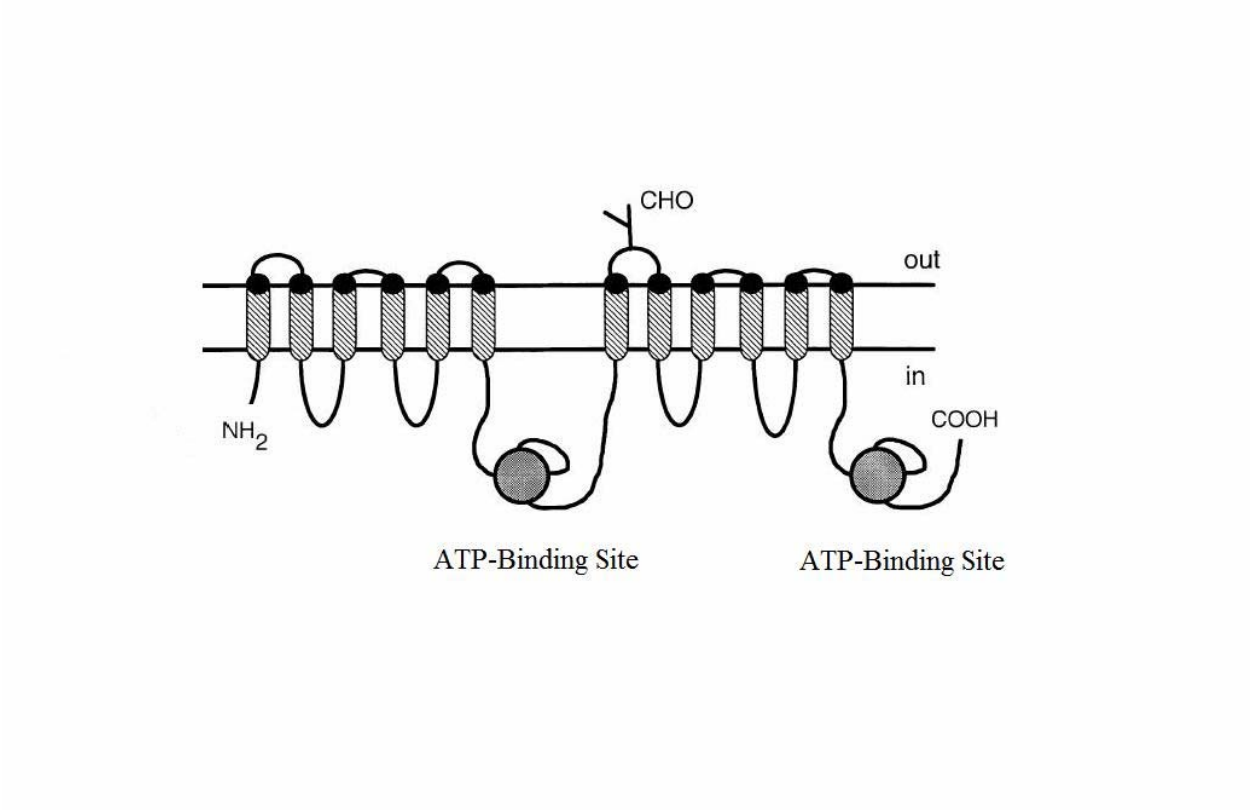

Modified from Borst et al. J Natl Cancer Inst, 2000.

ABCC1

MRP1 is a 190 kDa protein that contains 17 transmembrane helices (Leslie et al., 2001) (Figure 3). MRP1 is the product of the ABCC1 gene and is located on the basolateral membrane of cells. Like MDR1, MRP1 contains two nucleotide binding domains and uses ATP hydrolysis as its source of energy. In rodents there is only 1 functionally equivalent protein, mrp1, which is expressed in the liver, kidney, lung, intestine, and brain (Cherrington et al., 2002).

Cells with elevated levels of MRP1 show similar drug resistant profiles to cells that express elevated levels of MDR1 (Borst et al., 2000). This would suggest that MRP1 substrates are also substrates of P-gp. However, it appears that MRP1 transports glutathione, sulfate, or glucuronide conjugates (Jedlitschky et al., 1996). For example, doxorubicin and daunorubicin do not inhibit the transport of leukotriene, a model MRP1 substrate (Priebe et al., 1998), yet, the

glutathione conjugates of doxorubicin and daunorubicin do inhibit leukotriene transport. Conjugation may not be necessary for MRP1 transport. For example, vincristine is cotransported with reduced glutathione by MRP1 (Loe et al., 1998). This would explain how MRP1 is able to transport unconjugated molecules. The cotransport of unconjugated drugs with reduced glutathione may explain why Huisman et al. (Huisman et al., 2002) did not observe the transport of indinavir, saquinavir, and ritonavir in MRP1 transfected cells since glutathione levels were not measured. MRP1 is also able to transport multivalent organic anions like methotrexate without glutathione (Ishikawa et al., 2000). In general, MRP1 transport requires a negatively charged molecule. The different methods of transport (i.e. cotransport or conjugation) allow MRP1 to transport a variety of molecules.

Figure 3: Structure of MRP1.

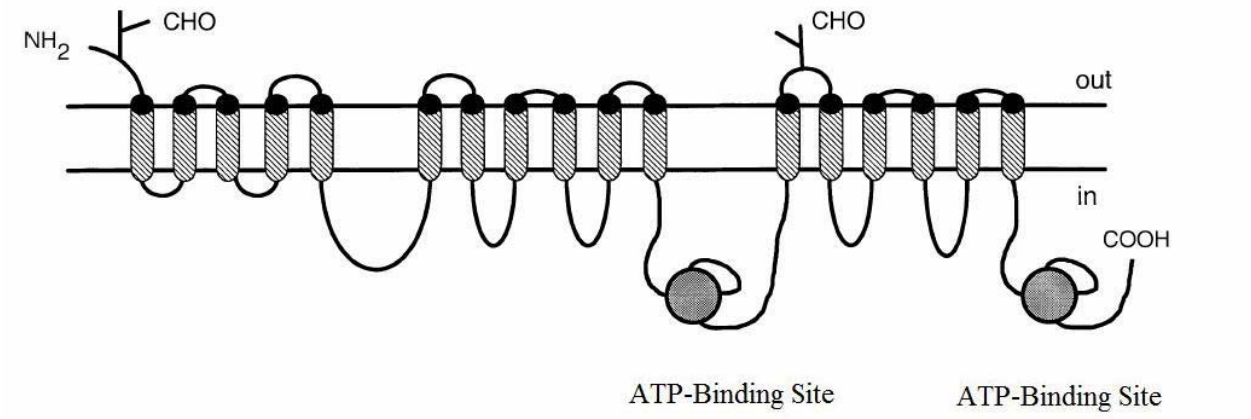

Modified from Borst et al. J Natl Cancer Inst, 2000.

C. Blood-Brain Barrier

The BBB is comprised of capillary endothelial cells that restrict the transport of endogenous and exogenous substances into and out of the CNS, and is responsible for maintaining the microenvironment of the brain (Huber et al., 2001). Brain capillary endothelial cells have tight junctions, as indicated by a high transendothelial electrical resistance (1100 to 2000 $\Omega \bullet m^2$) in rat brains (Wolburg and Lippoldt, 2002). The BBB is characterized by having limited paracellular diffusion and transcytosis activity (Bickel et al., 2001). Therefore, molecules must pass through the endothelial cells (transcellular) to enter the CNS. Hydrophilic molecules, which cannot readily pass through the lipid bilayer, would have limited distribution into the CNS. However, capillary endothelial cells have specialized proteins that transport molecules across the apical and basolateral membranes (Figure 4) (Huber et al., 2001). For example, glucose, which is an essential nutrient for the CNS, is transported by GLUT1, a facilitated transport protein (Klepper and Voit, 2002). A deficiency in GLUT1 causes low levels of glucose in the CNS, termed hypoglycorrhachia, which in turn causes abnormal physiologic functioning of the brain and is associated with seizures and developmental delay (Klepper and Voit, 2002). This deficiency illustrates the importance of the BBB on the microenvironment of the CNS.

Brain capillary endothelial cells are surrounded by astrocytes, a type of glial cell, which form foot processes (Prat et al., 2001). Although capillary endothelial cells form the BBB, surrounding cells, like astrocytes, are essential for the regulation and maintenance of the BBB (Prat et al., 2001; Wolburg and Lippoldt, 2002; Rieckmann and Engelhardt, 2003). For example, brain endothelial cells grown in the presence of glial cells show a significant increase in the expression of γ-glutamyl transferase, a marker of the BBB, and increased tight junctions (Abbott, 2002).

P-gp has been identified on the apical membrane of brain capillary endothelial cells (Demeule et al., 2000) and is responsible for transporting a variety of xenobiotics away from the CNS (Tanigawara, 2000). Its influence on the distribution of xenobiotics into the CNS can be seen in mdr1a and mdr1a/1b knockout mice (Borst and Schinkel, 1996). Table 1 lists the plasma

and brain mdr1a (-/-) to mdr1a (+/+) concentration ratios for a variety of xenobiotics that are transported by P-gp (Pardridge, 1998). It should be noted that the concentrations of the xenobiotics, with the exception of vinblastine, in the plasma and brain samples were determined by total radioactivity, and therefore, represents both the parent drug and their metabolite(s). The plasma concentrations of vinblastine, ivermectin, digoxin, and loperamide were greater in mdr1a knockout mice as indicated by the plasma ratio being greater than 1. This suggests that P-gp plays a role in the elimination of these drugs. The brain ratios for vinblastine, ivermectin, digoxin, and loperamide were substantially larger than the plasma ratios, indicating that P-gp plays a significant role in the distribution of these drugs into the CNS. The plasma ratios for cyclosporine A, dexamethasone, morphine, and ondansteron were not different in mdr1a knockout versus wild-type mice. However, there was an increase in the distribution of these drugs into the CNS. P-gp can also change the pharmacological or toxicological effects of a drug in the CNS. For example, mdr1a knockout mice are 100 times more sensitive to ivermectin CNS toxicity compared to wild-type mice (Schinkel et al., 1994). Also, the antinociceptive effects of morphine are altered in mdr1a knockout mice (Zong and Pollack, 2000).

There is confusion concerning the expression of MRP1 at the BBB. The mRNA of mrp1 has been found in isolated rat brain endothelial cells (Regina et al., 1998; Decleves et al., 2000) suggesting that it plays a role in the distribution of xenobiotics into the CNS. MRP1 has been detected in isolated and cultured bovine endothelial cells (Huai-Yun et al., 1998; Zhang et al., 2000a). However, MRP1 was not found in human capillary endothelial cells and the expression of MRP1 was associated with glial fibrillary acidic protein (GFAP), a marker of glial cells (Seetharaman et al., 1998a). This would suggest that MRP1 is expressed in glial cells and not in capillary endothelial cells. By contrast, the expression of MDR1 in isolated human brain endothelial cells was associated with the expression of platelet endothelial cell adhesion molecule (PECAM), a marker of endothelial cells (Seetharaman et al., 1998a), which is consistent with P-gp being expressed at the BBB. Interestingly, the expression of MRP1 has been shown to increase in cultured human brain endothelial cells compared to the originally isolated cells, whereas the expression of MDR1 decreases (Seetharaman et al., 1998b). Mrp1 also appears to be elevated in an immortalized rat brain endothelial cell line (RBE4), a cell line used for in vitro drug transport studies (Regina et al., 1998). It has been suggested that isolated brain endothelial cells are contaminated with glial cells which also express transport proteins

(Ballerini et al., 2002). The contamination with glial cells may explain why mrp1 has been detected in rat and bovine brain endothelial cells (Huai-Yun et al., 1998; Regina et al., 1998; Decleves et al., 2000; Zhang et al., 2000a). Since HIV protease inhibitors are transported by MRP1 (Jones et al., 2001a; Jones et al., 2001b; van der Sandt et al., 2001; Williams et al., 2002), determining the expression of MRP1 at the BBB would help to identify possible mechanisms for the transport of HIV protease inhibitors into the CNS.

Figure 4: Transport mechanisms at the blood-brain barrier.

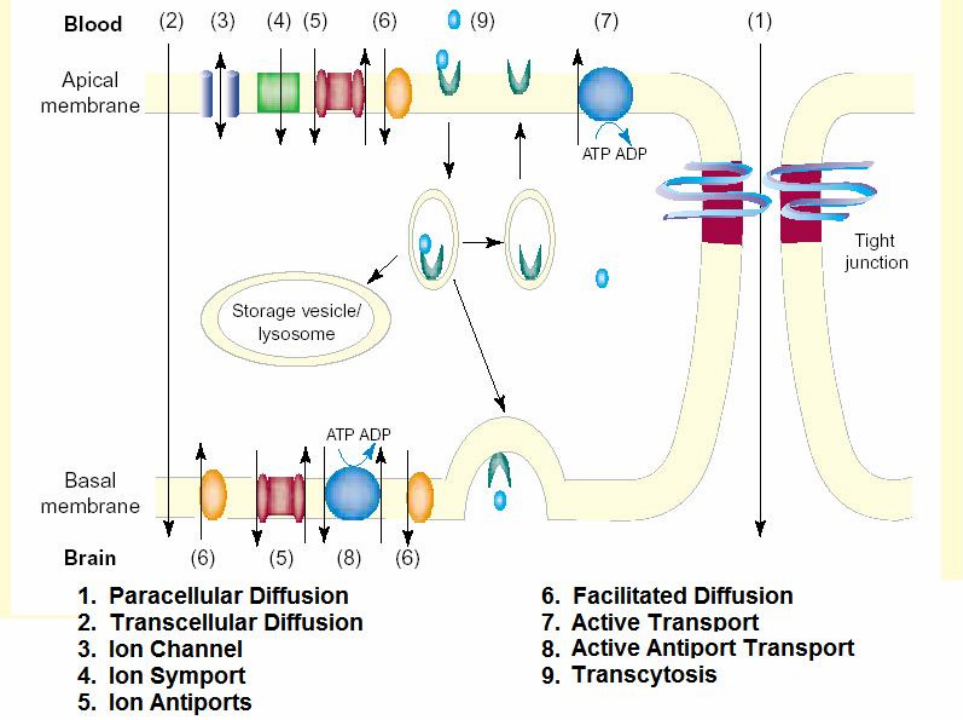

Huber et al. Trends Neurosci, 2001

Table 1: The distribution of xenobiotics into the CNS of mdr1a knockout and wild-type mice.

	mdr1a (-/-):mdr1a (+/+)	
Drug	**Plasma**	**Brain**
Vinblastine	2	22
Ivermectin	3	87
Digoxin	4	66
Cyclosporine A	1	17
Dexamethasone	1	2
Morphine	1	2
Ondansetron	1	4
Loperamide	2	13

D. HIV-Associated Dementia

HIV-associated dementia is a cognitive motor disorder that had an estimated prevalence of 20 to 30% in HIV-1-infected individuals during the early 1990s (Swindells et al., 1999; Kaul et al., 2001). The prevalence of HIV-associated dementia has decreased significantly with the advent of new antiretroviral drugs, like HIV protease inhibitors (Sacktor, 2002; Albright et al., 2003). However, HIV-associated dementia is still prevalent in HIV infected individuals even with these new drugs (Kaul et al., 2001; Sacktor, 2002; McArthur et al., 2003). The mechanism of HIV-associated dementia is poorly understood, however, it is known that the HIV does not infect neurons (Kaul et al., 2001). The HIV enters the CNS during the initial stages of infection and resides in the CNS thereafter. The pathology of HIV-associated dementia is associated with an increase in microglia cells, increased TNF-α mRNA in both microglia and astrocytes, and neuronal loss (Kaul et al., 2001). A proposed model by which neurons are damaged by the HIV-1 virus is shown in Figure 5. In this model, the HIV-1 virus infects microglia/macrophage cells in the CNS, which causes the release of neurotoxins that cause free radical damage to neurons. Another proposed mechanism is the HIV-1 virus releases gp120 surface proteins, which causes uninfected microglia cells to release neurotoxins that damage the neuron. Many HIV protease inhibitors and reverse transcriptase inhibitors do not distribute into the brain in sufficient

concentrations to affect HIV replication, hence, it is theorized that increasing the extent of distribution of HIV drugs would help to ameliorate the effects of HIV-associated dementia. One method to increase the distribution of HIV PIs would be to coadminister an MDR modulator with HIV protease inhibitors to inhibit P-gp at the BBB.

Figure 5: Proposed mechanism of HIV-associated dementia.

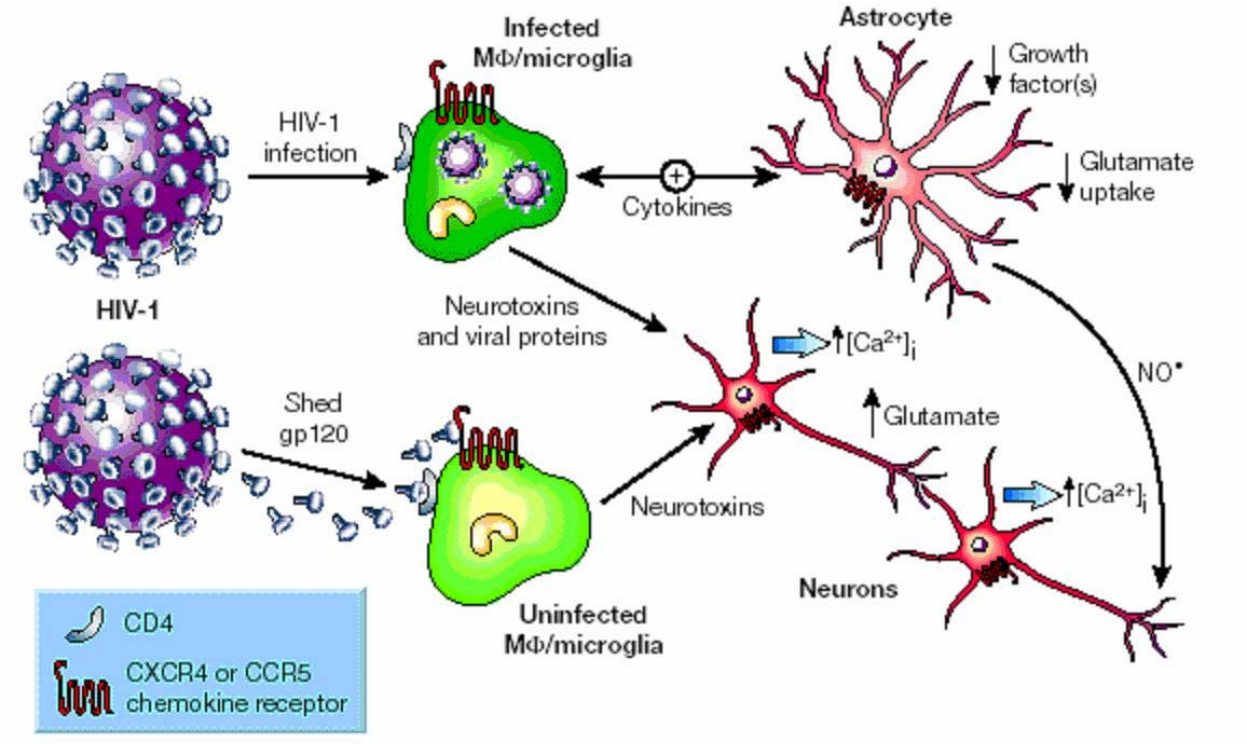

Kaul et al. Nature, 2001.

E. MDR Modulators

MDR modulators were first used to inhibit P-gp in cancer cell lines that were resistant to a variety of antineoplastic drugs (Tsuruo et al., 1983; Feng et al., 1991; Roepe, 1992). First generation MDR modulators include calcium channel blockers, calmodulin antagonists, cyclic peptides, and vinca alkaloid analogues (Ford, 1996). These first generation MDR modulators were therapeutic agents that were also substrates for P-gp. For example, verapamil, a calcium channel blocker, has been used clinically as an MDR modulator with doxorubicin, vinblastine, and vincristine (Raderer and Scheithauer, 1993). However, in these clinical studies, the measured plasma concentrations for verapamil (1-2 μM) were below the optimal in vitro concentrations to inhibit P-gp (6-10 μM). A limiting factor in achieving plasma concentrations of verapamil high enough to inhibit P-gp is the cardiotoxic effects of verapamil (Raderer and Scheithauer, 1993; Ford, 1996; Krishna and Mayer, 2000). Other first generation MDR modulators also caused unwanted pharmacological effects when administered in doses sufficient to inhibit P-gp.

Over time, a second generation of MDR modulators that were analogues of the first generation MDR modulators was utilized. The principal advantage of these second generation MDR modulators was their limited pharmacological effects. For example, dexverapamil, the R-enantiomer of verapamil, showed reduced cardiotoxic effects, and valspodar is a non-immunosuppressive analog of cyclosporine (Krishna and Mayer, 2000). However, both first and second generation MDR modulators showed significant effects on metabolism, and especially on the enzyme cytochrome P4503A4 (Lum et al., 1992; Raderer and Scheithauer, 1993; Lum and Gosland, 1995). For example, R-verapamil, valspodar, and cyclosporine have caused a decrease in the metabolic clearance of paclitaxel, etoposide, and doxorubicin (Bartlett et al., 1994; Berg et al., 1995; Boote et al., 1996). This overlap in substrates is not surprising since both P-gp and CYP3A4 substrates are characterized as large lipophilic molecules (Wang et al., 2001).

The relative selectivity of the MDR modulators for CYP3A4 and P-gp was determined by comparing the IC50 of P-gp in Caco-2 cells to the IC50 of CYP3A4 in liver microsomes (Wandel et al., 1999). Figure 6 shows the results of these experiments for cyclosporine and valspodar (PSC 833). There is no direct way to compare the IC50 of P-gp and CYP3A4 for each drug individually, however, the relative selectivity of cyclosporine and valspodar for CYP3A4

and P-gp can be compared. Since a higher concentration of valspodar was needed to inhibit CYP3A4 compared to cyclosporine, it can be concluded that cyclosporine is a more potent inhibitor of CYP3A4 than valspodar. On the other hand, a higher concentration of cyclosporine was needed to inhibit P-gp compared to valspodar, and therefore, it can be concluded that valspodar is a better inhibitor of P-gp. Unfortunately, these results do not indicate if valspodar or cyclosporine is a selective inhibitor of P-gp or CYP3A4. In fact, valspodar has been shown to inhibit the clearance of etoposide, a CYP3A4 substrate (Boote et al., 1996).

Third generation MDR modulators were designed based on the structure activity relationship of P-gp. Figure 7 shows the structure of GF120918, a third generation MDR modulator. Ideally, MDR modulators would inhibit P-gp without altering metabolism, which can lead to toxicities. Therefore, determining the selectivity of MDR modulators, like GF120918, would help to identify candidates to be used for MDR modulation clinically. GF120918 has been shown not to inhibit CYP3A4 metabolism in vitro (Cummins et al., 2002). GF120918 has also been shown to selectively inhibit P-gp transport without inhibiting CYP3A4 metabolism in a rat single-pass intestinal perfusion model (Cummins et al., 2003). This would further suggest that third generation modulators are able to inhibit P-gp transport without altering drug metabolism.

Figure 6: IC50 of valspodar (PSC 833) and cyclosporine for CYP3A4 metabolism and P-gp transport. The IC50 of cyclosporine and valspodar for the metabolism of nifedipine, a CYP3A4 substrate, was determined in human liver microsomes (shown on the left). The IC50 of cyclosporine and valspodar for the transport of digoxin, a P-gp substrate, across a Caco2 monolayer was determined (shown on right).

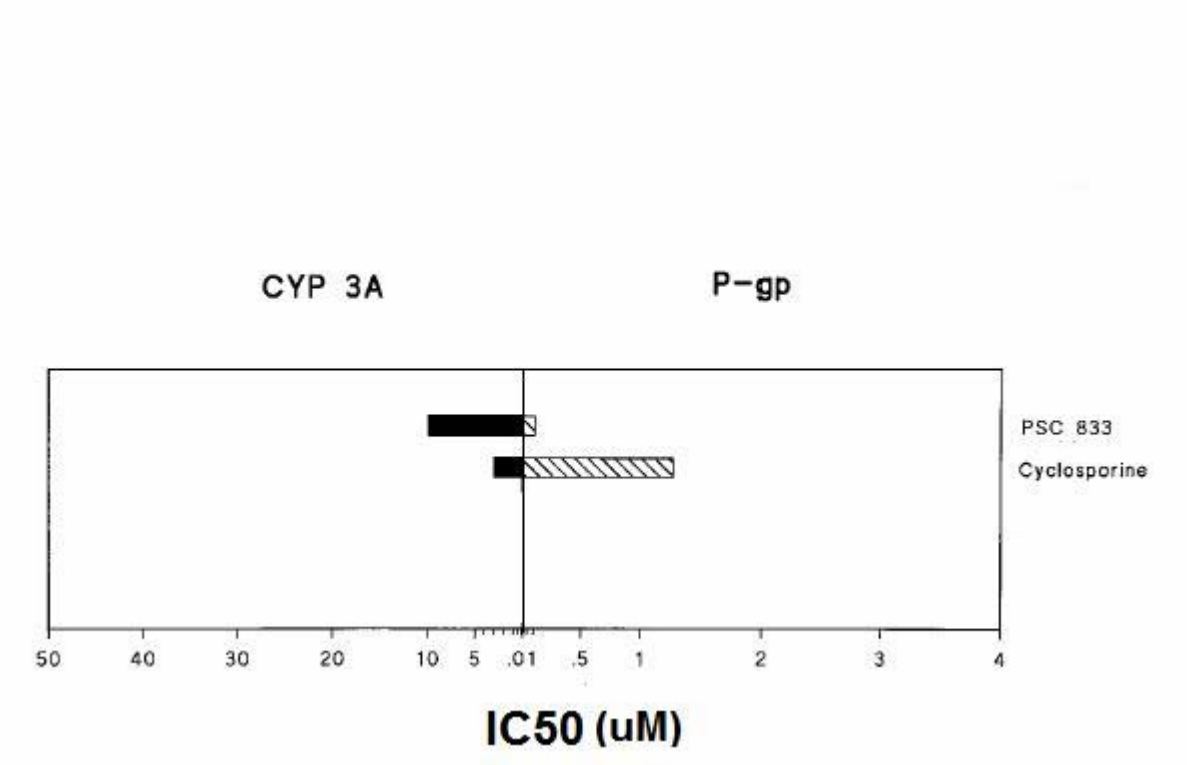

Modified from Wandel et al. Cancer Res. 1999.

Figure 7: Structure of GF120918

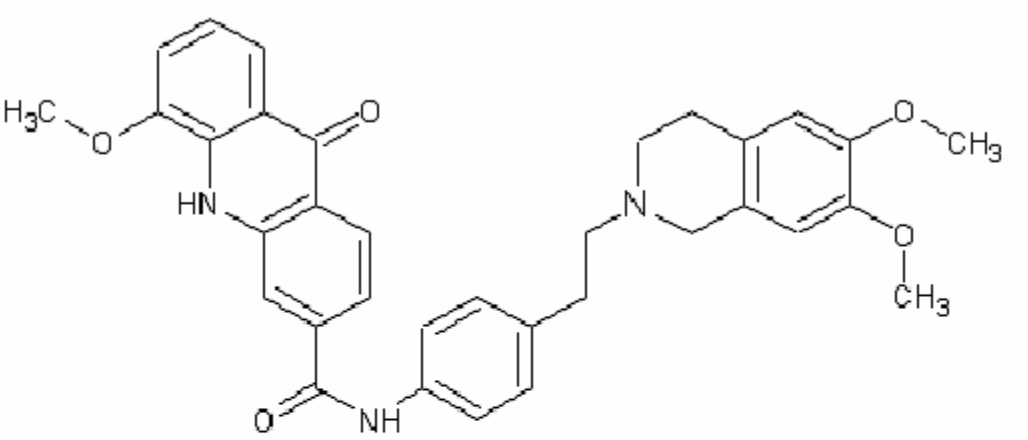

F. Distribution of HIV Protease Inhibitors into Breast Milk

There is little information concerning the distribution of most xenobiotics into breast milk. Even less is known about the mechanisms (i.e. passive diffusion and active transport) by which a xenobiotic can gain access to the milk from the plasma. Mammary epithelial cells, like brain capillary endothelial cells, regulate the distribution of xenobiotics into milk. Mammary epithelial cells form tight junctions that limit paracellular transport. Therefore, xenobiotics must enter into milk through the transcellular pathway. Lipophilicity, protein binding in milk and plasma, fat partitioning, and ionization have been used to predict the extent of xenobiotic accumulation in milk (Fleishaker et al., 1987). These models assume that xenobiotics passively diffuse into the breast. However, some drugs have been shown to be actively transported into milk, including cimetidine and nitrofurantoin (Oo et al., 1995; Gerk et al., 2001). The mRNA of many drug transporters, including ABCB1 and ABCC1, are expressed in lactating mammary epithelial cells (Alcorn et al., 2002). Preliminary studies in this lab have shown that the mRNA

of mdr1b, one of the rodent genes responsible for the production of P-gp, is expressed in rat mammary tissue using polymerase chain reaction (PCR) (Figure 8). This would suggest that P-gp could play a significant role in the distribution of P-gp substrates into breast milk, including HIV protease inhibitors.

The HIV viral load in breast milk is considered a risk factor for the transmission of HIV from mother to child (Fowler and Newell, 2002). The concentrations of zidovudine (AZT), a reverse transcriptase inhibitor used in the treatment of HIV, in breast milk are equivalent to that of maternal serum concentrations (Briggs et al., 1998). It has been shown that the transmission of the HIV through breastfeeding can be significantly reduced by using reverse transcriptase inhibitors (Fowler and Newell, 2002). This would suggest that other antiretroviral drugs, like HIV protease inhibitors, may also prevent the transmission of HIV through breast milk. HIV protease inhibitors are lipophilic, and therefore, the tight junctions of the mammary epithelial barrier should not prevent their distribution into milk. However, the protein expression and functionality of P-gp at the mammary epithelial barrier are unknown. Understanding the distribution and mechanisms by which HIV protease inhibitors enter into breast milk would help to determine if HIV protease inhibitors could be used to prevent the transmission of HIV through breast milk.

Figure 8: Expression of mdr1b in rat tissue. mRNA from male rat livers, female rat livers, lactating female rat livers, and female lactating mammary tissue was isolated and converted to cDNA. Beta2-microglobulin (housing keeping gene) and mdr1b were amplified using PCR. (In collaboration with R. Muller)

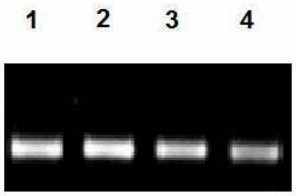

Beta2-microglobulin

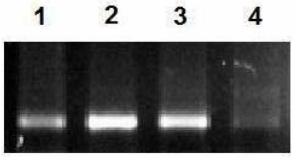

mdr1b

Lane	Tissue
1	Male Rat Liver
2	Female Rat Liver
3	Lactating Female Rat Liver
4	Lactating Rat Mammary Tissue

CHAPTER III. HYPOTHESIS AND SPECIFIC AIMS

The major thrust of the work presented in this dissertation will address the ability of P-gp to control the distribution of HIV protease inhibitors across the BBB, and the ability of MDR modulators to increase the distribution of HIV protease inhibitors into the CNS. This work will be guided by the following hypotheses and specific aims:

Hypothesis 1: The co-administration of GF120918 will increase the unbound brain to blood ratio of amprenavir in rats by inhibiting P-gp at the blood-brain barrier, but GF120918 will not alter the systemic clearance of amprenavir.

Specific Aim 1. To determine the effects of GF120918 on the CNS distribution of amprenavir into the CNS of rats.

Specific Aim 2. To determine the effects of GF120918 on the systemic clearance of amprenavir in rats.

Specific Aim 1 will determine if MDR modulators, like GF120918, can be used to increase the CNS distribution of HIV protease inhibitors. Since HIV protease inhibitors are extensively bound to plasma proteins, it is necessary to determine the unbound concentration of amprenavir in plasma and the CNS. This will avoid ambiguity concerning the effects of GF120918 on the plasma protein binding of amprenavir, versus the inhibition of P-gp at the BBB. The brain to blood ratio of unbound amprenavir will be compared in rats treated with GF120918 and control rats. Amprenavir is a substrate of CYP3A and therefore, specific Aim 2 will determine if GF120918 has a significant effect on the systemic clearance of amprenavir. Amprenavir will be given as a constant infusion and the systemic clearance of amprenavir will be determined from the plasma steady-state concentrations. The systemic clearance of amprenavir in the absence and presence of GF120918 will be compared.

Hypothesis 2: GF120918, unlike cyclosporine, will selectively inhibit P-gp transport relative to CYP3A metabolism in vitro

Specific Aim 3. To determine the in vitro inhibition constant (Ki) of GF120918 and cyclosporine for CYP3A4.

Specific Aim 4. To determine the in vitro inhibition constant (Ki) of GF120918 and cyclosporine for MDR1.

Specific Aims 3 and 4 will determine the in vitro selectivity of GF120918 and cyclosporine for P-gp and CYP3A4. An expression system for CYP3A4 will be used to determine the apparent inhibition constants of GF120918 and cyclosporine, using midazolam as a model CYP3A4 substrate. Nonlinear simultaneous fitting will be used to obtain the inhibition constants of GF120918 and cyclosporine for CYP3A4.

MDR1 transfected pig kidney cells (LLC-MDR1) and non-transfected kidney cells (LLC-PK1) will be used to determine the apparent inhibition constants of GF120918 and cyclosporine for P-gp, using doxorubicin as a model P-gp substrate. Nonlinear simultaneous fitting will be used to obtain the inhibition constant of GF120918 and cyclosporine for P-gp. The in vitro inhibition constants of P-gp and CYP3A4 will be compared to determine the selectivity of the MDR modulators. The selective inhibition determined in vitro will then be tested in vivo using the rat model.

Hypothesis 3: GF120918, unlike cyclosporine, will selectively inhibit P-gp transport at the BBB over CYP3A metabolism in vivo.

Specific Aim 5. To determine the selectivity of GF120918 and cyclosporine for CYP3A and P-gp inhibition using the rat model.

Specific Aim 5 will determine the selective inhibition of GF120918 and cyclosporine in vivo using the rat model. The CNS distribution of nelfinavir will be used as a marker for the effects of GF120918 and cyclosporine on P-gp at the BBB. The unbound brain to plasma ratio of nelfinavir in the presence and absence of GF120918 and cyclosporine will be compared to

determine the effects of the MDR modulators on P-gp at the BBB. The concentrations of the two MDR modulators will be measured to determine the concentrations needed to produce, or not produce, an effect at the BBB.

Midazolam will be used as a model CYP3A substrate to determine the effects of GF120918 and cyclosporine on CYP3A metabolism. Midazolam is metabolized by CYP3A in humans and rats (Kobayashi et al., 2002). Although midazolam appears to be a substrate of MDR1, the contribution of MDR1 to the overall transport of midazolam is negligible because the passive diffusion of midazolam is significantly greater than the MDR1 dependent transport (Kim et al., 1999; Tolle-Sander et al., 2003). Therefore, it will be assumed that the effects of the MDR modulators on the clearance of midazolam will be due to inhibition of CYP3A metabolism and not by P-gp-dependent elimination of midazolam. The oral clearance of midazolam will be used to determine the effects of GF120918 and cyclosporine on CYP3A metabolism. The systemic clearance of midazolam in rats is similar to that of hepatic-blood-flow, suggesting that the metabolism of midazolam is blood-flow rate limited in rats (Kotegawa et al., 2002). The effect of ketoconazole, a CYP3A inhibitor, was significantly greater for the oral clearance rather than the systemic clearance of midazolam (Kotegawa et al., 2002), again suggesting that the elimination of midazolam is blood-flow rate limited. Therefore, the most sensitive measure of CYP3A inhibition would be to determine the oral clearance of midazolam in the presence of GF120918 and cyclosporine. Nonlinear simultaneous fitting will be used to obtain the inhibition constant of GF120918 and cyclosporine for CYP3A.

Hypothesis 4: Mrp1 is localized to capillary endothelial cells in the CNS, and therefore, may play a role in the distribution of HIV protease inhibitors into the CNS.

Specific Aim 6. To determine the expression of mdr1a and mrp1 at the blood-brain barrier of rats.

Capillary endothelial cells will be isolated from rat brains. A fraction of the cells will be used to measure γ-glutamyl transferase activity, a marker of the BBB. The mRNA will be collected from the remaining cells and the expression of GFAP and PECAM will be determined by PCR as a measure of glial cell contamination and endothelial cell enrichment, respectively.

The expression profile of PECAM, GFAP, mrp1, mdr1a and the activity of γ-glutamyl transferase activity will be compared to determine if mrp1 is localized to the BBB. The mdr1a gene will be used as a positive control since it is known to be localized to the BBB. It is postulated that if mrp1 is localized to the BBB, then it will play a significant role in the CNS distribution of xenobiotics, including HIV protease inhibitors. Alternatively, if mrp1 is not localized to the BBB then it will be assumed that mpr1 does not play a significant role in the distribution of xenobiotics into the CNS.

Hypothesis 5: P-gp, located in lactating mammary epithelium , plays an important role in the transport of MDR substrates into milk.

Specific Aim 7. To determine the distribution of nelfinavir into rat milk.

Specific Aim 8. To determine if P-gp plays a significant role in the distribution of nelfinavir into rat milk.

The distribution of nelfinavir into rat milk will be determined by measuring the milk to plasma ratio of nelfinavir after a constant infusion. The role of P-gp at the mammary epithelial barrier will also be determined by analyzing the distribution of nelfinavir into rat milk in the presence and absence of the MDR modulator GF120918. After the milk sample is taken, the brain will be excised and the brain to plasma ratio of nelfinavir will be determined and used as a positive control for the inhibition of P-gp. Rat mammary tissue will also be excised from the rat after the brain has been removed. The protein expression of P-gp will be determined in both rat brain and mammary tissue.

CHAPTER IV. MATERIALS AND METHODS

A. Materials

Acetonitrile, sodium acetate, acetic acid, methanol, heptane, ethyl acetate, zinc sulfate heptahydrate were obtained from Fisher Scientific (Pittsburg, PA). Midazolam, doxorubicin, cyclosporine, dimethyl sulfoxide (DMSO), sodium phosphate, adenosine triphosphate (ATP), adenosine monophosphate (AMP), Mes (2-[N-morpholino] ethanesulfonic acid), EGTA (ethylene gycol-bis (beta-aminoethylether)- N,N,N',N'-tetraacetic acid), dithiothreitol, sodium azide, zinc acetate, ascorbic acid, sodium hydroxide, ammonium molybdate, (+/-)-verapamil hydrochloride, sodium orthovanadate, antifoam A concentrate, lauryl sulfate (SDS; sodium dodecylsulfate), Tween, hydroxypropylmethylcellulose, bovine Albumin Fraction V (BSA), cyclosporine A (cyclosporine) were obtained from Sigma-Aldrich (St. Louis, MO). Amprenavir, ^{14}C-amprenavir (96.5 μCi/mg), and GF120918 were a generous gift from GlaxoSmithKline (Research Triangle, NC). Polyethylene Glycol 400 (PEG-400) was obtained from Union Carbide Chemicals (Danbury, CT). 1-OH midazolam was a generous gift from Roche Laboratories. Cytochrome P4503A4 Supersomes are microsomes from insect cells (BT1-TN-5B1-4) that were infected with CYP3A4, P450 reductase, and cytochrome b5 cDNA and were obtained from BD Bioscience Company (Woburn, MA). Control Supersomes (no gene infected), CYP3A1 Supersomes (infected with CYP3A1, rat P450 reductase, and human cytochrome b5), CYP3A2 Supersomes (infected with CYP3A2, rat P450 reductase, and human cytochrome b5), rat liver microsomes, and the NADPH regenerating system ($NADP^+$, glucose-6-phosphate, $MgCl_2$, glucose-6-phosphate dehydrogenase), and crude membrane vesicles (MDR1 infected and control) were also purchased from BD Bioscience Company (Woburn, MA). Supersomes were kept at -70 ºC and the NADPH regenerating system was kept at -20 ºC prior to use, as indicated by manufacture. LLC-PK1 (pig kidney epithelial) cells were obtained from American Type Culture Collection (Manassas, VA). LLC-MDR1 cells (MDR1 transfected LLC-PK1 cells) were a generous gift from Dr. A. Schinkel (van der Sandt et al., 2000). MDR1-baculovirus was a gift from Dr. U. Subrahmanyeswara Rao (University of North Carolina). SF9 cells, SFM II-900 media, trypsin, and M-199 media were obtained from Invitrogen (Carlsbad, CA). ^{3}H-Vincristine (250 μCi•ml^{-1}) was obtained from Moravek Biochemicals (Brea, CA). Cyclosporine D was obtained from Novartis Pharmaceuticals Company. The solid phase

extraction column (Bond Elute LRCTM, C18, 200mg/10mL) was obtained from Varian (Harbor City, CA). Midazolam•HCl was obtained from Bedford Laboratories (Bedford, OH). Nelfinavir was extracted from Viracept tablets (Agouron Pharmaceuticals, Inc., a Pfizer Company, Ann Arbor, MI), yielding a white solid having a purity of 98.6% by microtitration and exhibiting a single peak by HPLC. C219 (mouse anti-human P-gp) and JSB1 (mouse anti-hamster P-gp) primary antibodies were obtained from Signet Laboratories (Dedham, MA). Alkaline phosphatase linked IgG1 (rabbit anti-mouse) and IgG2a (rabbi anti-mouse) antibodies were obtained from ZYMED Laboratories Inc. (San Francisco, CA). NBT (nitro blue tetrazolium)-BCIP (5-bromo-4-chloro-3-indolyl-phosphate) was obtained from Pierce (Rockford, IL).

B. Intracerebral Microdialysis of Amprenavir

1. Study Design

Five rats were dosed orally with 250 mg kg^{-1} of GF120918 in suspension (0.5% hydroxypropylmethylcellulose, 1% Tween-80) for four consecutive days. On the third day, the cannula was placed in the left femoral vein, a CMA/20 microdialysis probe was placed in the jugular vein, and a CMA/12 microdialysis probe guide was placed in the frontal cortex (3 mm anterior and 3 mm lateral from bregma). On the fourth day, a CMA/12 microdialysis probe was placed in the probe guide. The animal was placed in an Awake Animal System (Bioanalytical Systems Inc., IN), which prevents the different tubing (i.e. microdialysis tubes and femoral vein cannula) from tangling. Approximately 2 hours after the fourth daily dose of GF120918, the rat was given a constant intravenous (i.v.) infusion of amprenavir (26.8 mg•h^{-1}•kg^{-1}, 0.05 ml•h^{-1}) in PEG-400. Dialysate (Na^+ 155 mM; K^+ 2.9 mM; Ca^{2+} 2 mM; Mg^{2+} 0.7 mM; Cl^- 138mM; HCO_3^- 25 mM; and glucose 6.0 mM (pH 7.4)) was perfused through the probes at a rate of 1µl•min^{-1}. Samples were taken from the CMA/12 and CMA/20 probes every 45 minutes over 5.25 hours. For the control group, five rats were treated identically as the treatment group with the exception that the animals were given suspension vehicle without GF120918.

2. Animals

Ten adult male Sprague-Dawley rats (250 - 350 g) were used in all experiments. Animals were purchased from Harlan laboratories (Indianapolis, IN). Animals were maintained under a 12:12-hr light/dark cycle and had access to food and water ad lib prior and during the experiments.

3. Microdialysis Surgery

Equipment:

1 Scalpel and Blade * (George Tiemann and Co., Plainview, NY)
1 Scissor * (George Tiemann and Co., Plainview, NY)
1 Microsurgical scissor * (George Tiemann and Co., Plainview, NY)
2 Forceps * (George Tiemann and Co., Plainview, NY)
1 Ryder needle holder * (George Tiemann and Co., Plainview, NY)
Trocar * (George Tiemann and Co., Plainview, NY)
Vessel Dilator (George Tiemann and Co., Plainview, NY)
Skin Button (Instech Laboratories, PA) *
Gauze *
2-3cc Syringes (George Tiemann and Co., Plainview, NY)
4-2 inch Suture (George Tiemann and Co., Plainview, NY)
1 Suture and Needle (George Tiemann and Co., Plainview, NY)
Koft Animal Stereotaxic (David Koft Instruments, Tujunga, CA)
Skull Drill (Messner Emtronic, Western, Germany)
CMA/20 Microdialysis Probes (CMA/Microdialysis, Acton, MA)
CMA/12 Guide Cannula (CMA/Microdialysis, Acton, MA)
CMA/12 Microdialysis Probes (CMA/Microdialysis, Acton, MA)
Introducer (CMA/Microdialysis, Acton, MA)
Heat Lamp
BAS® Animal Bowl (Bioanalytical Systems Inc., West Lafayette, IN)
BAS Raturn ((Bioanalytical Systems Inc., West Lafayette, IN)

* Autoclaved prior to use.

Solutions:

Ketamine (100mg/ ml) (Fort Dodge Laboratories, Inc., Fort Doge, Iowa)

Xylazine (20 mg•ml^{-1}) (Butler Company, Columbus, OH)

0.9% Sodium chloride solution (Abbott Laboratories, Chicago, IL)

Cannulas:

Cannulas were prepared using 2.5 feet of PE-50 tubing (Becton, Dickinson, Sparks, MD) and 3.5 cm of silastic tubing (Dow Corning, Midland, MI). The silastic tubing was soaked in ethyl ether for approximately 30 seconds and then placed over the PE-50 tubing. The silastic tubing extended 3.5 cm from the PE-50 tubing. Cannulas were stored in 70% ethanol.

Preoperative:

Each rat was injected intraperitoneally (i.p.) with 1 ml•kg^{-1} of 3:1 vol:vol Ketamine: Xylazine solution. After approximately 20 minutes the toe reflex was checked. The area around the femoral and jugular veins and the shoulder blade were shaved. The shaved areas were generously wiped with betadine solution and alcohol. The rat was placed on a surgical board with the arms and feet tied so that the leg and arm were taut but not blocking blood-flow. The cannulas were connected to 22 gauge needles, which were attached to the syringes filled with saline. Saline was washed through the tubing to remove any alcohol. A sterilized drape was placed over the animal with the femoral and jugular vein areas exposed.

Cannulation of Femoral Vein:

Holding the scalpel at 30° to the skin, and pulling the skin apart, an incision approximately 0.75 inch long was made on the skin over the femoral vein. The connective tissue around the femoral vein was removed using forceps and the femoral vein was isolated from the femoral artery and nerve. Approximately 2 cm of the femoral vein was cleaned of all extraneous tissue. Forceps were placed under the vein and a piece of suture was placed around the vein at the distal end. The suture was tied to prevent blood-flow into the vein (Figure 9). Next, a second piece of suture was placed around the vein proximal to the first suture. Tension was

placed on the vein by clamping the tied suture with a pair of Ryder needle holders and gently pulling the suture. A small incision was made on the vein close to the tied suture. With the aid of a vessel dilator, the silastic tubing end of the cannula was inserted into the vein using forceps. Once the silastic tubing was completely inserted into the vein, the other suture was tied. Another incision was made dorsal midline between the scapulae. A trocar was passed under the skin from the incision at the femoral vein to the dorsal midline incision. The cannula was passed through the trocar and secured with a skin button on the back of the rat.

Figure 9: Cannulation of Femoral Vein.

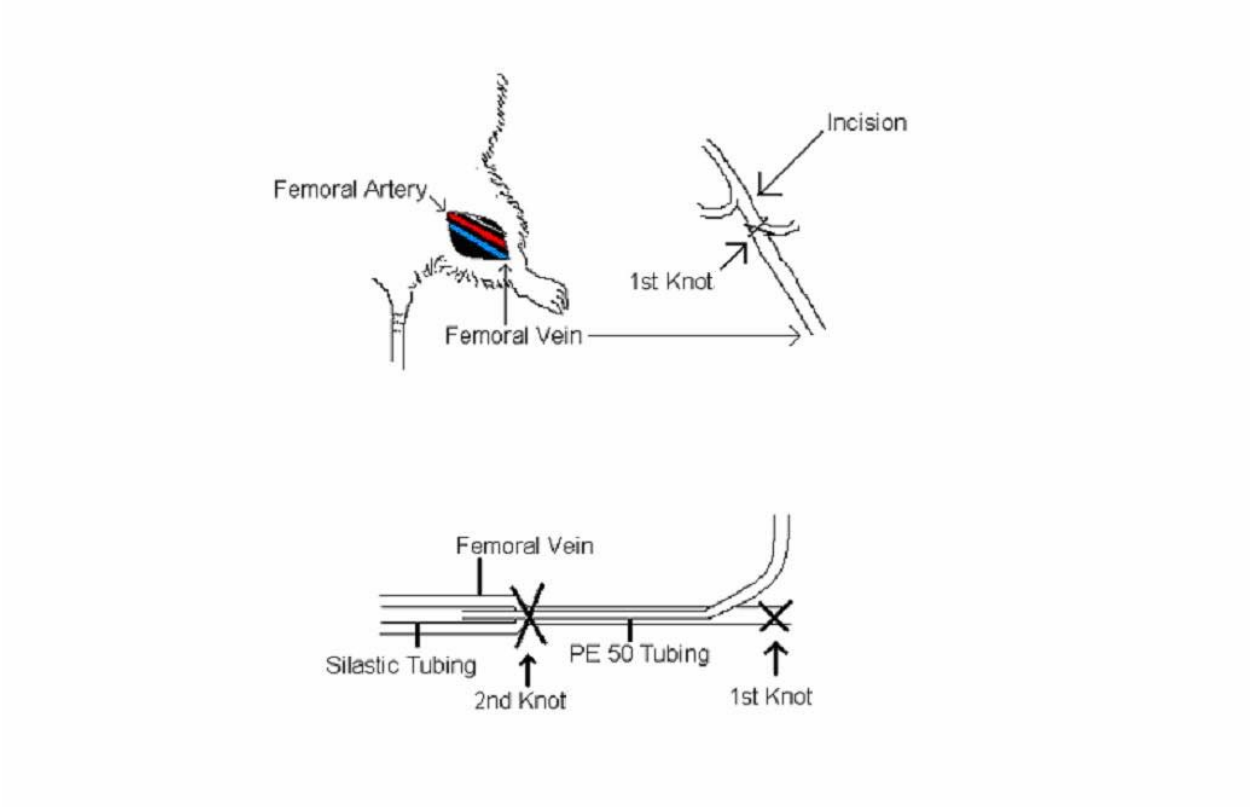

Insertion of the CMA®/20 Probe:

A small incision was made (0.75 inch) in the skin over the pectoral muscle on the left side of the midline. The jugular vein was exposed but not isolated. A needle with a plastic guide (Introducer) was inserted into the pectoral muscle and then into the jugular vein. The needle was removed and a CMA®20 probe was placed in the plastic guide. The probe was sutured to the pectoral muscle and the plastic guide was removed. The CMA®20 inlet and outlet tubes were passed under the skin to the dorsal midline incision with the aid of a trocar. The inlet and outlet tubes were secured to the back of the rat with a skin button. The surgical button was then sutured to the fascia and muscle on the back. All incisions were then sutured.

Insertion of the CMA®/12 Guide Cannula:

An incision was made on the top of the head to expose approximately 3 cm of the skull anterior from bregma. A stereotaxic device was used to locate the frontal cortex (3 mm anterior and 3 mm lateral from bregma), and a small hole was made in the skull using a skull drill. Two screws were placed approximately 2 cm anterior and posterior from the hole. The dura matter was broken with a 25 gauge needle. A CMA®/12 Cannula Guide was then lowered into the brain over 10 minutes. The CMA®/12 Cannula Guide was secured to the skull by placing dental cement over the guide and the two screws.

Postoperative Recovery:

All incision sites, with the exception of the skull, were cleaned with hydrogen peroxide and alcohol. The animal was then placed in a BAS® animal bowl under external heat (heat lamp). The rat was monitored closely until the effects of the anesthesia wore off. The animal was then connected to the BAS® Awake Animal System to prevent the cannula and tubing from twisting.

4. Microdialysis Experiment

Equipment:

FEP Tubing (4 pieces, 0.5 m long) (CMA/Microdialysis, Acton, MA)

1 cc Glass syringe with needle (CMA/Microdialysis, Acton, MA)

Tubing Adapters (6) (CMA/Microdialysis, Acton, MA)

CMA/100 Microinjection Pump (CMA/Microdialysis, Acton, MA)

Insertion of the CMA/12 Probe:

The FEP tubing was connected to the inlet and outlet ports of the microdialysis probes using tubing adapters. A CMA/12® probe was prepared as described by the manufacture. The dummy guide was removed from the CMA/12® guide cannula using forceps. The CMA/12® probe was then inserted into the cannula and sealed with super glue. The CMA/20® probe was prepared as described by the manufacture. Dialysate was perfused through the probes at a rate of 1 μl•min^{-1} using a CMA/100 microinjection pump. The probes were equilibrated for at least 1 hour prior to sampling.

Sampling:

Samples were collected in HPLC Inserts (Sun International, NC) for 45 minutes at a rate of 1 μl•min^{-1}. A 15 μl sample was removed and placed in a 4 mL scintillation vial (Fisher) for retrodialysis. ^{14}C-Amprenavir was analyzed using a Packard Tri-Carb liquid scintillation analyzer (Packard Instrument Co., CT). The remaining sample was used for amprenavir analysis by HPLC.

Retrodialysis

Retrodialysis was used to determine the in vivo recovery of amprenavir. A known concentration of ^{14}C-labeled amprenavir in the microdialysis dialysate was perfused through the probe. The amount of amprenavir recovered from the brain or blood in vivo was determined by the fraction of ^{14}C-labeled amprenavir lost. Fraction loss was determined by the following equation.

$$\%\,\text{Recovery} = \frac{dpm_{before} - dpm_{after}}{dpm_{before}} \bullet 100 \qquad \text{Equation 1}$$

Where dpm_{before} is the disintegration per minute in the dialysate before being perfused through the probe, and dpm_{after} is the disintegration per minute in the dialysate after being perfused through the probe.

The assumption that the fraction of amprenavir lost through the microdialysis probe would be equal to the amount recovered was tested in vitro. A known concentration of amprenavir was placed in the dialysate to determine the fraction loss when perfused through a probe. In vitro recovery was determined by placing a known concentration of amprenavir in a beaker with a probe being perfused with blank dialysate. Recovery was determined by dividing the concentration of amprenavir in the dialysate by the concentration in the beaker. The blood and brain samples were corrected by dividing the concentration of amprenavir in the dialysate by the recovery of the probe. The specific activity of ^{14}C-amprenavir was measured (4.06 pg/dpm), and used to determine the contribution of ^{14}C-amprenavir to the overall mass of amprenavir (radiolabeled and non-radiolabeled amprenavir) in the dialysate. The mass of non-radiolabeled amprenavir was determined by subtracting the ^{14}C-amprenavir mass from the overall mass of amprenavir in the dialysate.

5. HPLC Analysis of Amprenavir

Amprenavir was analyzed using a reverse phase (C18 microbore column, Bioanalytical Systems Inc., IN) microbore HPLC system. A CMA/200 sample injector (CMA/Microdialysis, MA)) with a mobile phase consisting of 60% H_2O and 40% acetonitrile (vol:vol) at a flow rate of 0.1 ml min^{-1} was used. Amprenavir was detected with a fluorescence detector (Bioanalytical Systems Inc., IN) with an excitation and emission wavelength of 244 and 340 nm, respectively. A 10 µl sample was injected onto the column. Amprenavir had a retention time of 6.85 minutes. The limit of detection for amprenavir was 100 ng•ml^{-1}. Intra-day and inter-day assay precisions (% C.V.) were less than 10%. The intra-day and inter-day accuracy were between 90 - 110%. The chromatograms were analyzed with a C-R3A Shimadzu Chromatopac for the peak height of amprenavir (Figure 10).

Figure 10: HPLC Chromatogram of amprenavir in dialysate.

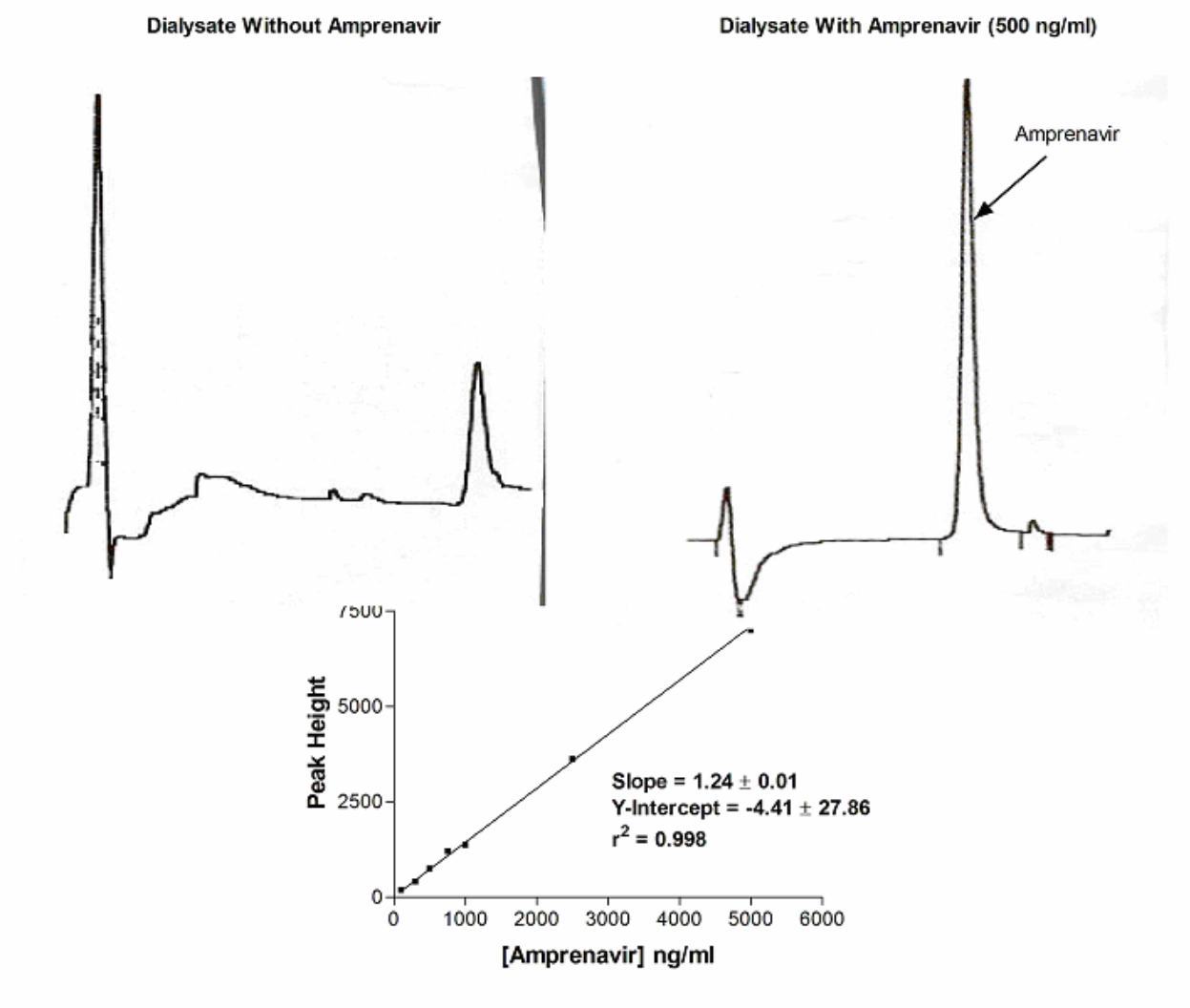

6. Statistical Analysis

The unbound brain to blood ratio (BBR) was calculated by dividing the brain concentration by the plasma concentration. A two-way ANOVA with a Bonferroni post-hoc test was used to examine the effect of time and treatment on the BBR. A p value less than 0.05 was considered statistically significant.

B. Determination of the In Vitro Inhibition Constants of GF120918 and Cyclosporine for Cytochrome P4503A4.

1. Study Design

CYP3A4

Cytochrome P4503A4 Supersomes with P450 reductase and cytochrome b_5 were used to determine the inhibition constants of the MDR modulators GF120918 and cyclosporine. Midazolam (Figure 11) was used as a model substrate of CYP3A4, which is metabolized to 1-OH midazolam (Figure 11). The reaction mixture consisted of a 200 µl solution contain 10 pmol CYP3A4 Supersomes or control insect Supersomes (no CYP3A4), 1.3 mM $NADP^+$, 3.3 mM glucose-6-phosphate, 0.4 $U \bullet ml^{-1}$ glucose-6-phosphate dehydrogenase, and 3.3 mM $MgCl_2$ at 37 ºC. The reaction was initiated with the addition of midazolam at 0, 0.5, 1, 2, 7, 20, 50, 100, or 200 µM and incubated at 37 ºC. For the inhibition studies 2 $\mu g \bullet ml^{-1}$ of GF120918 or 18 $\mu g \bullet ml^{-1}$ of cyclosporine was added using DMSO as a solubilizing agent (0.5% vol. DMSO, control samples also contained 0.5% DMSO). The reaction was stopped with the addition of 200 µl of ice cold methanol. The sample was vortexed for 5 minutes followed by centrifugation at 1800 g with an IEC clinical centrifuge for 5 minutes. A 300 µl aliquot was taken and dried down under nitrogen at 37 ºC. The sample was resuspended in 100 µl of HPLC mobile phase and analyzed by HPLC for 1-OH midazolam.

CYP3A2 and Rat Liver Microsomes

CYP3A2 Supersomes were treated identically to the CYP3A4 Supersomes, with the exception that the concentrations of midazolam were between 0 to 1 mM. Rat liver microsomes were treated the same as the Supersomes with the exception that 0.2 mg of total protein was used.

2. HPLC Analysis of Midazolam

Samples were analyzed by a previously reported HPLC method (Ma and Lau, 1996). A LC-10ADvp Shimadzu LC pump, SCL-10Avp system controller, SIL-10ADvp auto injector, and a SPD-10Avp UV-VIS detector were used to analyze 1-OH midazolam. The mobile phase

consisted of methanol:acetonitrile:14.9 mM sodium acetate at pH 3 (10:23:67, vol:vol:vol). A reverse phase SUPELCOSIL ABZ+ Plus column (25 cm X 4.6 mm, 5 µm) was used to separate 1-OH midazolam. A 50 µl sample was injected onto the column at a flow rate of 1 ml•min^{-1} and was analyzed by ultraviolet detection (U.V.) at 230 nm. The recovery of midazolam was 85%. Midazolam had a retention time of 6.12 minutes and was analyzed by Class-VP v5.03 software (Shimadzu Corporation, Columbia, MD) for peak height.

3. Statistical Analysis

The apparent inhibitory constant (Ki) was determined using simultaneous nonlinear regression. Cyclosporine has been shown to be a competitive inhibitor of CYP3A4 (Wandel et al., 1999) and therefore the formation rate of 1-OH midazolam versus substrate concentration was modeled assuming competitive inhibition (Equation 2). GF120918 did not show any inhibition of CYP3A4 at a concentration of 0.12 µg•ml^{-1} (Cummins et al., 2002) and therefore 2 µg•ml^{-1} of GF120918 was used for these studies. The 95% confidence intervals for the Km and Vmax of midazolam in the presence and absence of GF120918 were estimated using nonlinear regression assuming one binding site (GraphPad Prism 3.03, San Diego, CA). The Michaelis-Menten parameters were compared in order to determine what type of inhibition (i.e. competitive, non-competitive, uncompetitive), if any, occurs in the presence of GF120918. Simultaneous fitting of the data WinNonlin 4.0 (Pharsight Corp., San Francisco, CA) was used to estimate the inhibitory constant for cyclosporine.

$$\text{Formation rate of 1-OH Midazolam} = \frac{[\text{Midazolam}] \bullet \text{Vmax}}{[\text{Midazolam}] + \text{Km}\left(1 + \frac{[\text{Inhibitor}]}{\text{Ki}}\right)} \qquad \text{Equation 2}$$

Figure 11: Structure of midazolam, 1'-hydroxy midazolam, and 4-hydroxy midazolam.

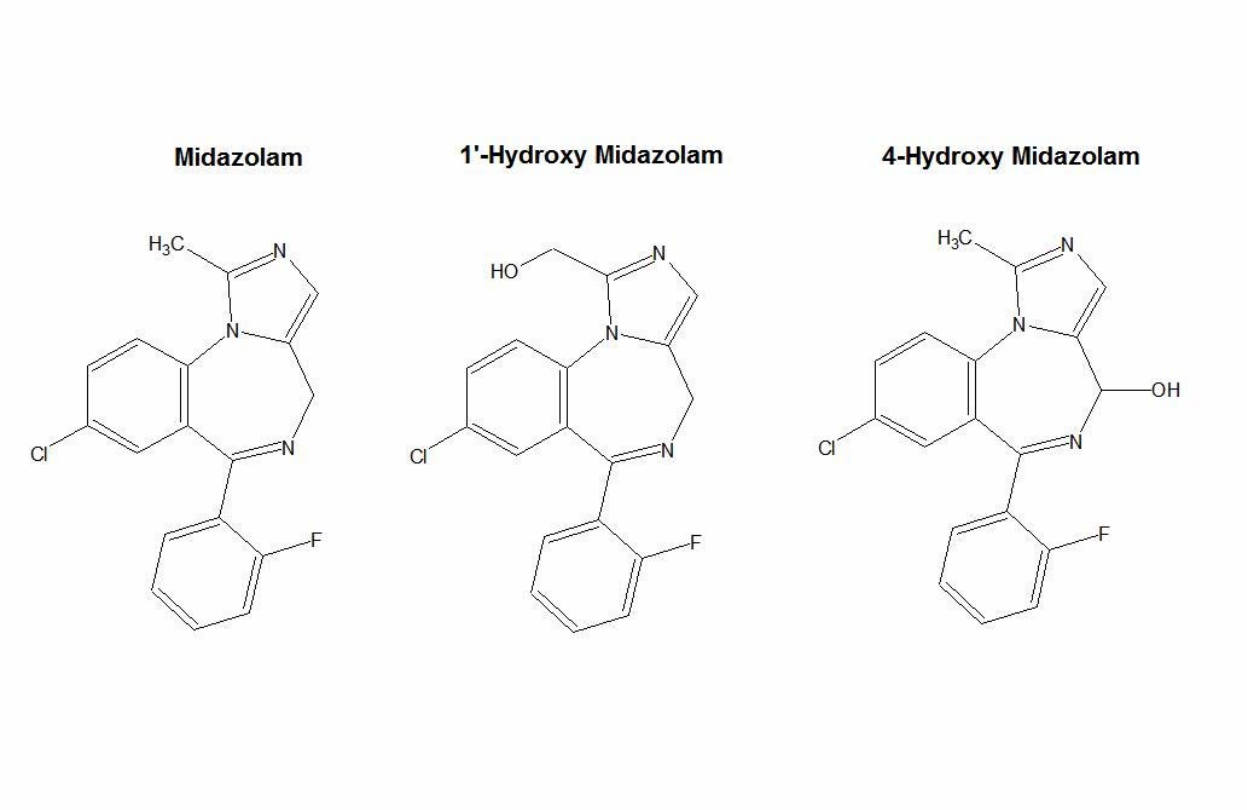

C. Determination of the In Vitro Inhibition Constants of GF120918 and Cyclosporine for P-gp.

1. MDR1 Transfected LLC-PK1 Cells

MDR1 transfected LLC-PK1 cells were used to determine the P-gp-dependent flux of doxorubicin, a model P-gp substrate. Both LLC-PK1 and LLC-MDR1 cells were cultured in M-199 medium containing L-glutamine, streptomycin (0.1 $\mu g \cdot ml^{-1}$), penicillin (0.1 $U \cdot ml^{-1}$), and 5% FBS at 37 ºC with 5% CO_2 in Costar triangle flasks (Fisher Scientific). For the transport studies cells were seeded onto polycarbonate Snapwells (12 mm diameter, 0.4 um, Corning Costar Corp., Cambridge, MA) at a density of 1.2×10^5 $cells \cdot cm^2$. The cells were cultured for 5 to 7 days with the medium being replaced after 3 days. Cell monolayer confluence was determined by the transepithelial electrical resistance using a Millicell meter (Millipore Corp., Cambridge,

MA). The monolayer was considered confluent when the TEER value was greater than 130 $\Omega \cdot cm^2$, as previously reported in the literature (van der Sandt et al., 2000).

After the cells reached confluence, the Snapwells were placed in a side by side diffusion chamber system (Navicyte, Inc., San Diego, CA). The diffusion chambers were incubated at 37 ºC by a RTE-110 recirculating water bath (Neslab Instruments, Portsmouth, NH). Five ml of medium was added to the apical compartment and 5 ml of medium containing 0, 10, 20, 40, 100, or 200 μM of doxorubicin was added to the basolateral compartment. For the inhibition studies, 0.2 $\mu g \cdot ml^{-1}$ of GF120918 or 18 $\mu g \cdot ml^{-1}$ of cyclosporine was added to the media in the apical and basolateral compartments using DMSO as a solubilizing agent (0.5% vol. of DMSO, controls also contained 0.5% DMSO). The transport study was stopped by removing the media in the two compartments. The P-gp-dependent flux of doxorubicin was determined by subtracting the transport of doxorubicin from the basolateral to apical compartment in the LLC-PK1 cells from the LLC-MDR1 cells.

2. HPLC Analysis of Doxorubicin

The concentration of doxorubicin in the medium samples was analyzed by a previously reported HPLC method (Fogli et al., 1999). A LC-10ADvp Shimadzu LC pump, SCL-10Avp system controller, SIL-10ADvp auto injector, and a RF-10Axl fluorescence detector were used to analyze doxorubicin. The mobile phase consisted of 50 mM monobasic sodium phosphate at pH 4.0 and acetonitrile (65:35, vol:vol). A reverse phase SUPELCOSIL ABZ+ Plus column (25 cm X 4.6 mm, 5 μm) was used to separate doxorubicin. A 100 μl sample from the medium was vortexed with 500 μl of acetonitrile for 5 minutes. The sample was then centrifuged at 1800 g for 5 minutes using an IEC clinical centrifuge. The supernatant was decanted and dried down under nitrogen at 37 ºC. The sample was then resuspended in 100 μl of mobile phase and a 50 μl sample was injected onto the HPLC system. The recovery of doxorubicin was 81%. Doxorubicin had a retention time of 14.3 minutes and was analyzed by Class-VP v5.03 software (Shimadzu Corporation, Columbia, MD) for the peak height of doxorubicin (Figure 12).

3. Statistical Analysis

GF120918 and cyclosporine have been shown to be competitive inhibitors of P-gp (Bohme et al., 1993; Wallstab et al., 1999), and therefore the P-gp-dependent flux of doxorubicin versus substrate concentration was modeled assuming competitive inhibition. The apparent inhibitory constants of GF120918 and cyclosporine were estimated using simultaneous nonlinear regression with WinNonlin 4.0 (Pharsight Corp., San Francisco, CA).

Figure 12: HPLC chromatogram of doxorubicin in cell media.

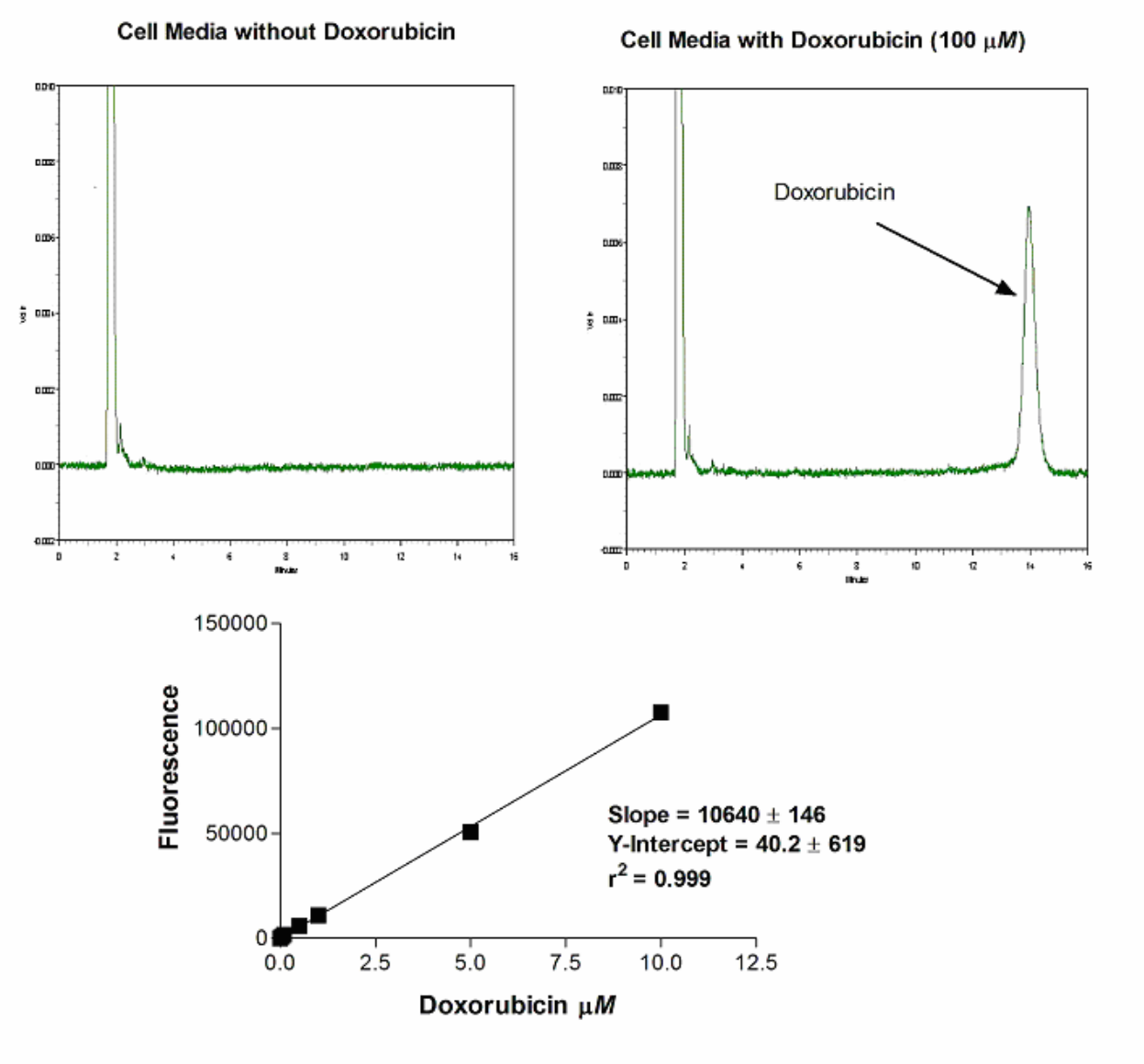

D. Inhibition of P-gp at the BBB by GF120918 and Cyclosporine.

1. Study Design

Nelfinavir was used as a model substrate for P-gp. The effect of P-gp modulation by GF120918 and cyclosporine was determined by measuring the CNS distribution of nelfinavir. The concentrations of GF120918 and cyclosporine were determined and compared to the in vitro results for inhibition of P-gp (Chapter IV.C).

The systemic clearance and terminal half-life of nelfinavir were determined by giving 3 rats an intravenous bolus dose of nelfinavir (12 $mg \bullet kg^{-1}$ in 0.1 ml of DMSO). Both femoral and jugular veins were cannulated for drug delivery and plasma sampling, respectively. Plasma samples were taken at 0, 1, 5, 10, 20, 30, 40 minutes and 1, 1.7, 2.3, 3, 3.7, 4.3, and 5 hours for the analysis of nelfinavir. The results from these studies were used to determine the rate and duration of nelfinavir's infusion needed to produce steady-state plasma concentrations. In order to determine the blood concentration time-profile of cyclosporine, 3 rats were given an i.v. bolus dose of cyclosporine (20 $mg^{-1} \bullet kg^{-1}$, in DMSO). Both femoral and jugular veins were cannulated for drug delivery and blood sampling, respectively. Blood samples were collected at 5 minutes, 1, 2, 3, and 4 hours after the i.v. bolus dose. The plasma concentration time-profile of GF120918 was determined by giving an i.v. bolus dose of GF120918 (10 $mg^{-1} \bullet kg^{-1}$, in DMSO). Plasma samples were collected at 5, 10, 30 minutes, and 1, 2, 3, 4, and 5 hours after the i.v. bolus dose.

For the CNS distribution studies, the femoral and jugular veins of 15 rats were cannulated for drug delivery and blood/plasma sampling, respectively. Approximately 24 hours after the surgery 5 rats were given either an i.v. dose of DMSO (0.1 ml), GF120918 (10 $mg \bullet kg^{-1}$), or cyclosporine (20 $mg \bullet kg^{-1}$). Five minutes after the dose of the MDR modulator or DMSO, a constant infusion of nelfinavir (2.7 $mg \bullet hr^{-1}$, 1.5 $ml \bullet min^{-1}$ H_2O pH =2) was given for 4 hours. Plasma samples were taken at 0, 0.5, 1, 2, 3, and 4 hours after the start of the infusion for the analysis of nelfinavir. Two additional blood or plasma samples were taken at 0.5 and 4 hours for the analysis of cyclosporine or GF120918, respectively. After the 4 hour blood/plasma sample, the animal was decapitated. The top part of the skull was removed and the brain was excised and immediately frozen.

2. Animals

Fifteen adult male Sprague-Dawley rats (250 - 350 g) were used in all experiments. Animals were purchased from Harlan laboratories (Indianapolis, IN). Animals were maintained under a 12:12-hr light/dark cycle and had access to food and water ad lib prior and during the experiments.

3. Surgery

Cannulation of Femoral and Jugular Veins:

The surgery for the cannulation of the femoral vein is described in section Chapter IV.A.3. For the cannulation of the jugular vein, an incision into the skin above the jugular vein was made. The jugular vein was cannulated in the same way the femoral vein was cannulated. The cannula was then passed under the skin with the aid of a trocar, to the dorsal midline incision. The cannula was secured to the back of the rat with a skin button.

4. HPLC Analysis of Nelfinavir, GF120918, and Cyclosporine

The concentrations of nelfinavir in plasma and brain samples were analyzed with an HPLC method. A LC-10ADvp Shimadzu LC pump, SCL-10Avp system controller, SIL-10ADvp auto injector, and a SPD-10Avp UV-VIS detector (254 nm) were used to analyze nelfinavir. The mobile phase consisted of acetonitrile and 200 mM acetate buffer (48:52, vol:vol) with a flow rate of 1.5 ml•min^{-1}. A reverse phase SUPELCOSIL ABZ+ Plus column (25 cm X 4.6 mm, 5 µm) at 37 ºC was used to separate nelfinavir. A 100 µl plasma sample was vortexed with 500 µl of acetonitrile for 5 minutes. The sample was then centrifuged at 1800 g for 5 minutes using an IEC clinical centrifuge. The supernatant was decanted and dried down under nitrogen at 37 ºC. The sample was resuspended in 100 µl of mobile phase and a 50 µl sample was injected onto the HPLC system. Nelfinavir had a retention time of 14.5 minutes. The recovery of nelfinavir from plasma was 86%. The limit of detection of nelfinavir was 50 ng•ml^{-1}. The chromatograms were analyzed by Class-VP v5.03 software (Shimadzu) for the peak height of nelfinavir (Figure 13a).

For the analysis of nelfinavir in the brain, a 1 gram brain sample was homogenized in 2.5 ml of phosphate buffered saline at pH 7.4 with a Tissumizer (TeKmar, OH). Acetonitrile (12.5 ml) was added to the homogenate and vortexed for 10 minutes. The sample was centrifuged at 400 g for 10 minutes and the supernatant was decanted and dried down under nitrogen at 37 ºC. The sample was resuspended in 1 ml of mobile phase and passed through an Acrodisc CR13 mm syringe filter (Gelman Laboratory). The solution was dried down under nitrogen at 37 ºC, and then resuspended in 100 µl of mobile phase. A 50 µl sample was injected onto the HPLC system. The recovery of nelfinavir from brain homogenates was 86%. The chromatograms were analyzed by Class-VP v5.03 software (Shimadzu) for the peak height of nelfinavir (Figure 13b).

GF120918 plasma samples were analyzed with a previously reported HPLC method (Kemper et al., 2001). A LC-10ADvp Shimadzu LC pump, SCL-10Avp system controller, SIL-10ADvp auto injector, and a RF-10Axl fluorescence detector (excitation wavelength = 260 nm, emission wavelength = 460 nm) were used to analyze GF120918. The mobile phase consisted of acetonitrile and 50 mM sodium acetate buffer at pH 4.2 (35:65, vol:vol) with a flow rate of 1 $ml \bullet min^{-1}$. A reverse phase SUPELCOSIL ABZ+ Plus column (25 cm X 4.6 mm, 5 µm) was used to separate GF120918. A 100 µl plasma sample was vortexed with 500 µl of acetonitrile for 5 minutes. The supernatant was decanted and dried down under nitrogen at 37 ºC. The sample was resuspended in 100 µl of mobile phase and a 50 µl sample was injected onto the HPLC system. GF120918 had a retention time of 5.3 minutes. The recovery of GF120918 from plasma was 84%. The limit of detection of GF120918 was determined to be 25 nM. The chromatograms were analyzed by Class-VP v5.03 software (Shimadzu Corporation, Columbia, MD) for the peak height of GF120918 (Figure 14).

Cyclosporine blood samples were analyzed with HPLC by the lab of Dr. Jimmi Hatton (University of Kentucky). A LC-10AD auto injector, SCL-10AD system controller, SIL-10AD autoinjector, and a SPD-10Avp UV-VIS detector (214 nm) were used to analyze cyclosporine. The mobile phase consisted of acetonitrile, water, and methanol (51:31:18, vol:vol:vol) with a flow rate of 1 $ml \bullet min^{-1}$. A Supelcosil™ LC-18 column (5 cm X 4.6 mm ID, 3µm) at 80 ºC was used to separate cyclosporine. A 100 µl blood sample was vortexed with 3 ml of 182 mM zinc sulfate, methanol, and acetonitrile (47:32:21, vol:vol:vol) containing 50 µg of cyclosporine D (internal standard) for 45 seconds, followed by centrifugation for 5 minutes. The supernatant was decanted and added to a solid phase extraction column. Acetonitrile and water (8 ml, 50:50,

vol:vol) was added to the solid phase extraction column. Ethyl acetate (2 ml) was used to elute cyclosporine from the column. The eluted solution was dried under air at 60 ºC. The sample was reconstituted in acetonitrile, water, methanol (51:31:18, vol:vol:vol) and vortexed for 1 minute. Heptane (1 ml) was added to the sample and centrifuged for 3 minutes. The bottom layer was removed and a 50 µl sample was injected onto the HPLC system. The chromatograms were analyzed by Class-VP v5.03 software (Shimadzu Corporation, Columbia, MD) for peak area.

Figure 13: Chromatogram of nelfinavir in plasma and brain.

a.

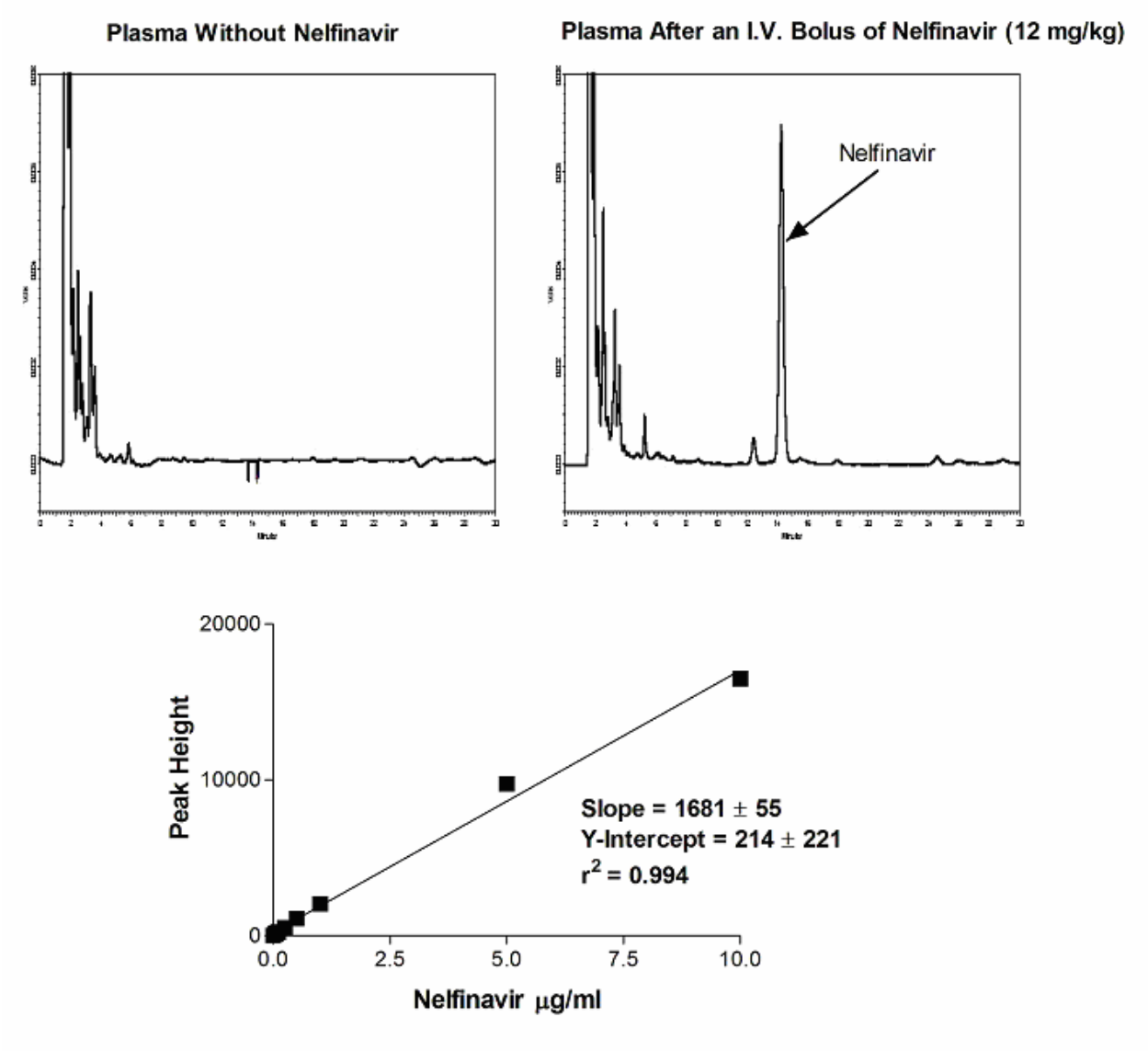

Figure 13: (Continued)

b. Brain

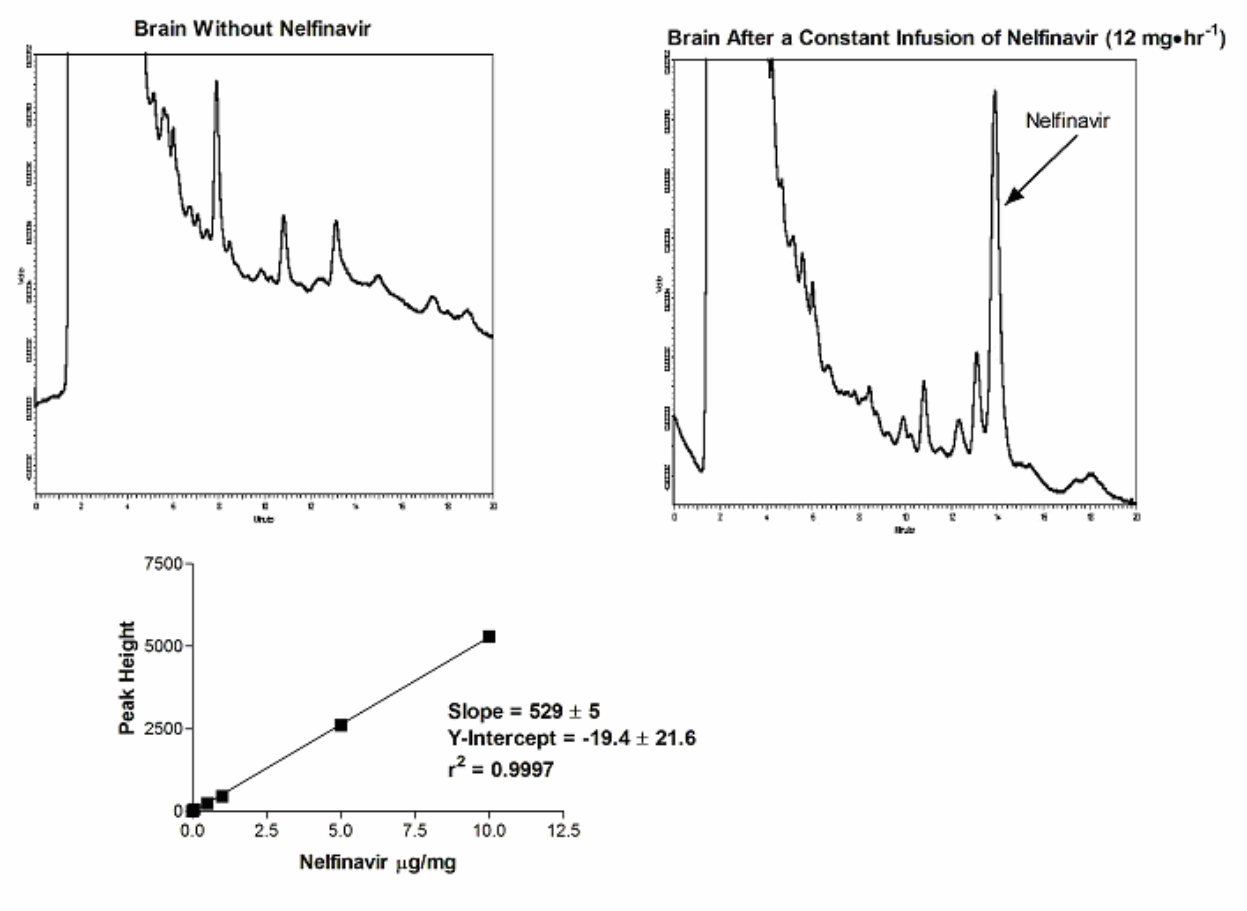

Figure 14: Chromatogram of GF120918 in plasma.

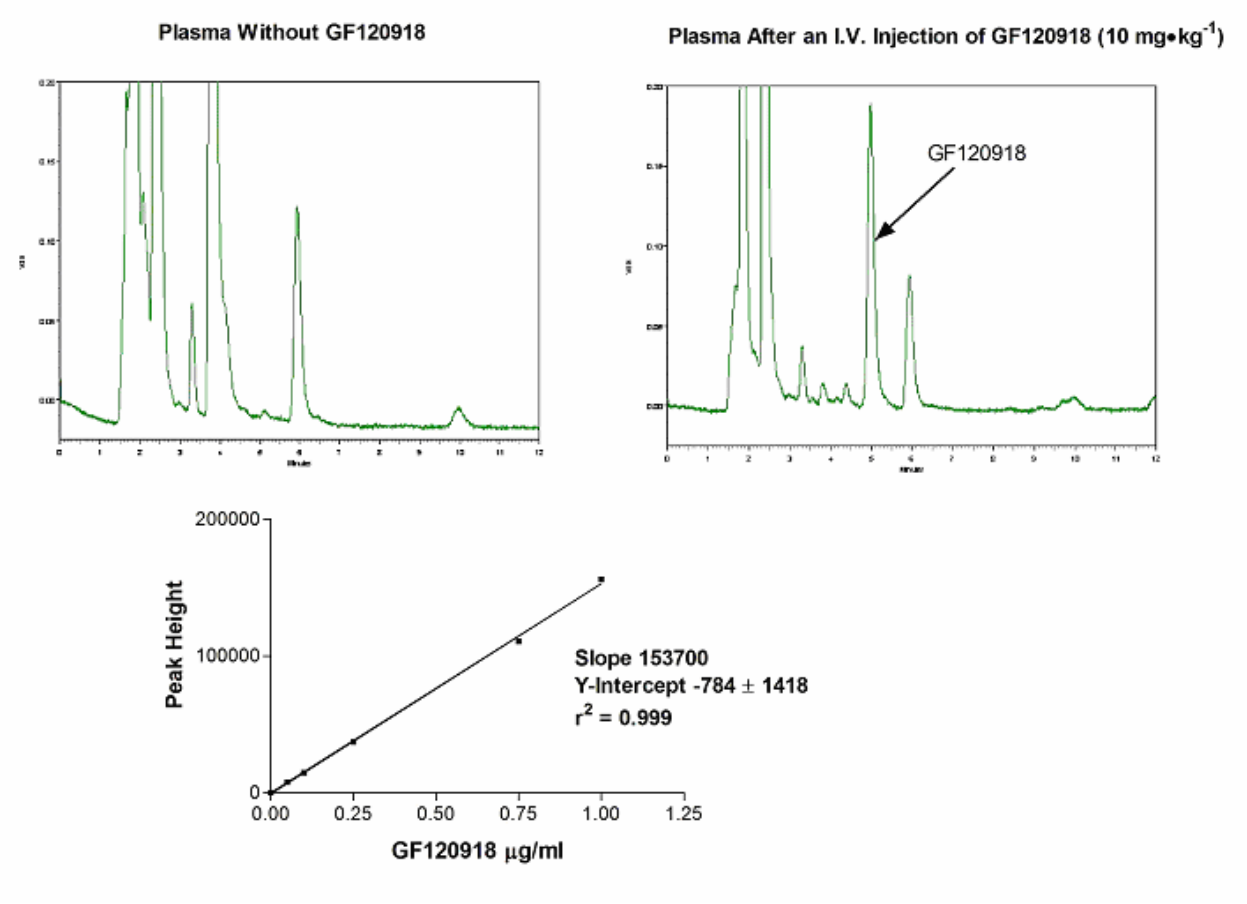

5. Statistical Analysis

A one-way ANOVA was used to determine if the concentration of nelfinavir at the 4th hour of the infusion, were different between the 3 groups (control, GF120918, and cyclosporine). The brain to plasma ratio of nelfinavir was used to determine the extent of nelfinavir distribution into the CNS. The brain to plasma ratios were compared using a one-way ANOVA (nonparametric) and a Tukey's post-hoc test. A p value less than 0.05 was considered statistically significant.

E. In Vivo Studies with Midazolam

1. Study Design

Midazolam was used as a model CYP3A substrate to determine the effects of GF120918 and cyclosporine on hepatic metabolism. Jugular and femoral cannulas were placed in 15 rats for drug delivery and blood/plasma sampling. Approximately 24 hours after the surgery 5 rats were given either an i.v. dose of DMSO (0.1 ml), GF120918 (10 mg•kg^{-1}), or cyclosporine (20 mg•kg^{-1}) in DMSO (0.1 ml). Five minutes after the injection of the MDR modulator or DMSO an oral gavage of midazolam (15 mg•kg^{-1}) was given. Plasma samples were taken at 0, 5, 10, 20, and 30 minutes and at 1, 1.5, 2, 3, 4, and 5 hours. Two additional blood or plasma samples were taken at 0.5 and 4 hours for the analysis of cyclosporine or GF120918, respectively.

2. Animals

Fifteen Adult male Sprague-Dawley rats (250 - 350 g) were used in all experiments. Animals were purchased from Harlan laboratories (Indianapolis, IN). Animals were maintained under a 12:12-hr light/dark cycle and had access to food and water ad lib prior and during the experiments.

3. Surgery

Cannulas were placed in the femoral and jugular vein as described in Chapter IV.D.3.

4. HPLC Analysis of Midazolam, GF120918, and Cyclosporine

The concentration of midazolam in plasma was analyzed by a previously reported HPLC method (Ma and Lau, 1996) and is described in Chapter IV.B.5. A 100 µl plasma sample was vortexed with 500 µl of acetonitrile for 5 minutes. The sample was then centrifuged for 5 minutes at 1800 g using an IEC clinical centrifuge. The supernatant was decanted and dried down under nitrogen at 37 ºC. The sample was resuspended in 100 µl of mobile phase and a 50 µl sample was injected onto the HPLC system (Figure 15). Midazolam had an extraction efficiency of 88%. GF120918 and cyclosporine samples were analyzed by HPLC as described in Chapter IV.D.4.

Figure 15: Chromatogram of midazolam before and after an oral gavage of midazolam•HCl (15 mg•kg^{-1}).

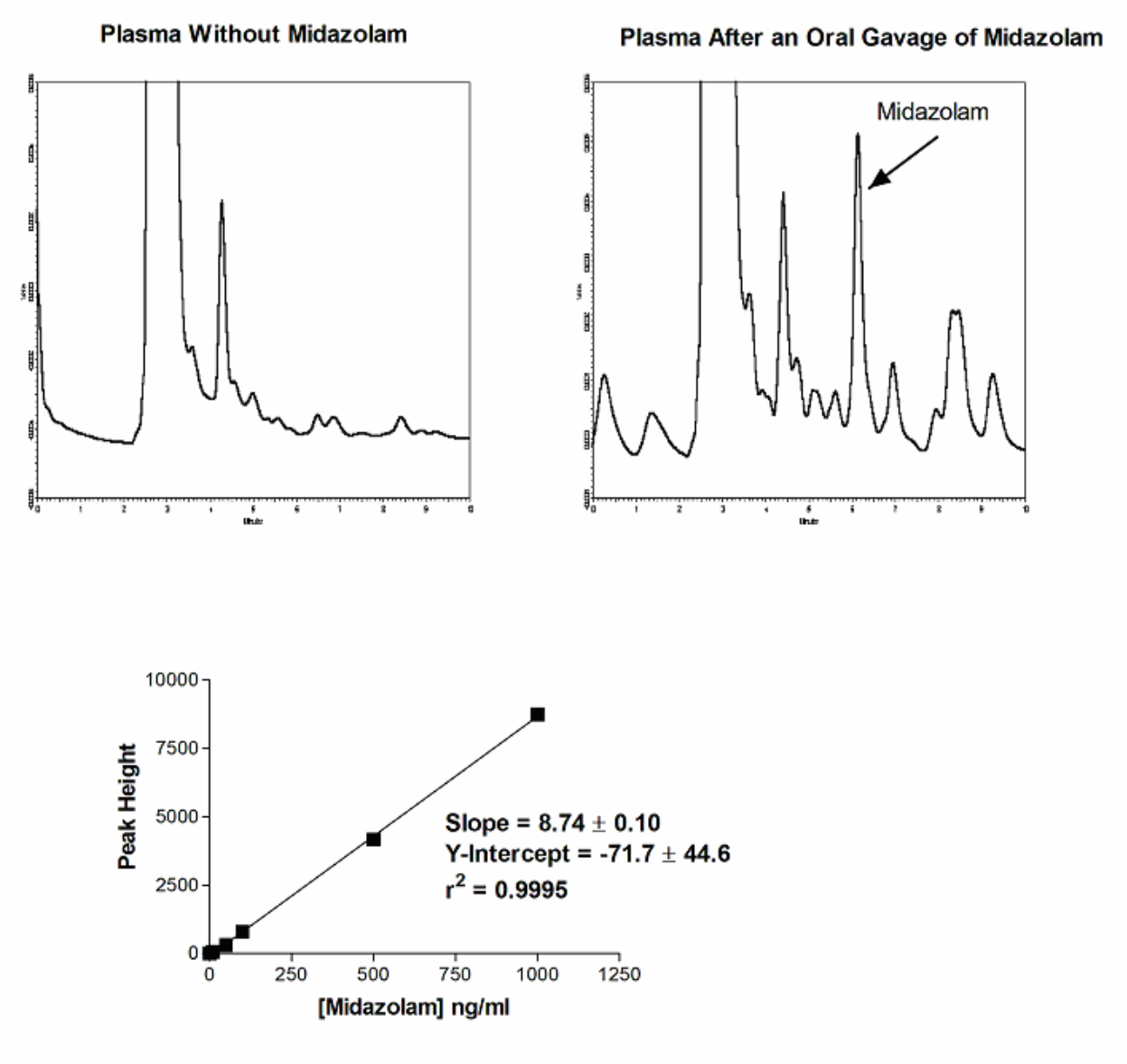

5. Statistical Analysis

The oral clearance of midazolam was determined using noncompartmental pharmacokinetic analysis by WinNonlin 4.0 (Pharsight, CA). The area under the curve (AUC) was determined using the linear trapezoidal method. The terminal half-life was estimated using the last 4 data points and was used to extrapolate the terminal AUC. Oral clearance was calculated by taking the dose of midazolam and dividing it by the AUC. A one-way ANOVA (nonparametric) and a Tukey's post-hoc test were used to determine if there was a significant difference between the 3 groups. A p value of less than 0.05 was considered statistically significant.

F. The mRNA Expression of Mdr1a and Mrp1 at the BBB

1. Study Design

Male rat brains were homogenized and the capillary endothelial cells were isolated using the capillary depletion method (Triguero et al., 1990). In this method (for details see below), brain capillary endothelial cells are isolated using density centrifugation. Two fractions are created, a capillary enriched fraction and a capillary depleted fraction. The mRNA from the capillary enriched fraction, capillary depleted fraction, and whole brain homogenates were collected and reverse transcribed to cDNA. PECAM and GFAP were amplified by PCR and were used as a marker of endothelial cell and glial cell expression, respectively. The mRNA expression of mdr1a and mrp1 was also determined in the capillary enriched fraction, capillary depleted fraction, and whole brain homogenates to determine their localization (i.e. at the BBB or in the parenchyma) in the CNS.

The mRNA expression of β-actin, PECAM, GFAP, mdr1a, and mrp1 was initially determined using qualitative PCR, however, it became necessary to use quantitative PCR to measure the relative expression of the 5 genes. In addition, a small aliquot from the capillary enriched fraction, capillary depleted fraction, and whole brain homogenate was used to determine the activity of γ-glutamyl transferase, a marker of the BBB.

2. Isolation of Brain Capillary Endothelial Cells

Brain capillary endothelial cells were isolated using the capillary depletion method (Triguero et al., 1990). Male Sprague-Dawley rat brains were ordered from Pel-Freez Biologicals (Rogers, AK). A 0.5 gram brain sample was homogenized with 3.5 ml of physiologic buffer containing 10 mM HEPES, 141 mM NaCl, 4 mM KCl, 2.8 mM $CaCl_2$, 1 mM $MgSO_4$, 1 mM NaH_2PO_4, and 10 mM D-glucose (pH 7.4) with a Dounce glass homogenizer. Dextran (26%, 4 ml) was mixed with the brain homogenate and centrifuged at 5400 g for 15 minutes at 4 ºC. Two layers were formed after centrifugation, a top layer (depleted of endothelial cells) and a bottom layer (enriched with endothelial cells).

3. γ-Glutamyl Transferase

An aliquot from the capillary depleted and enriched fraction, and the whole brain homogenate was used to determine the activity of γ-glutamyl transferase. The activity was determined using the procedure outlined by the manufacture (Sigma Diagnostic, Procedure No. 545). A 20 µl sample from the capillary depleted fraction, capillary enriched fraction, and whole brain homogenates was incubated with 2.3 µmol γ-glutamyl-p-nitroanilide and 50 µmol of glycylglycine at 37 ºC for 20 minutes. The reaction was stopped with the addition of acetic acid (2 ml). Sodium nitrite (1 mg) was added and the solution was incubated for 3 minutes at room temperature. Ammonium sulfamate (1 mg) was added and the solution was incubated at room temperature for 3 minutes. Finally 0.523 mg of naphthylethylenediamine was added. The solution was transferred to a cuvette and the absorption was measured by a Shimadzu UV-2501 PV spectrophotometer at 550 nm.

4. Reverse Transcription and PCR Methods

RNA samples were reverse transcribed (RT) using Superscript First-Strand Synthesis System for RT-PCR (Invitrogen, Carlsbad, CA). One to 5 µg of total RNA was placed into a PCR tube containing 1 mM dNTP and 50 ng of oligo (dT). The sample was incubated at 65 ºC for 5 minutes and allowed to cool on ice. RT buffer, $MgCl_2$ (5 mM), DTT (0.01 M),

RNaseOUT, and SuperScript II RT were added to the PCR tube. The sample was incubated at 42 ºC for 50 minutes followed by 70 ºC for 15 minutes. The sample was placed on ice before RNase H was added and incubated at 37 ºC for 20 minutes.

For qualitative PCR, the samples contained 1 µg of cDNA, 1X PCR buffer, 1.5 mM $MgCl_2$, 0.2 mM dNTP mix, 0.2 µM sense primer, 0.2 uM antisense primer, and 0.04 units/µl of *taq* DNA polymerase. PCR amplification contained three steps for each cycle. In the first step, the sample was incubated at 94 ºC for 1 minute. In the second step, the sample was incubated at 62 ºC for 1 minute to allow the primers to anneal to the cDNA. In the final step, the sample was incubated at 72 ºC for 1 minute for amplification. The PCR samples were amplified between 25 to 50 cycles using a Peltier Thermal Cycler (DNA engine). PCR samples were run on 1.5% agarose gels with ethidium bromide and analyzed by U.V. radiation.

For quantitative PCR, cDNA samples were amplified using the SYBR Green PCR Core Reagent system (Applied Biosystems, Foster City, CA). The PCR samples contained approximately 1µg of cDNA, 1X SYBR green, 3 mM $MgCl_2$, 1.25 mM dNTP mix, 0.01 µM fluorescein, 0.5 µM sense and antisense primers, and 2.5 units/µl of Taq polymerase. The samples were incubated at 94 ºC for 4 minutes before PCR amplification was initiated. There were 3 steps for each cycle. In the first step the sample was incubated at 94 ºC for 1 minute. In the second step the sample was incubated at 64 ºC for 1 minute, and finally in the third step the sample was incubated at 72 ºC for 1 minute. The PCR samples were amplified up to 50 cycles using the iCycler Real-Time PCR Detection System (Bio-Rad Laboratories, Hercules, CA). Intercalated SYBR green was measured by fluorescence with an excitation wavelength of 490 nm and an emission wavelength of 515 nm during the elongation step (72 ºC for 1 minute). PCR products were run on a 1.5% agarose gels with ethidium bromide and analyzed with a Chemi-Imager 4000 (Alpha Innotech Corporation, San Leandro, CA).

5. Primers for Qualitative PCR

PCR primers were designed with Vector NTI 7.1 (Infomax Inc., Frederick, Maryland), using the mRNA sequence.

a. β-Actin (Serazin-Leroy et al., 1998) (Gene Bank No. V01217, Product Size 763bp)

Sense Primer: GAT CTT GAT CTT CAT GGT GCT AGG

Antisense Primer: TTG TAA CAA ACT GGG ACG ATA TGG

b. PECAM (Gene Bank No. U77697, Product 334-695 (361 b.p.))

Sense: TGC GAA ATG CTC TCC AAA CC

Antisense: CAG AGC ACC GAA GCA CCA TT

c. GFAP (Gene Bank No. NM_017009, Product size 54-609 (555 b.p.))

Sense: GCC GCT CCT ATG CCT CCT CCG A

Anti-sense: ATC TCC TCC TCC AGC GAC TCA

d. Mdr1a (Decleves et al., 2000) (Gene Bank No. S66618, Product Size 440 b.p.)

Sense: CCC GTC TTG ATC ATG TGG CC

Anti-sense: GGA CAG AAA CAG AGG ATC GC

e. Mrp1 (Decleves et al., 2000) (Gene Bank No. X96394, Product Size 394)

Sense: AGG CTC TGG CTT GGC TCT AT

Anti-sense: CTG GCT TGG TGT GAA CTG AT

6. Quantitative PCR

a. β-Actin (Gene Bank No. V01217, Product Size 2574-3040 (255 b.p. without intron)

Sense: TCT CTT CCA GCC TC CTT CC
Antisense: ATA GAG CCA CCA ATC CAC AC

b. PECAM (Gene Bank No. U77697, Product Size 80-257 (177 b.p.))
Sense: ACA TAA CAG AGC TGT TTC CCA GGC
Antisense: TCT CCT CGG CAA TCT TGC TGA A

c. GFAP (Gene Bank No. NM_017009, Product Size 234-420 (186 b.p.))

Sense: TGT TGG TAG TAA GCT GGT CCA G
Anti-sense: AGA TGA TGG AGC TCA ATG ACC G

d. Mdr1a (Gene Bank No. AF286167, Product Size 5-120 (115 b.p.))

Sense: AGC TCG AAG AAG ACC TTA ACG G
Antisense: CGA AAC ATT GTG AGC ACA CTG ACC

e. Mrp1 (Decleves et al., 2000) (Gene Bank No. X96394, Product Size 394)

Sense: AGG CTC TGG CTT GGC TCT AT
Antisense: CTG GCT TGG TGT GAA CTG AT

G. The Distribution of Nelfinavir into Rat Milk and the CNS

1. Study Design

A cross-over design was used to determine the distribution of nelfinavir into milk. Jugular and femoral cannulas were placed in 8 rats for drug delivery and plasma sampling. Approximately 24 hours after the surgery, the pups were removed from the mother to allow milk accumulation in the mammary ducts. A constant infusion of nelfinavir (2.7 $mg \bullet hr^{-1}$, 1.5 $ml \bullet min^{-1}$ H_2O pH =2) was given. At the 6^{th} hour of the infusion either DMSO (0.1 ml) or GF120918 (10 $mg \bullet kg^{-1}$) in DMSO (0.1 ml) was given. Plasma samples were taken at 0, 1, 3, 5, 6, 7, and 8 hours. The milk was collected after the 8^{th} hour plasma sample. After a 24 hour washout period the animals were given a second constant infusion of nelfinavir (2.7 $mg \bullet kg^{-1}$). The rat was given the opposite treatment from the previous day (either DMSO or GF120918) at the 6^{th} hour. Plasma samples were taken at 0, 1, 3, 5, 6, 7, and 8 hours. The milk was collected after the 8^{th} hour plasma sample was taken. Brain and mammary tissue were excised for nelfinavir analysis (brain only) and protein expression of P-gp (brain and mammary tissue).

2. Animals

Eight adult female lactating Sprague-Dawley rats with pups (250 - 350 g) were used in all experiments. Animals were purchased from Harlan laboratories (Indianapolis, IN). Animals were maintained under a 12:12-hr light/dark cycle and had access to food and water ad lib prior and during the experiments.

3. Surgery

Cannulas were placed in the femoral and jugular vein as described in Chapter IV.D.3.

4. HPLC Analysis of Nelfinavir

The plasma and brain concentrations of nelfinavir were determined using the HPLC method described in Chapter IV.D.5. The milk samples were treated and analyzed identically to that of the plasma samples (Figure 16).

Figure 16: Chromatogram of nelfinavir in milk.

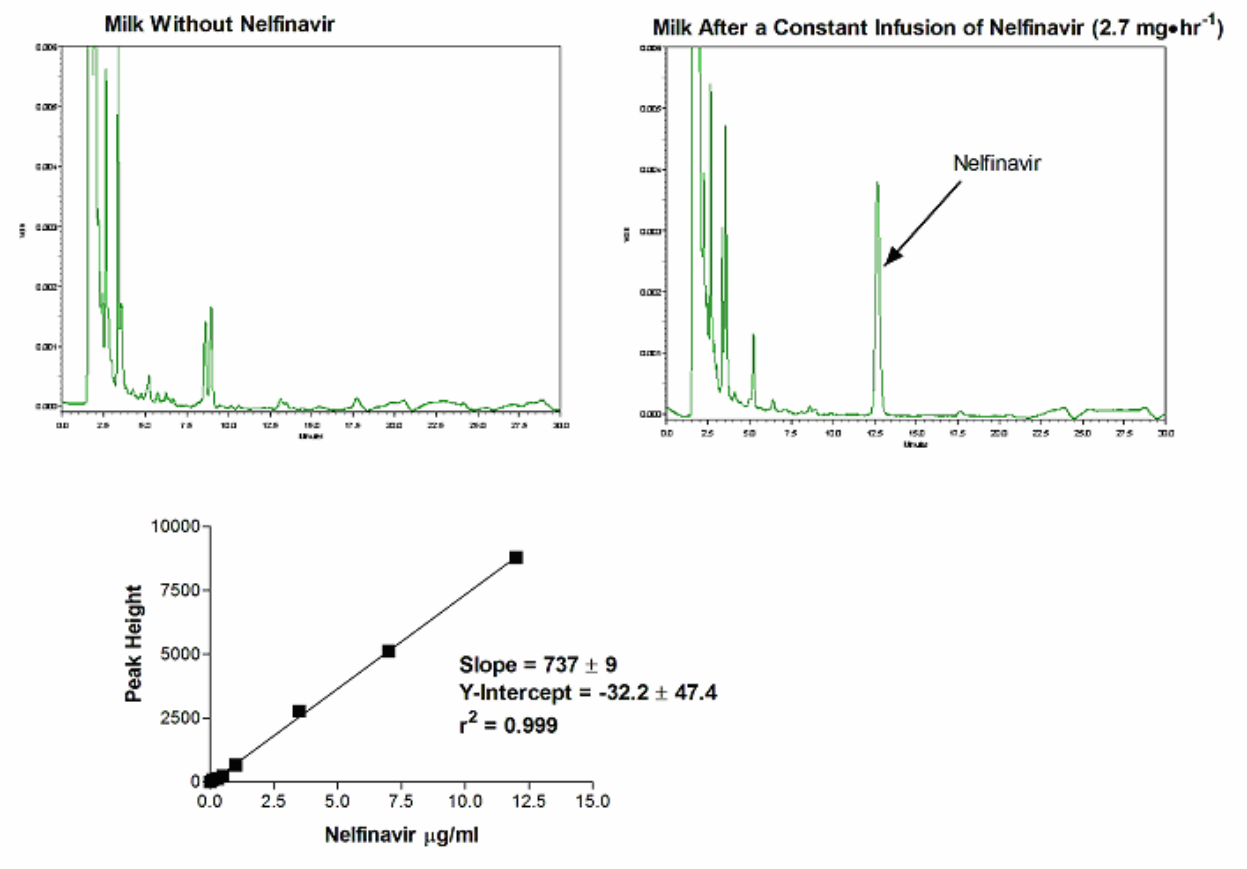

5. Statistical Analysis

A student t-test (parametric) was used to determine if there was a significant difference in the plasma concentrations at the 8th hour, the milk to plasma ratio, and the brain to plasma ratio of nelfinavir between the control and GF120918 animals.

6. Protein Expression of P-gp in Rat Mammary, Brain, and Liver Tissues.

The protein expression of P-gp in rat mammary, brain, and rat liver tissues was determined by western blots. Approximately 0.5 grams of rat mammary, brain, and liver tissues were homogenized in 5 ml of hypotonic lysis buffer (10 mM Tris HCl, 10 mM NaCl, 10 $\mu g \bullet ml^{-1}$ leupeptin, 10 $\mu g \bullet ml^{-1}$ aprotinin, 1 mM phenylmethylsulfonyl fluoride) using a Tissumizer (TeKmar, OH). The homogenate was then centrifuge at 3000 g for 15 minutes at 4ºC to remove nuclear and particulate matter. The supernatant was decanted and centrifuged at 40000 g for 30 minutes at 4ºC. The supernatant was decanted and the remaining pellet was resuspended in 1 ml of hypotonic lysis buffer solution. A small aliquot (20 µl) was used to determine total protein concentration using the method of Lowry *et al.* (Lowry et al., 1951).

Homogenized samples (40 µg of total protein) were incubated at 70 ºC for 5 minutes and loaded onto a 4-12% NuPage Bis-Tris gel. The proteins were separated with electrophoresis chromatography for 1 hour at 200 volts (constant) and 120 mA (initial). The protein was transferred from the gel to a polyvinylidene difluoride (PVDF) membrane at 25 volts (constant) and 160 mA (initial) for 2 hours. The membrane was blocked over night at 4 ºC with 5% albumin in TBST buffer. The membrane was incubated with C219 or JSB1 primary antibody (200 $ng \bullet ml^{-1}$, 20 ml) for 1 hour. The membrane was then washed 3 times with TBST buffer (50 ml) for 15 minutes each time. The membrane was then incubated with either IgG1 secondary antibody (1:25000 dilution in 20 ml of 5% albumin-TBST buffer, used with JSB1 primary antibody) or IgG2a secondary antibody (1:25000 dilution in 20 ml of 5% albumin-TBST buffer, used with C219 primary antibody) for 1 hour. The membrane was then washed 3 times with TBST buffer (50 ml) for 15 minutes each time. The membrane was imaged using the NBT/BCIP staining according to the manufacturer's instruction.

CHAPTER V. RESULTS AND DISCUSSION

A. Intracerebral Microdialysis of Amprenavir

1. Microdialysis In Vitro Recovery

The microdialysis technique was used to determine the unbound concentration of amprenavir in the blood and CNS of rats after an oral administration of GF120918. One critical step of the microdialysis technique is to determine the fraction of a drug recovered from the sampling fluid. Relative recovery is a term used to describe the extraction efficiency and is defined as the concentration of a drug in the dialysate fluid divided by the concentration in the sampling fluid. The relative recovery of amprenavir was estimated using the retrodialysis technique, which assumed that the fraction of amprenavir lost through the microdialysis probe is equal to relative recovery of the amprenavir. The in vitro recovery and loss of amprenavir were determined to be 0.45 ± 0.05 and 0.44 ± 0.03, respectively, and are shown in Figure 17. There was no statistical difference between the in vitro recovery and loss, and therefore, it was assumed that retrodialysis would be an accurate measurement of in vivo recovery.

2. Intracerebral and Blood Concentrations of Amprenavir

According to information from GlaxoSmithKline (personal communication) the plasma half-life of amprenavir is approximately 45 minutes in rats, and therefore a constant infusion of amprenavir for 5.25 hours should produce steady-state concentrations in blood. Figure 18 shows the concentration-time profile of amprenavir for a representative animal in the control and GF120918 treated animals. The blood and brain concentrations of amprenavir did not reach steady-state by 5.25 hours, as can be seen in Figure 18. There are many plausible reasons for this discrepancy. One possible reason is because PEG-400, the vehicle used for amprenavir, caused changes in the elimination of amprenavir. A second possible reason is the microdialysis procedure produced stress on the animals, which caused changes in the elimination of amprenavir. Because steady state concentrations in the blood were not produced, the effects of GF120918 on the systemic clearance of amprenavir could not be accurately measured.

Figure 17: In vitro loss and recovery of amprenavir through a microdialysis probe. CMA-12 microdialysis probes were placed in a solution containing amprenavir (1 µg/ml). The microdialysis probes were perfused with ^{14}C-amprenavir, and the in vitro recovery and loss of amprenavir were determined. Each data point represents the average of 3 different probes. Results are shown as mean ± S.D..

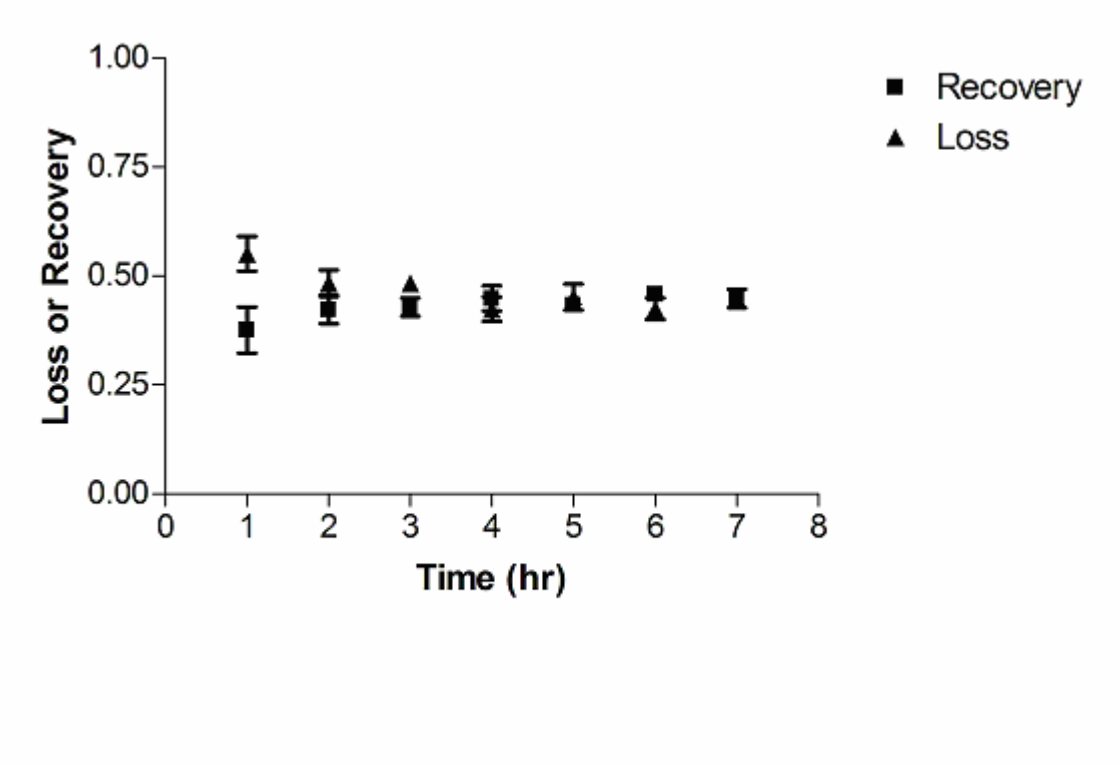

Figure 18: Concentration-time profile of unbound amprenavir in the blood and CNS dialysates of a representative rat. Amprenavir was infused (26.8 mg•h^{-1}•kg^{-1}) for 5.25 hours. (a) Control animal. (b) GF120918 (250 mg•kg^{-1}) treated animal.

a. Control Animal

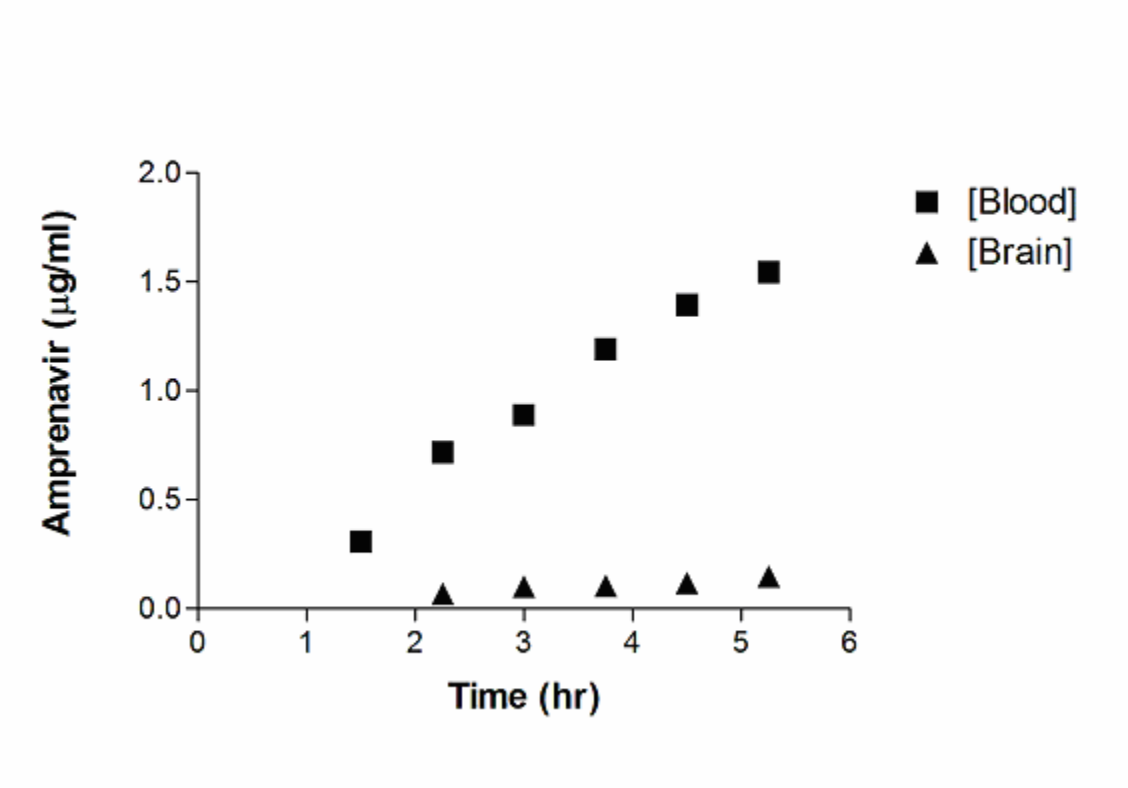

Figure 18: (Continued)

b. GF120918 Treated Animal

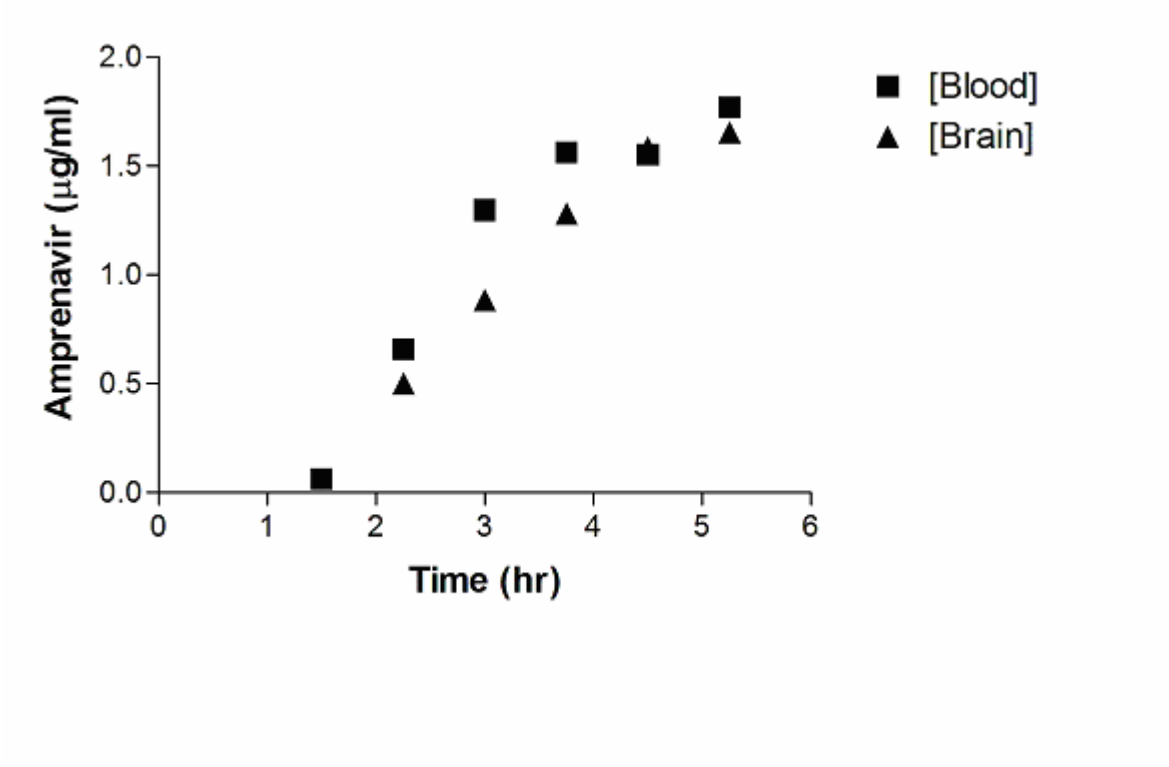

Although steady-state concentrations of amprenavir were not achieved, the concentration-time profile of amprenavir in the blood and CNS parallel one another. The BBR of amprenavir at the last 4 time points was not significantly different ($p = 0.80$) from one another within the control or GF120918 treated groups (Figure 19). This indicates that the distribution of amprenavir into the CNS is rapid. The initial CNS concentrations of amprenavir in the control group were below the limit of detection and therefore could not be used in the analysis. There was a statistically significant difference ($p < 0.001$) in the BBR of amprenavir between the control and GF120918 treated groups at each time point. As a result, the unbound concentration, and thus the effective concentration, of amprenavir was increased in the extracellular fluid of the CNS in the presence of a MDR modulator (GF120918). There was no effect of GF120918 ($p = 0.20$) on the blood concentrations at each time point (Figure 20) between the control and GF120918 treated animals. This would indicate that the increase in the distribution of amprenavir into the CNS is due to alterations at the BBB (i.e. inhibition of P-gp), and not due to changes in the plasma protein binding of amprenavir by GF120918.

The increase in the distribution of amprenavir into the CNS in the presence of GF120918 was similar to the increase in the BBR (13 fold based on total radioactivity) seen in whole body autoradiography studies in mice at 2 hours post dose (Polli et al., 1999). There was a high degree of variability in the BBR of amprenavir for the GF120918 treated animals. The variability can be attributed to varying plasma concentrations of GF120918 for each animal. The co-administration of an MDR modulator with a protease inhibitor may have a significant effect on decreasing HIV viral load in the CNS. The decrease in viral load could potentially ameliorate the effects of HIV-associated dementia.

Figure 19: Unbound brain to blood ratio of amprenavir in rats. The unbound brain to blood ratio was determined at the last 4 time points of the infusion of amprenavir (26.8 mg•h^{-1}•kg^{-1}) after an oral dose of GF120918 (250 mg•kg^{-1}) or vehicle. Each time point represents 5 rats for each group and is shown as mean ± S.D..

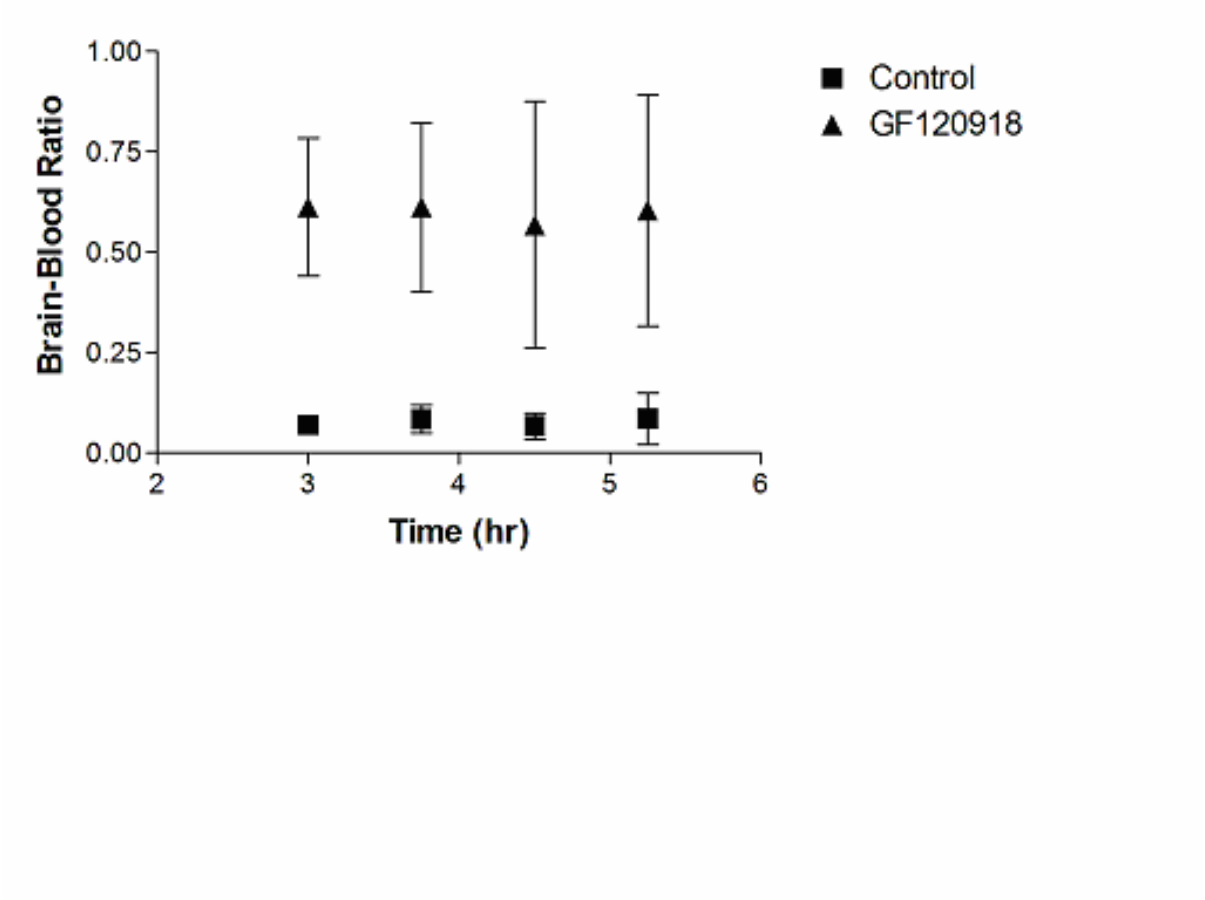

Figure 20: Blood dialysate concentrations of amprenavir in control and GF120918 treated animals. A constant infusion of amprenavir was given (26.8 mg•h^{-1}•kg^{-1}) for 5.25 hr to control and GF120918 treated animals (n = 5 rats for each group). Results shown as mean ± S.D..

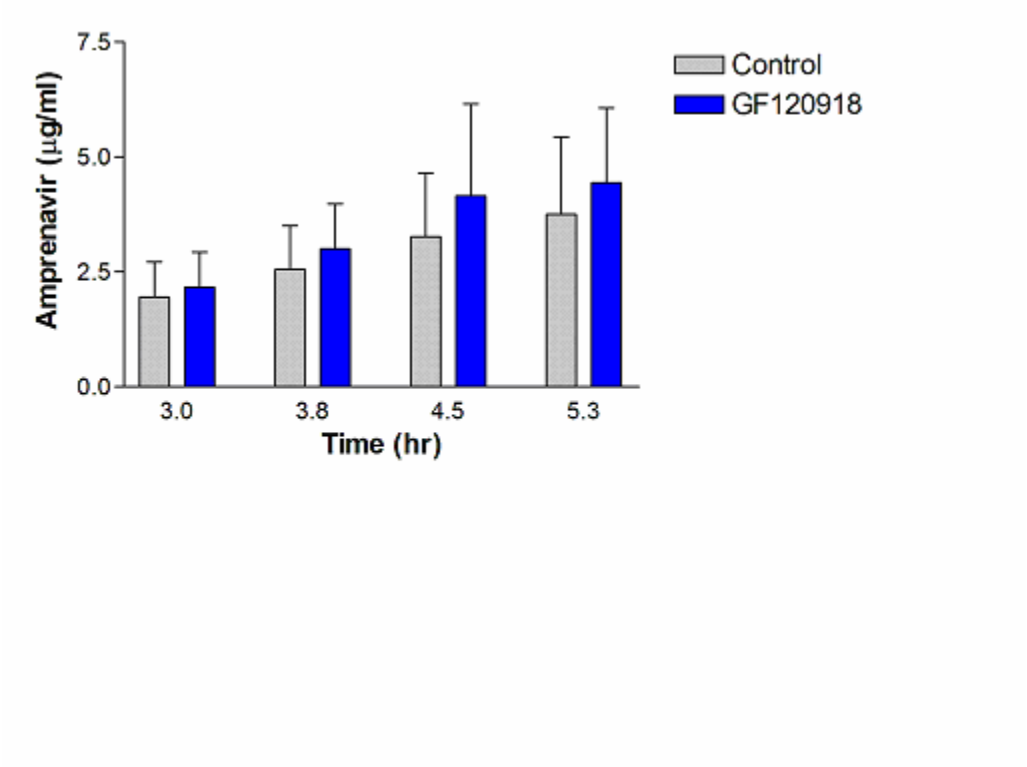

B. In Vitro Inhibition of Cytochrome P4503A

1. Inhibition of CYP3A4 (Human)

Since many MDR modulators significantly alter CYP3A4 metabolism, it was deemed necessary to determine if GF120918 inhibits CYP3A4. An in vitro expression system for CYP3A4 was used to determine the Ki of GF120918 and cyclosporine. Midazolam was used as a model CYP3A substrate, and is metabolized to 1-hydroxy midazolam by CYP3A4. Figure 21 shows the formation of 1-hydroxy midazolam over 20 minutes by the CYP3A4 expression system with 5 μM midazolam. The formation of 1-hydroxy midazolam appears to be linear up to 15 minutes ($r^2 = 0.94$). For the inhibition studies with cyclosporine and GF120918, midazolam was incubated with the CYP3A4 expression system for 10 minutes.

Figure 22 shows the Michaelis-Menten curve for the formation of 1-hydroxy midazolam by CYP3A4. The apparent Km and Vmax were determined to be 3.26 μM (1.80 to 4.70, 95% confidence interval (C.I.)) and 32.0 pmol•min^{-1} (29.2 to 34.8, 95% C.I.), respectively. The apparent Km of midazolam in human liver microsomes has been reported to be 3.9 and 11.7 μM (Andrews et al., 2002; Patki et al., 2003). In a recombinant CYP3A4 expression system, the apparent Km of midazolam has been reported to be 0.8 μM, 5.4 μM, 3.1 μM, and 4.4 μM using infected insect cells, transfected b-lymphoblastoid cells, transformed yeast cells, and transformed *E. coli cells*, respectively (Andrews et al., 2002; Patki et al., 2003). The Km determined in this dissertation (3.26 μM) is within the reported values for CYP3A4 expression systems (0.8 – 5.4 μM). The Michaelis-Menten curves for 1-hydroxy midazolam in the presence of cyclosporine and GF120918 are shown in Figures 23 and 24, respectively, and the kinetic parameters are shown in Table 2. GF120918, at a concentration of 3.33 μM, had no statistically significant effect on the apparent Km or Vmax of midazolam. This is consistent with other reports that showed no inhibition of CYP3A4 metabolism by GF120918 with a concentration of 0.200 to 5 μM (Cummins et al., 2002; Cummins et al., 2003). Therefore, it was concluded that GF120918 is not an inhibitor of CYP3A4, at least up to concentrations of 5 μM. Cyclosporine significantly increased the Km of midazolam, but showed no effect on Vmax. This is consistent with other reports that have shown cyclosporine to be a competitive inhibitor of CYP3A (Abel and Back, 1993; Wandel et al., 1999). The apparent Ki of cyclosporine was determined to be 1.64 μM (0.95 to 2.32, 95% C.I.). The apparent Ki of cyclosporine has been reported to be 4.9 μM and

6.8 μM using human liver microsomes (Abel and Back, 1993; Wandel et al., 1999). Differences between the Ki reported in these studies versus the reported values could be a result of non-specific binding of cyclosporine to the different metabolizing systems used (human liver microsomes versus CYP3A4 expression systems), or due to differences in the CYP3A4 activity in human liver microsomes versus CYP3A4 expression system. The in vitro results are consistent with results from the use of cyclosporine as an MDR modulator clinically, where it has been shown to inhibit the metabolism of doxorubicin, daunorubicin, and etoposide (Lum et al., 1992; Bartlett et al., 1994; List et al., 2001). The inhibition of CYP3A4 mediated metabolism by cyclosporine can potentially increase the concentration of other co-administered CYP3A4 substrates to toxic levels. GF120918, on the other hand, could potentially inhibit P-gp without altering CYP3A4 metabolism, which makes it a better candidate as an MDR modulator clinically.

Table 2: Apparent Km and Vmax of midazolam in the presence and absence of cyclosporine and GF120918.

Treatment	Vmax pmol•min^{-1} (95% C.I.)	Km μM (95% C.I.)
Control	32.0 (29.2 to 34.8)	3.26 (1.80 to 4.70)
Cyclosporine (15 μM)	29.3 (26.4 to 32.2)	26.4 (17.6 to 25.2)
GF120918 (3.33 μM)	26.8 (25.0 to 28.5)	3.80 (2.63 to 4.97)

Figure 21: Formation of 1-hydroxy midazolam by the CYP3A4 expression system over time. Midazolam (10 µM) was incubated in the presence of CYP3A4 Supersomes (20 pmol of P450) and the formation of 1-hydroxy midazolam was determined at different time points. Results are shown as mean (in triplicate) ± S.D..

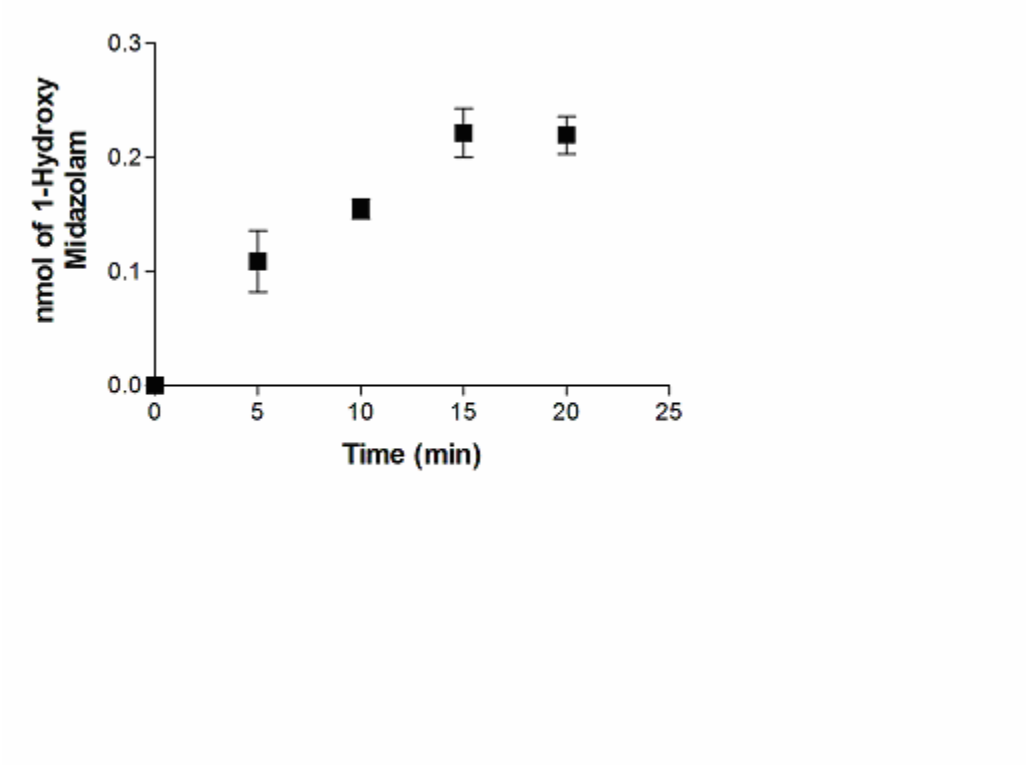

Figure 22: Michaelis-Menten curve for the formation of 1-hydroxy midazolam. The formation of 1-hydroxy midazolam was determined using CYP3A4 Supersomes (20 pmol of P450) at varying concentration of midazolam (0 to 200 μM). Results are shown as the mean (duplicate) for the formation of 1-hydroxy midazolam.

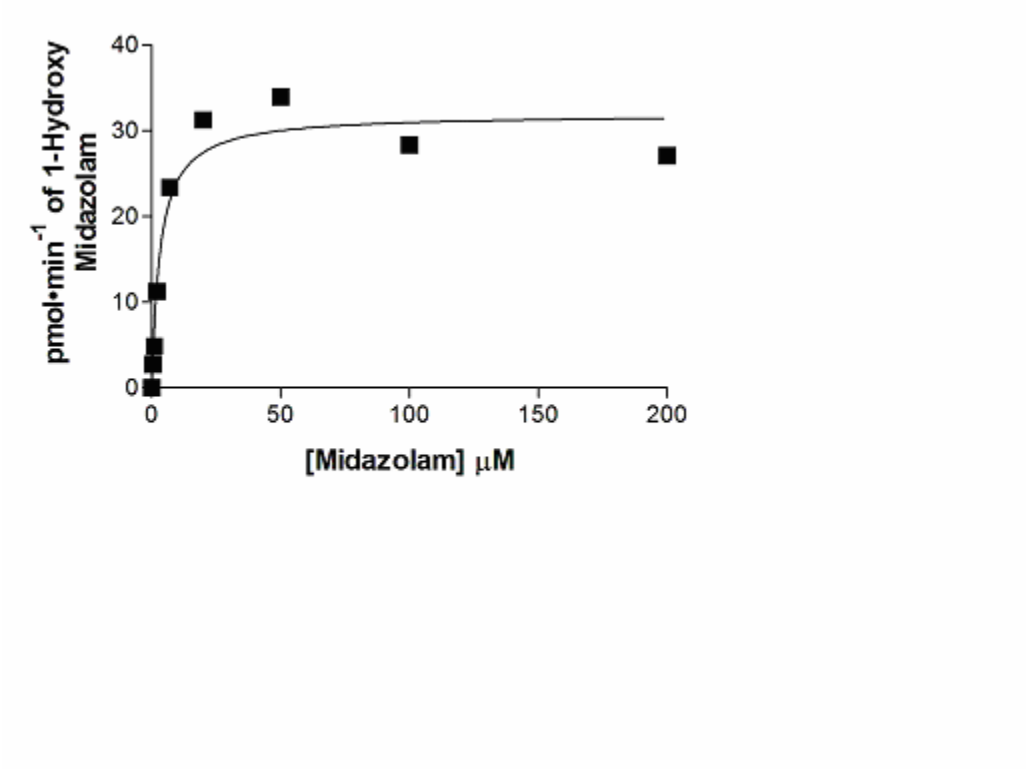

Figure 23: Michaelis-Menten curve for the formation of 1-hydroxy midazolam in the presence of cyclosporine. The formation of 1-hydroxy midazolam was determined using CYP3A4 Supersomes (20 pmol of P450) at varying concentration of midazolam in the presence of cyclosporine (15 μM). Results are shown as the mean (duplicate) for the formation of 1-hydroxy midazolam.

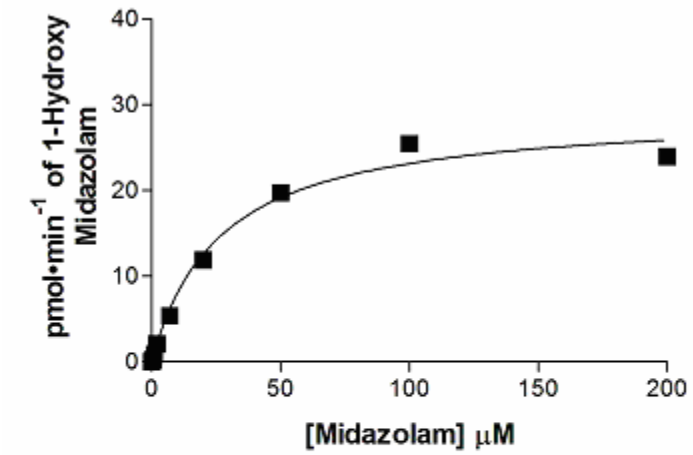

Figure 24: Michaelis-Menten curve for the formation of 1-hydroxy midazolam in the presence of GF120918. The formation of 1-hydroxy midazolam was determined using CYP3A4 Supersomes (20 pmol of P450) at varying concentration of midazolam in the presence of GF120918 (3.33 μM). Results are shown as the mean (duplicate) for the formation of 1-hydroxy midazolam.

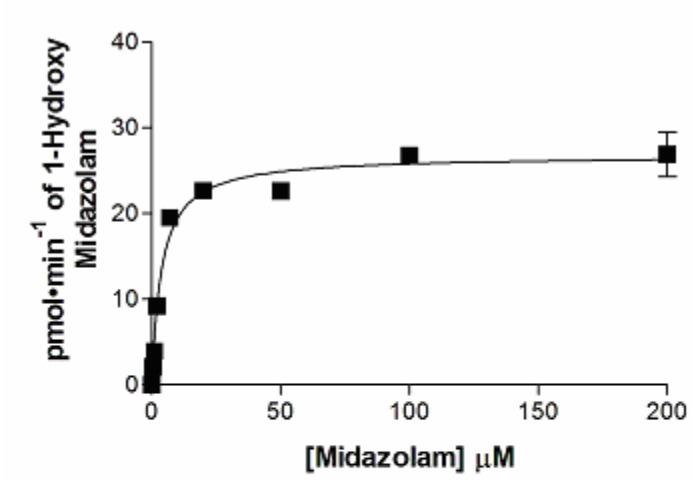

2. Inhibition of CYP3A1 and CYP3A2 (Rat)

Midazolam is predominately metabolized to 4-hydroxy midazolam by CYP3A1 and CYP3A2, and to 1-hydroxy and 1,4-dihydroxy midazolam to a lesser extent in rats (Ghosal et al., 1996; Higashikawa et al., 1999; Kobayashi et al., 2002). The 4-hydroxy midazolam metabolite standard was not available, so the formation of 1-hydroxy midazolam was used to determine the inhibitory effects of GF120918 and cyclosporine on CYP3A in rats. Figure 25 shows the formation of 1-hydroxy midazolam by CYP3A2 over 20 minutes. The formation of 1-hydroxy midazolam appeared to be linear up to 10 minutes ($r^2 = 0.98$) and therefore, midazolam was incubated for 5 minutes for the inhibition studies.

Figure 26 shows the formation of 1-hydroxy midazolam by CYP3A2 when incubated with midazolam from 0 to 1 mM. The formation of 1-hydroxy midazolam initially increases, followed by a decrease in activity at higher concentrations of midazolam. This type of profile was also seen in the formation of 1,4-dihydroxy midazolam in rat liver microsomes by Ghosal et al. (Ghosal et al., 1996). This profile could be due to the existence of a second binding site (Hutzler and Tracy, 2002), which causes allosteric changes that reduce the activity of CYP3A2. At lower concentrations of midazolam (Figure 27), the formation of 1-hydroxy midazolam appears to follow Michaelis-Menten kinetics. The apparent Km and Vmax was determined to be 3.46 μM (1.93 to 4.99, 95% C.I.) and 16.9 pmol•min^{-1} (15.3 to 18.4, 95% C.I.), respectively, and is shown in Table 3. The formation of 1-hydroxy midazolam in the presence of cyclosporine or GF120918 is shown in Figures 28 and 29, respectively. The apparent Km and Vmax values for the formation of 1-hydroxy midazolam in the presence of cyclosporine and GF120918 were 5.10 μM (3.01 to 7.18, 95% C.I.), 14.0 pmol•min^{-1} (12.6 to 15.5, 95% C.I.) and 5.18 μM (2.90 to 7.46, 95% C.I.), 15.3 pmol•min^{-1} (13.6 to 17.0, 95% C.I.), respectively (Table 3). GF120918 showed no effect on the in vitro metabolism of midazolam by CYP3A2, which is consistent with the in vitro CYP3A4 results. However, cyclosporine also showed no effect on the in vitro metabolism of midazolam by CYP3A2, which is inconsistent with the CYP3A4 results. A possible reason for this result is that the inhibition by cyclosporine could be masked by the inhibitory effects of midazolam at higher concentrations. Another possible explanation for the lack of effect by cyclosporine is that cyclosporine inhibits the formation of 4-hydroxy midazolam (the primary metabolite of CYP3A2), but not the formation of 1-hydroxy midazolam. Since midazolam is

metabolized by CYP3A1 and CYP3A2, the CYP3A1 expression system was also used to determine the effects of cyclosporine and GF120918 on CYP3A metabolism.

Table 3: Kinetic parameters for the formation of 1-hydroxy midazolam by CYP3A2.

Treatment	Vmax pmol•min^{-1} (95% C.I.)	Km μM (95% C.I.)
Control	16.9 (15.3 to 18.4)	3.46 (1.93 to 4.99)
Cyclosporine (15 μM)	14.0 (12.6 to 15.5)	5.10 (3.01 to 7.18)
GF120918 (3.33 μM)	15.3 (13.6 to 17.0)	5.18 (2.90 to 7.46)

Like CYP3A2, the formation of 1-hydroxy midazolam by CYP3A1 initially increases, but then decreases at higher concentrations of midazolam (Figure 30). The decrease in activity at higher concentrations of midazolam made the CYP3A1 and CYP3A2 system difficult to interpret, and therefore, rat liver microsomes were used to determine the effects of cyclosporine and GF120918. The formation of 1-hydroxy midazolam appeared to be linear for 30 minutes (r^2 = 0.96, Figure 31), using rat liver microsomes, and therefore, the rat liver microsomes were incubated for 10 minutes for the inhibition studies. Figure 32 shows the formation of 1-hydroxy midazolam when incubated with midazolam from 0 to 500 μM. The kinetic parameters from these studies are shown in Table 4. The apparent Km for the formation of 1-hydroxy midazolam has been reported to be 32.3 μM by Ghosal et al. (Ghosal et al., 1996), which is lower than the Km (99.4 μM) from these studies. The difference in the Km values could be explained by the fact that the concentration range of midazolam used by Ghosal et al. (0 to 120 μM) was lower than the present studies (0 to 500 μM). If the analysis of the kinetic parameters is done using the results from 0 to 120 μM midazolam (Figure 33), the apparent Km becomes 48.4 μM (27.5 to 69.3, 95% C.I.), which is in good agreement with the 32.3 μM reported value. The formation of 1-hydroxy midazolam by rat liver microsomes in the presence of cyclosporine or GF120918 is shown in Figures 34 and 35, respectively. There was no statistical difference in the apparent Km for the formation of 1-hydroxy midazolam in the presence of cyclosporine or GF120918 (Table 4). The apparent lack of inhibition by cyclosporine in the CYP3A2 and in rat liver microsomes is difficult to explain, since cyclosporine has been shown to inhibit the elimination of etoposide, a CYP3A substrate, in rats (Burgio et al., 1996). Since the apparent Km for the formation of 1-

hydroxy midazolam was higher in the presence of cyclosporine (but not statistically different from the control Km), it is possible that the lack of statistical significance is due to too few data points, i.e., a lack of statistical power. As mentioned previously, it is possible that cyclosporine does not inhibit the formation of 1-hydroxy midazolam in rats, but rather inhibits the formation of 4-hydroxy midazolam, the primary metabolite of CYP3A1 and CYP3A2. Since cyclosporine did not inhibit the formation of 1-hydroxy midazolam in rats, it is impossible to determine what effects, if any, GF120918 has on CYP3A1 and/or CYP3A2.

Table 4: Kinetic parameters for the formation of 1-hydroxy midazolam by rat liver microsomes.

Treatment	Vmax pmol•min^{-1} (95% C.I.)	Km μM (95% C.I.)
Control	21.5 (19.0 to 23.9)	99.4 (66.6 to 132)
Cyclosporine (15 μM)	19.1 (15.3 to 22.9)	174 (91.7 to 257)
GF120918 (3.33 μM)	17.8 (14.7 to 20.9)	126.8 (67.8 to 186)

Figure 25: Formation of 1-hydroxy midazolam by CYP3A2. The formation of 1-hydroxy midazolam in the presence of midazolam (10 µM) was determined over 25 minutes using CYP3A2 Supersomes (20 pmol of P450). Results are shown as the mean (duplicates) for the formation of 1-hydroxy midazolam.

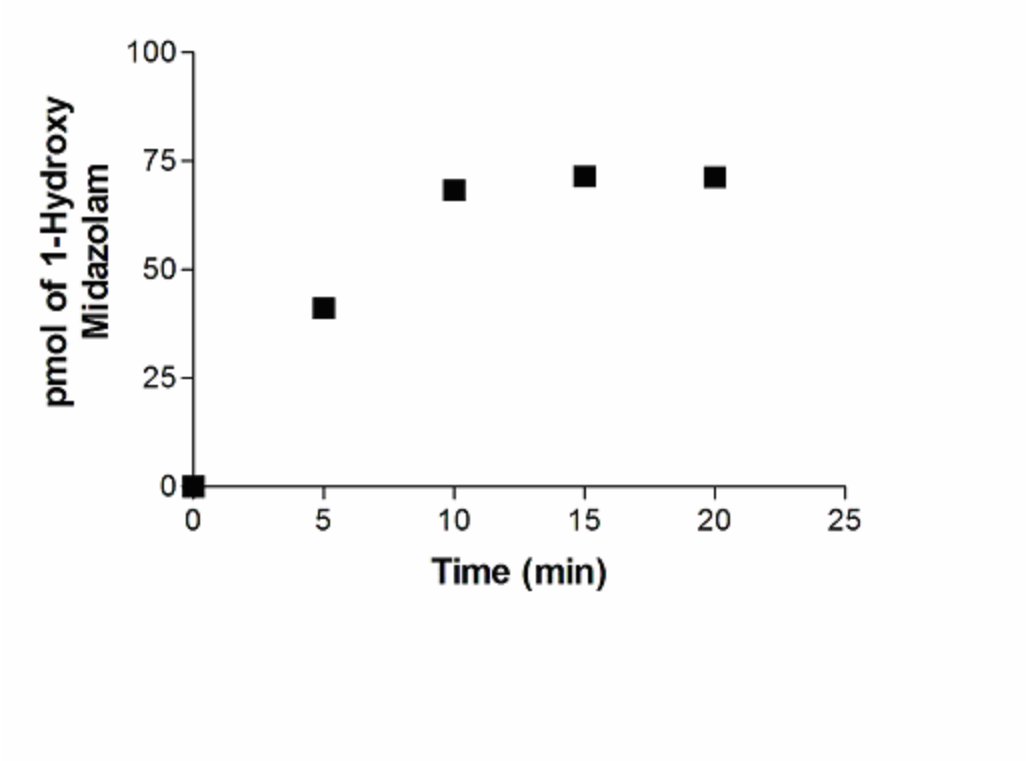

Figure 26: Formation of 1-hydroxy midazolam by the CYP3A2. The formation of 1-hydroxy midazolam in the presence of midazolam (10 µM) was determined using CYP3A2 Supersomes (20 pmol of P450) at varying concentration of midazolam. Results are shown as the mean (duplicate) for the formation of 1-hydroxy midazolam.

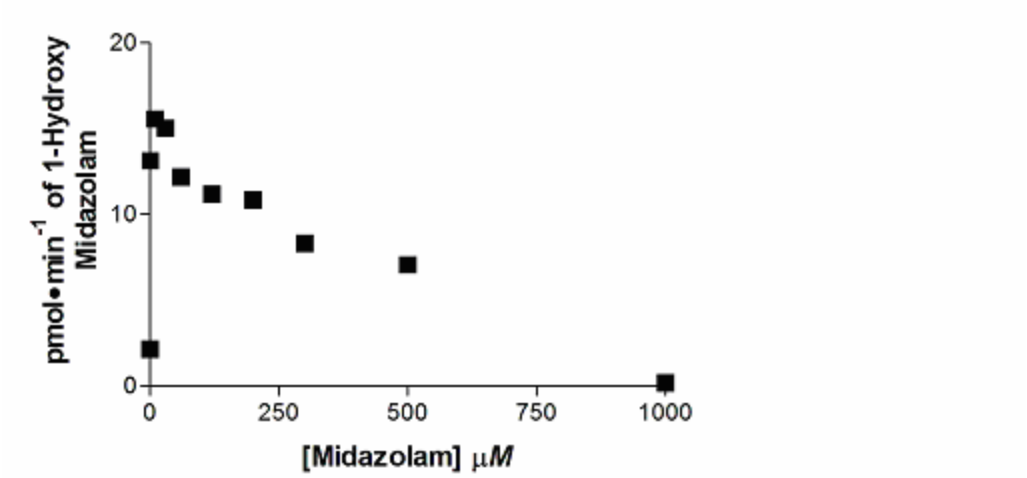

Figure 27: Formation of 1-hydroxy midazolam by CYP3A2 expression system. Midazolam (0 to 60 µM) was incubated with the CYP3A2 Supersomes (20 pmol P450) for 5 minutes. Results are shown as the mean (duplicate) for the formation of 1-hydroxy midazolam.

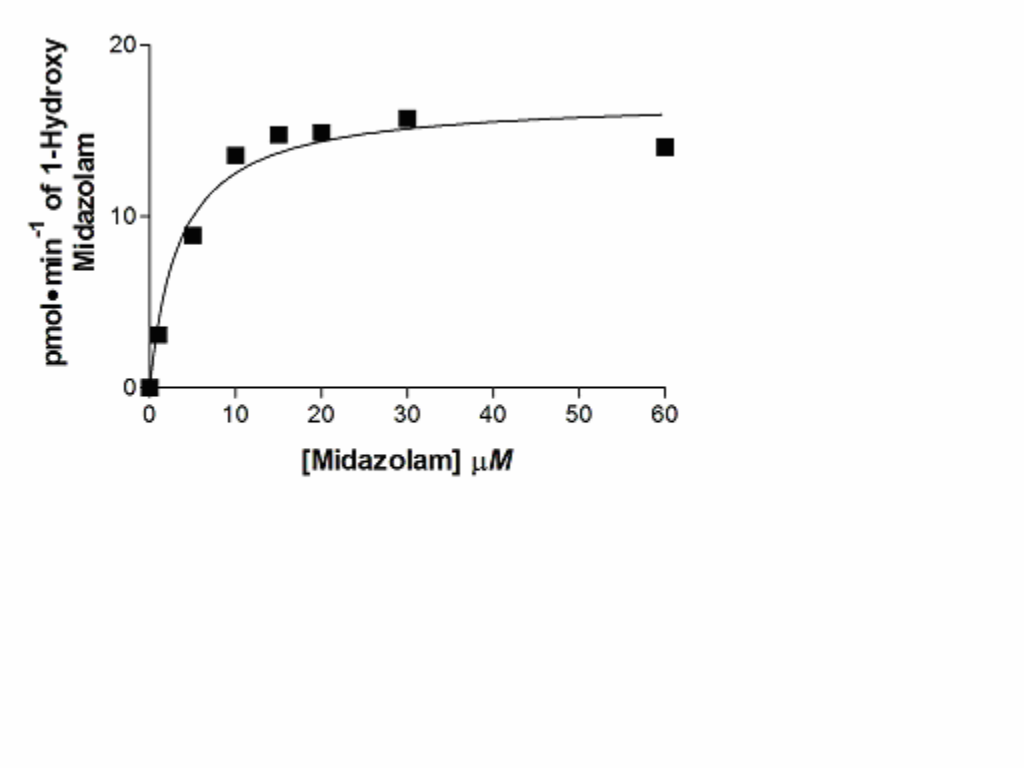

Figure 28: Formation of 1-hydroxy midazolam in the presence of cyclosporine by CYP3A2. The formation of 1-hydroxy midazolam was determined using CYP3A2 Supersomes (20 pmol of P450) at varying concentration of midazolam in the presence of cyclosporine (15 µM). Results are shown as the mean (duplicate) for the formation of 1-hydroxy midazolam.

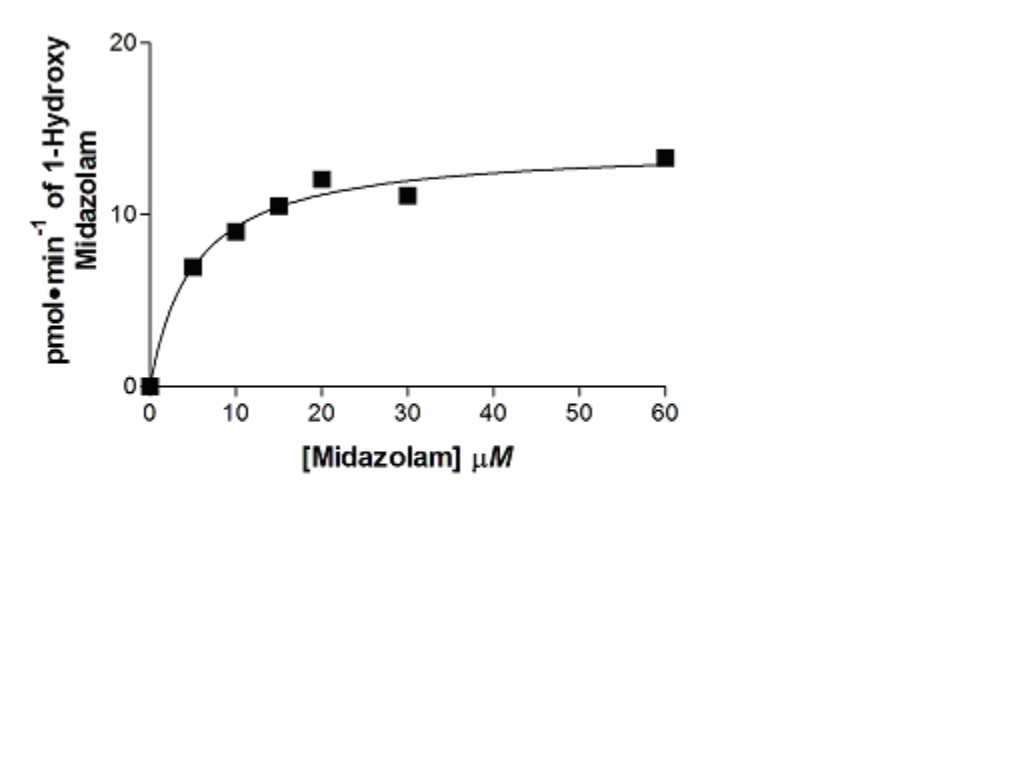

Figure 29: Formation of 1-hydroxy midazolam in the presence of GF120918 by CYP3A2. The formation of 1-hydroxy midazolam was determined using CYP3A2 Supersomes (20 pmol of P450) at varying concentration of midazolam in the presence of GF120918 (3.33 µM). Results are shown as the mean (duplicate) for the formation of 1-hydroxy midazolam.

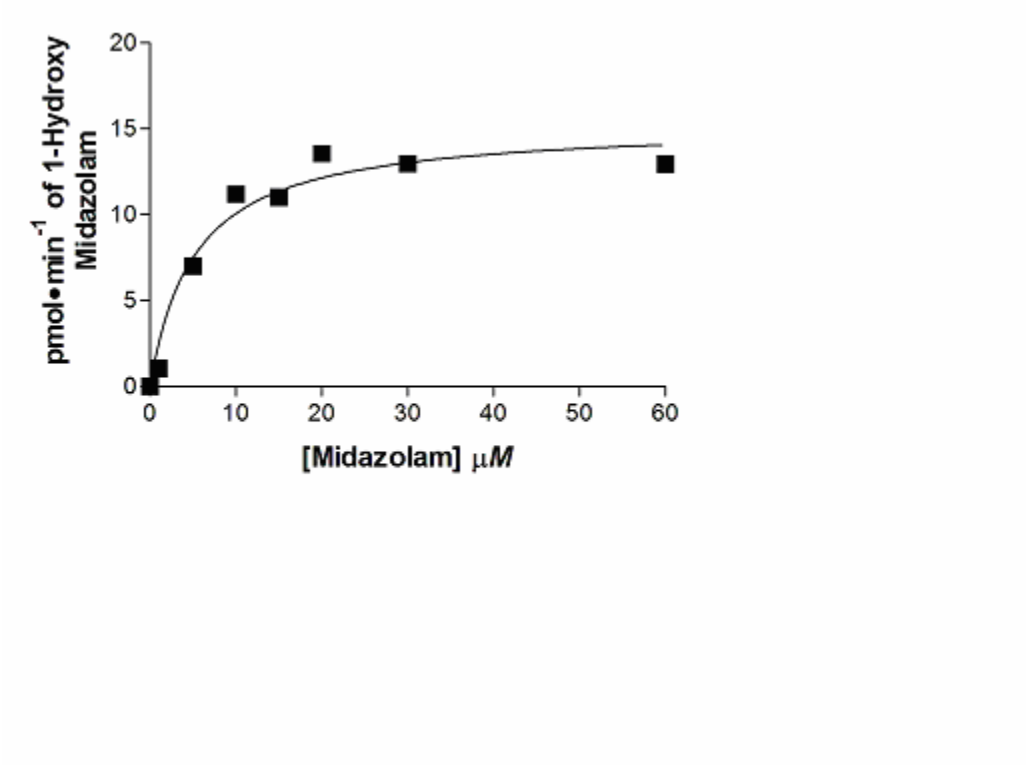

Figure 30: Formation of 1-hydroxy midazolam by the CYP3A1. The formation of 1-hydroxy midazolam in the presence of midazolam (10 µM) was determined using CYP3A1 Supersomes (20 pmol of P450) at varying concentration of midazolam. Results are shown as the mean (duplicate) for the formation of 1-hydroxy midazolam.

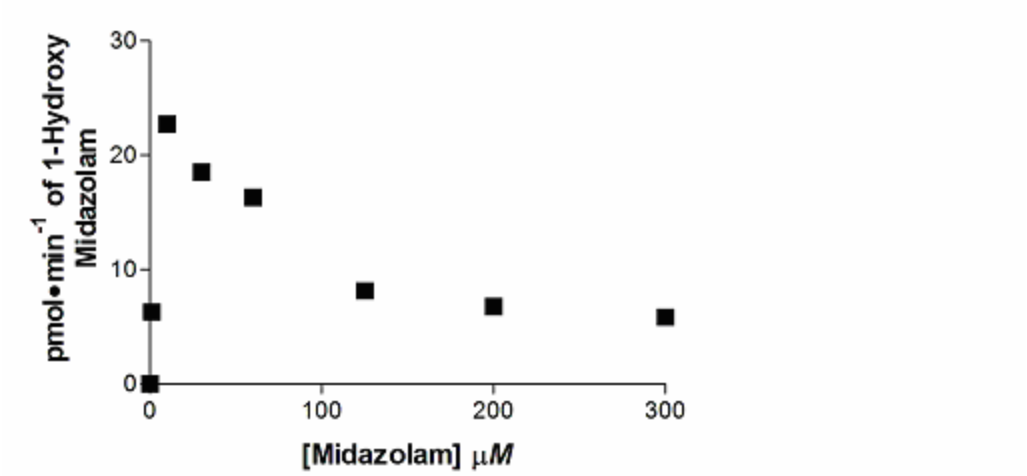

Figure 31: Formation of 1-hydroxy midazolam using rat liver microsomes. The formation of 1-hydroxy midazolam was determined over 30 minutes, using rat liver microsomes (0.2 mg/ml protein). Results are shown as the mean (duplicate) for the formation of 1-hydroxy midazolam.

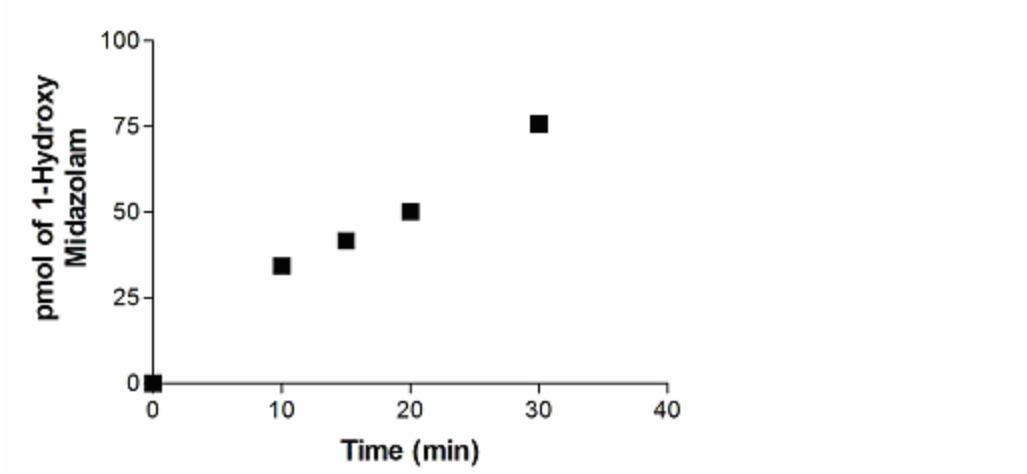

Figure 32: Formation of 1-hydroxy midazolam by rat liver microsomes. The formation of 1-hydroxy midazolam was determined using rat liver microsomes (0.2 mg/ml protein) at varying concentration of midazolam. Results are shown as the mean (duplicate) for the formation of 1-hydroxy midazolam.

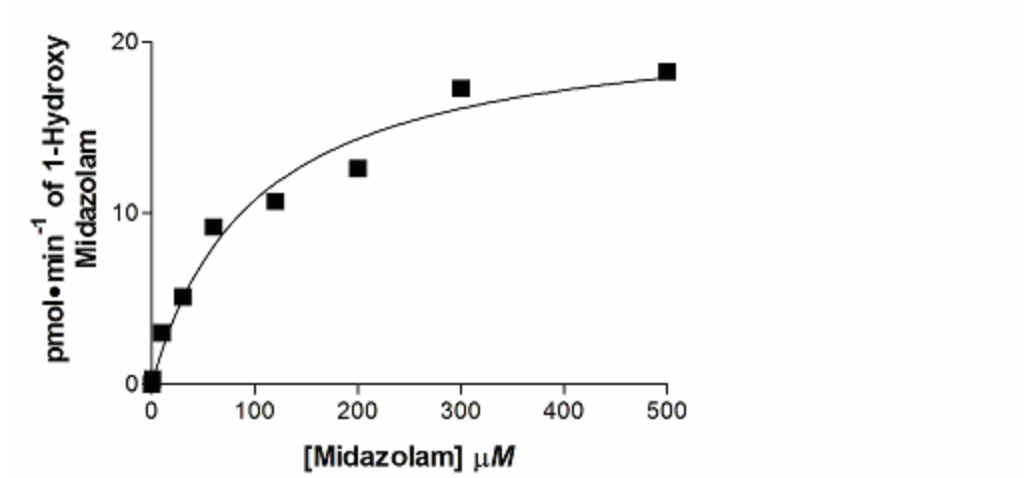

Figure 33: Formation of 1-hydroxy midazolam by rat liver microsomes (0 to 120 µM). The formation of 1-hydroxy midazolam was determined using rat liver microsomes (0.2 mg/ml protein) at varying concentration of midazolam. Results are shown as the mean (duplicate) for the formation of 1-hydroxy midazolam.

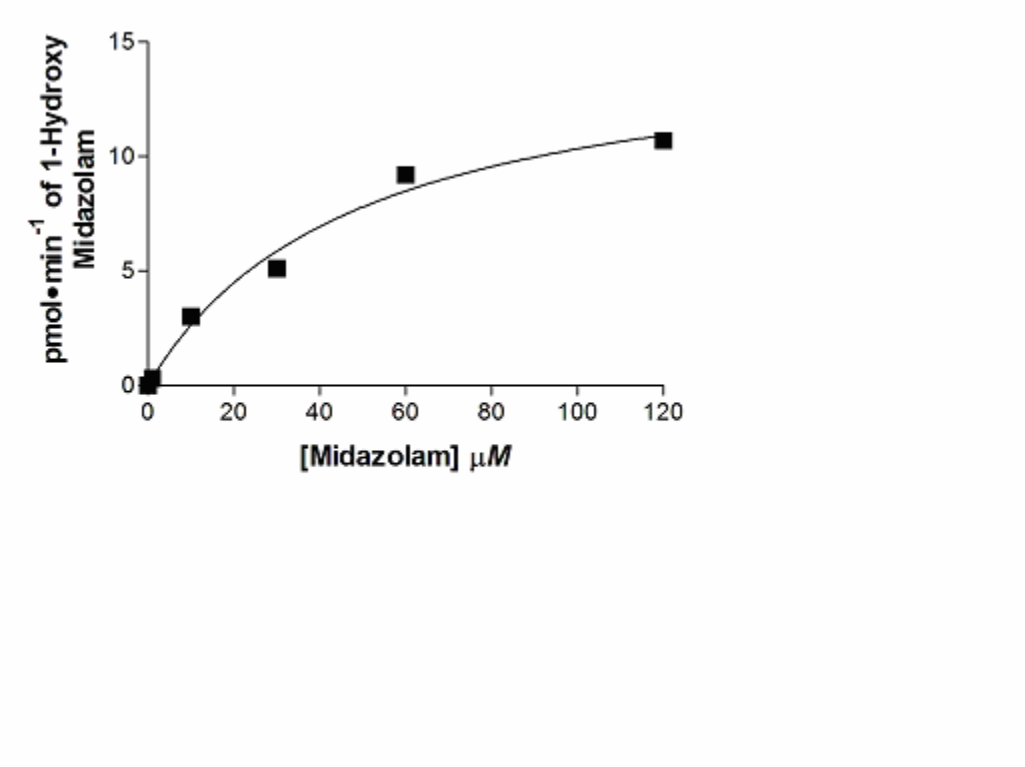

Figure 34: Formation of 1-hydroxy midazolam by rat liver microsomes in the presence of cyclosporine. The formation of 1-hydroxy midazolam was determined using rat liver microsomes (0.2 mg/ml protein) at varying concentration of midazolam in the presence of cyclosporine (15 µM). Results are shown as the mean (duplicate) for the formation of 1-hydroxy midazolam.

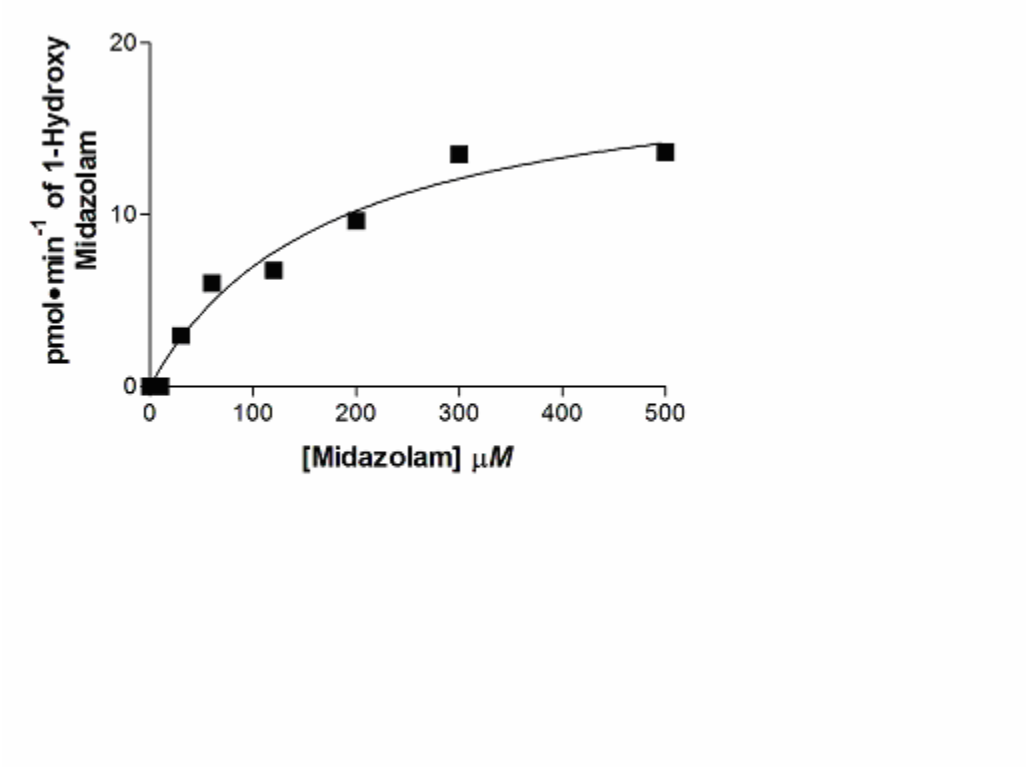

Figure 35: Formation of 1-hydroxy midazolam by rat liver microsomes in the presence of GF120918. The formation of 1-hydroxy midazolam was determined using rat liver microsomes (0.2 mg/ml protein) at varying concentration of midazolam in the presence of GF120918 (3.33 µM). Results are shown as the mean (duplicate) for the formation of 1-hydroxy midazolam.

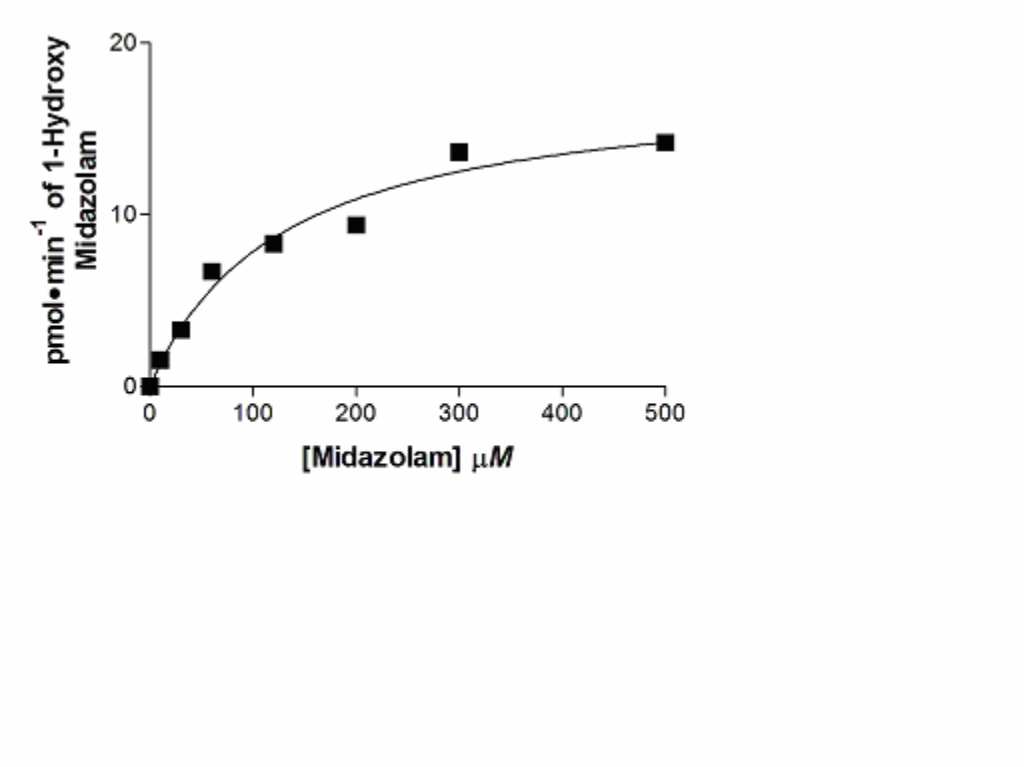

C. In Vitro Inhibition of MDR1

MDR1 Transfected LLC-PK1 Cells

The P-gp-dependent transport of doxorubicin across a cell monolayer was employed to determine the inhibition constants for cyclosporine and GF120918. The time course for the P-gp-dependent transport (basolateral to apical) of doxorubicin (5 μM) appeared to be linear for 4 hours ($r^2 = 0.85$, Figure 36). For the P-gp inhibition studies, the transport of doxorubicin was determined for 3 hours. Figure 37 shows the P-gp-dependent transport of doxorubicin (basolateral to apical) from 0 to 200 μM. The apparent Km and Vmax values for doxorubicin were determined to be 65.7 μM (40.0 to 91.5, 95% C.I.) and 37.9 pmol•hr^{-1} (31.8 to 44.0, 95% C.I.), respectively, and are shown in Table 5. Both cyclosporine and GF120918 significantly reduced the P-gp-dependent transport of doxorubicin (Figures 38 and 39). The Ki of GF120918 was determined to be 84.7 nM (53.1 to 116, 95% C.I.), which is higher than the reported value of 35 nM using rat liver membrane vesicles (Wallstab et al., 1999). The differences in the Ki values could be due to differences in the MDR1 (human) versus mdr1a and mdr1b (rat) transporters or the two different types of in vitro systems (MDR membrane vesicles versus MDR1 transfected cells). Since GF120918 showed no inhibition of CYP3A4 up to 3.33 μM and the apparent Ki for P-gp is 35 nM, this would suggest that GF120918 should be able to selectively inhibit P-gp in vivo. The apparent Ki of cyclosporine for P-gp was determined to be 2.96 μM (1.84 to 4.09, 95% C.I.). The apparent Ki value for cyclosporine has been reported to be 1.5 μM using rat liver membrane vesicles (Bohme et al., 1993). Again, the differences in the apparent Ki values could be due to differences in the MDR1 (human) versus mdr1a and mdr1b (rat) transporters or differences in the in vitro systems used. The confidence intervals for the Ki of cyclosporine for P-gp and CYP3A4 overlapped, which suggests that cyclosporine is unable to inhibit P-gp without inhibiting CYP3A4 metabolism. Some caution must be taken in this analysis though, since the inhibition constants in these studies did not take into account such effects as binding of cyclosporine to the transport (LLC-MDR1 cells) and metabolism (CYP3A4 Supersomes) systems.

Figure 36: The basolateral to apical transport of doxorubicin across LLC-PK1 and LLC-MDR1 monolayer. LLC-MDR1 and LLC-PK1 cells were grown to a confluent monolayer and placed in a side by side diffusion chamber system. Doxorubicin (5 μM) was placed in the basolateral compartment and the transport of doxorubicin in the apical compartment was measured over time. Each time point was done in triplicate and the results are shown as mean ± S.D..

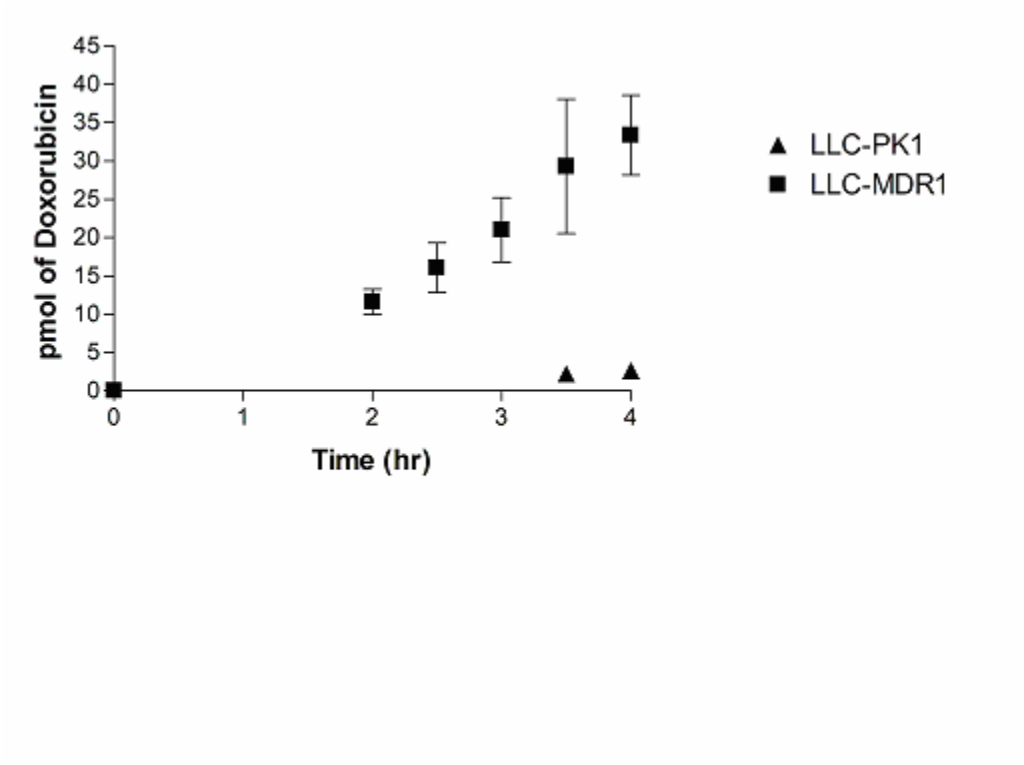

Figure 37: The P-gp-dependent transport of doxorubicin. The transport of doxorubicin to the apical compartment was determined at varying concentration of doxorubicin (0 to 200 μM) in the basolateral compartment. Results are shown as mean (triplicate) ± S.D..

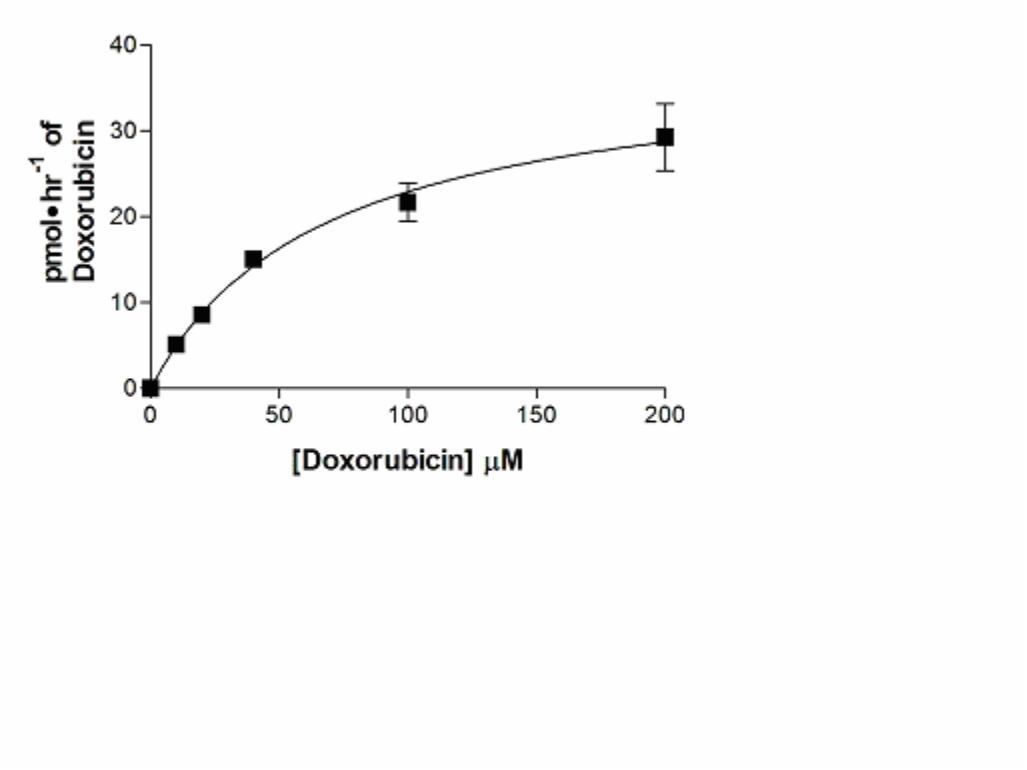

Figure 38: The P-gp-dependent transport of doxorubicin in the presence of cyclosporine. The transport of doxorubicin to the apical compartment was determined at varying concentrations of doxorubicin (0 to 200 µM) in the basolateral compartment in the presence of 15 µM cyclosporine. Results are shown as mean (triplicate) ± S.D..

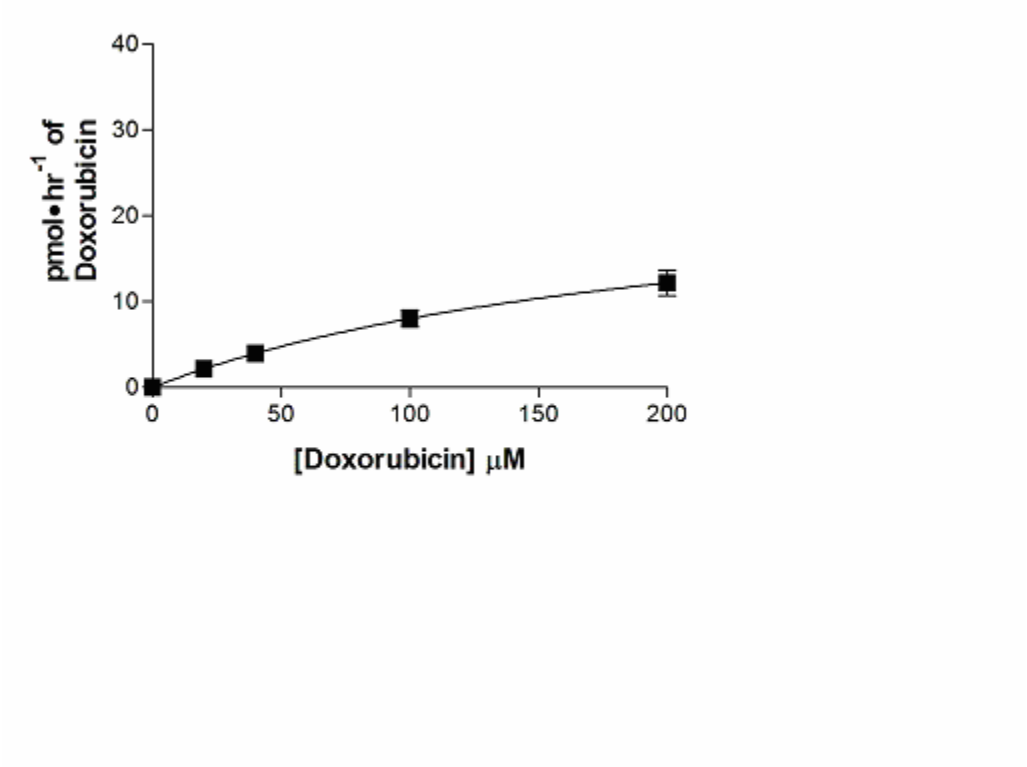

Figure 39: The P-gp-dependent transport of doxorubicin in the presence of GF120918. The transport of doxorubicin to the apical compartment was determined at varying concentrations of doxorubicin (0 to 200 µM) in the basolateral compartment in the presence of 0.33 µM GF120918. Results are shown as mean (triplicate) ± S.D..

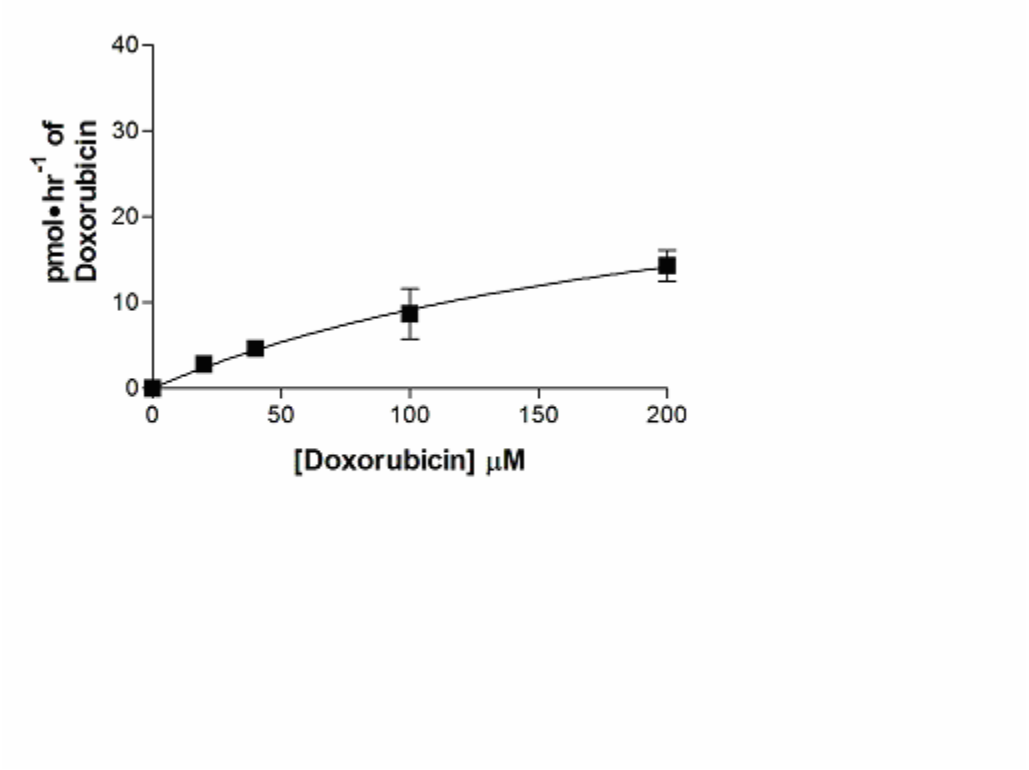

Table 5: Apparent Km and Ki values of doxorubicin, cyclosporine, and GF120918.

	Km µM (95% C.I.)	Ki µM (95% C.I.)
Doxorubicin	65.7 (40.0 to 91.5)	--
Cyclosporine	--	2.96 (1.84 to 4.09)
GF120918	--	0.085 (0.053 to 0.116)

D. In Vivo Inhibition of P-gp

Nelfinavir was used as a model P-gp substrate to determine the effects of GF120918 and cyclosporine on P-gp at the BBB. Using mdr1a knockout mice, P-gp shows its greatest effect on nelfinavir in limiting its CNS distribution compared to the other HIV protease inhibitors (Choo et al., 2000). Therefore, nelfinavir was chosen as the model P-gp substrate. The concentrations of GF120918 and cyclosporine were measured and compared to the in vitro inhibitory constants of P-gp.

1. Pharmacokinetic Studies with Nelfinavir

An i.v. bolus dose of nelfinavir (12 $mg \bullet kg^{-1}$) was given to 3 rats in order to determine the pharmacokinetics of nelfinavir. Figure 40 shows the concentration-time profile of nelfinavir over 5 hours. Table 6 shows the pharmacokinetic results from the i.v. bolus. The systemic clearance (12 $ml \bullet min^{-1}$) of nelfinavir is very close to the hepatic blood-flow of a rat (Davies and Morris, 1993) (13.8 $ml \bullet min^{-1}$). This would suggest that the clearance of nelfinavir is blood-flow rate limited, and therefore, any inhibition of its metabolism would not likely affect its systemic clearance. This is important since nelfinavir is metabolized by CYP3A4 in humans (Baede-van Dijk et al., 2001) and most likely is metabolized by CYP3A in rats. The volume of distribution of nelfinavir is well above the total body water of a rat indicating that nelfinavir is well distributed throughout the body.

Figure 40: Concentration-time profile of nelfinavir after an I.V. bolus. Three rats were given an I.V. bolus of nelfinavir (12 mg•kg^{-1}). Insert shows the log concentration time profile. Results are shown as mean ± S.D..

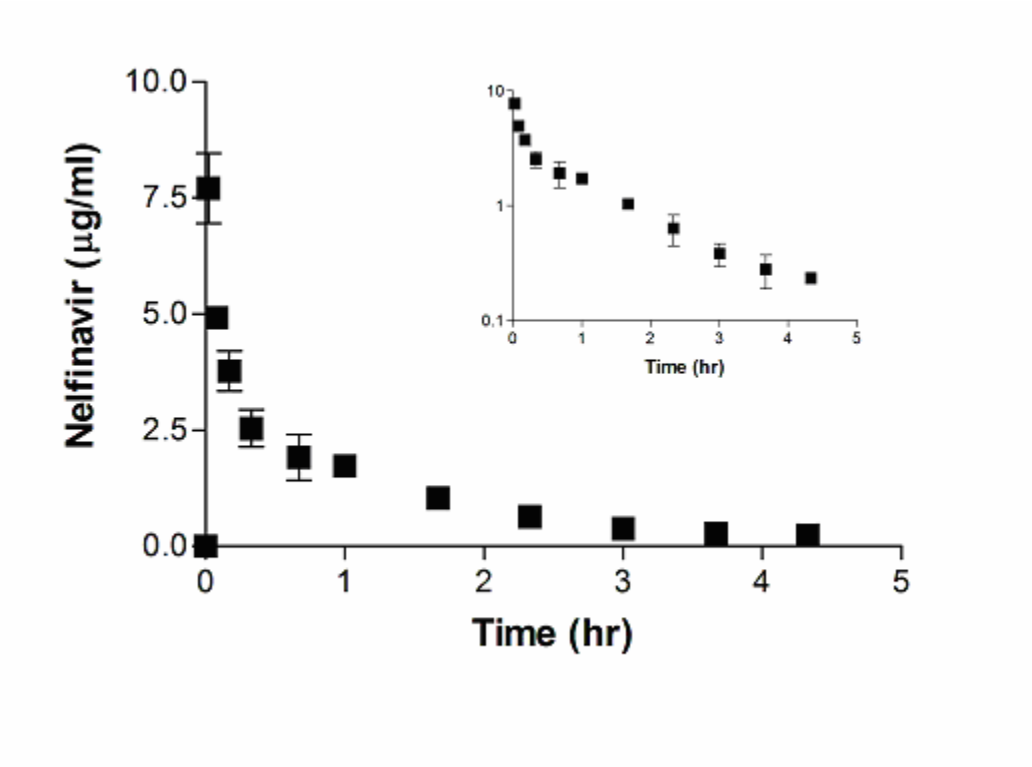

Table 6: The systemic clearance, volume of distribution$_{Steady\text{-}State}$, and terminal half-life of nelfinavir. Parameters were determined using noncompartmental pharmacokinetics analysis by Winnonlin 4.0.

	Mean ± Standard Deviation
Systemic Clearance	12 ± 5 ml•min^{-1}
Volume of Distribution$_{Steady\text{-}State}$	2.8 ± 0.3 L•kg^{-1}
Terminal Half-Life	1.0 ± 0.2 hr

2. Pharmacokinetics of Cyclosporine

An i.v. bolus dose of cyclosporine (20 mg•kg^{-1}) was given to 3 rats in order to determine the concentrations of cyclosporine that would be achieved during the infusion study with nelfinavir. The concentration-time profile of cyclosporine is shown in Figure 41. The blood concentrations of cyclosporine at 1 hour and 4 hour post injection were 18.2 μM ± 5.5 and 4.40 μM ± 0.5, respectively. These values are above the reported in vitro Ki value of cyclosporine for P-gp (2.96 μM) and CYP3A4 (1.64 μM).

Figure 41: Concentration-time profile of cyclosporine after an I.V. injection. Cyclosporine (20 mg•kg^{-1}) was given as an i.v. bolus dose to 3 rats. Blood samples were collected every hour, for 4 hours. Results are shown as mean (triplicate) ± S.D..

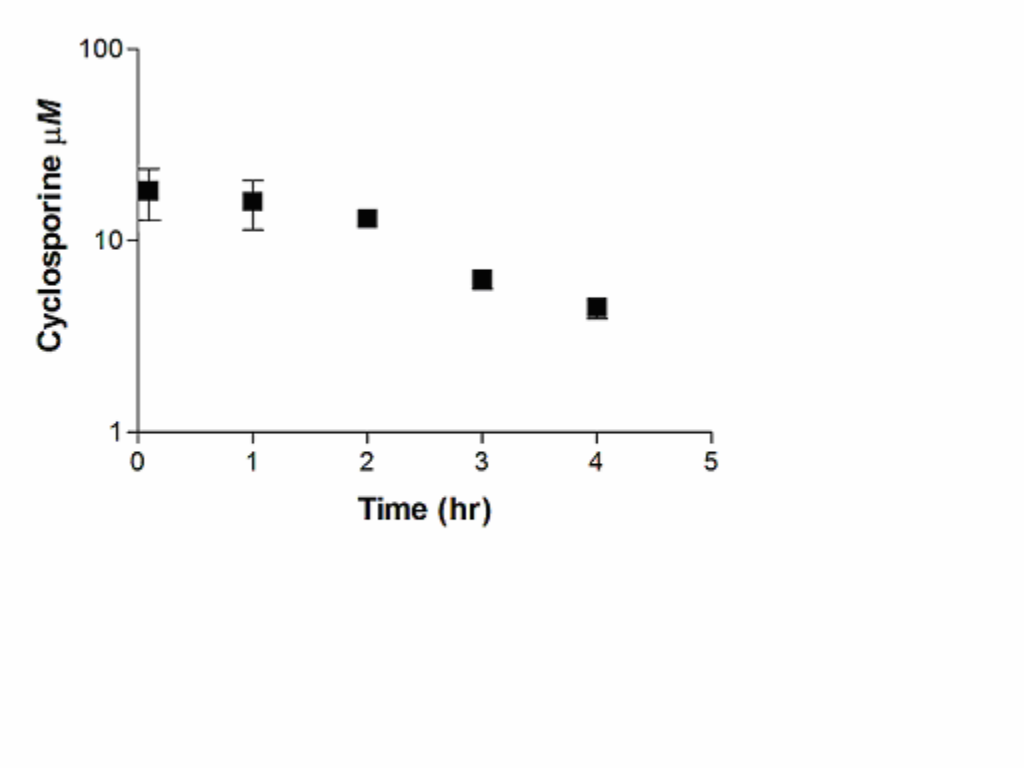

3. Pharmacokinetics of GF120918

An i.v. bolus dose of GF120918 (10 mg•kg^{-1}) was given to 3 rats in order to determine what concentrations of GF120918 would be achieved during the infusion study with nelfinavir. The concentration-time profile of GF120918 is shown in Figure 42. The concentrations of GF120918 at 1 hour and 4 hour post i.v. dose, were 4.31 μM ± 0.40 and 1.70 μM ± 0.65, respectively. The plasma concentrations of GF120918 observed in the rats were well above what was observed in mice given the same i.v. dose of GF120918 (Hyafil et al., 1993). Differences in the distribution and/or elimination of GF120918 might explain the higher concentrations. The concentrations of GF120918 were high enough to inhibit P-gp based on the in vitro inhibitory constant.

Figure 42: Concentration-time profile of GF120918 after an i.v. injection. GF120918 (10 mg•kg^{-1}) was given as an i.v. bolus dose to 3 rats. Results are shown as mean (triplicate) ± S.D..

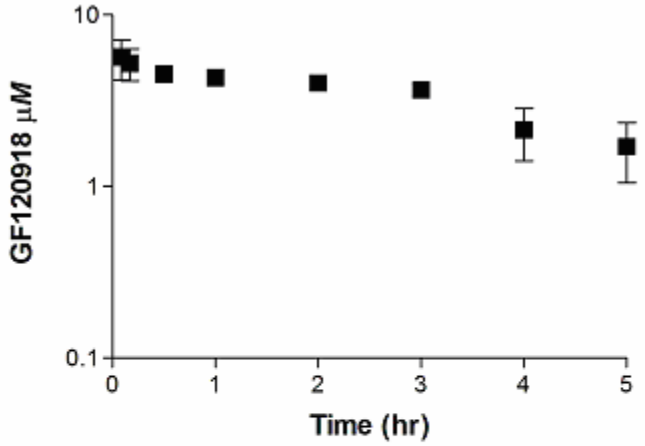

4. CNS Distribution of Nelfinavir

Figure 43 shows the plasma concentration-time profile of nelfinavir from a representative rat from the control, cyclosporine, and GF120918 treated animals. Nelfinavir was infused at a constant rate of 2.7 $mg \bullet hr^{-1}$, which should produce a steady-state concentration of 3.75 $\mu g \bullet ml^{-1}$. Nelfinavir appeared to be approaching steady-state plasma concentrations by 4 hours, with a mean plasma concentration of 2.20 ± 2.05, 1.45 ± 0.11, and 1.40 ± 0.52 $\mu g \bullet ml^{-1}$ for the control, cyclosporine, and GF120918, respectively, at 4 hours. There was no statistical difference ($p = 0.06$) between the 3 groups, although there was a significant amount of variation within each group. This variation is consistent with the i.v. bolus results which showed a significant amount of variation in the systemic clearance.

The brain concentrations (mean ± s.d.) of nelfinavir after the 4 hour infusion for control, cyclosporine, and GF120918 treated animals were 0.247 ± 0.274, 0.402 ± 0.267, and 9.56 ± 3.39, respectively. The brain to plasma ratio of nelfinavir is shown in Figure 44 (mean ± s.d). There was a statistically significant difference ($p < 0.001$) between the control and GF120918 treated animals. However, there was no statistical difference ($p > 0.05$) in the brain to plasma ratio of nelfinavir between the control and cyclosporine treated animals.

The concentrations of cyclosporine and GF120918 at 30 minutes and 4 hours are shown in Table 7 (mean ± s.d.). The concentrations of GF120918 were well above the in vitro inhibition constant for P-gp (0.085 μM). These results are consistent with the microdialysis data (Chapter 5.A.) and another report which used GF120918 to inhibit P-gp at the BBB to increase the distribution of amprenavir and nelfinavir into the CNS (Edwards et al., 2002; Savolainen et al., 2002). The concentrations of cyclosporine were within the range of the in vitro inhibition constant for P-gp (2.96 μM), however, no inhibition of P-gp at the BBB was observed. One possible explanation for this discrepancy is that cyclosporine is extensively bound in blood (Lemaire and Tillement, 1982). Cyclosporine is 44% bound to RBC and 95% bound to plasma proteins in rats. Accounting for the binding of cyclosporine from the RBC and plasma proteins the theoretical free concentration at 30 minutes and 4 hours would be 0.147 and 0.081 μM, respectively, and therefore cyclosporine would be well below the in vitro Ki for P-gp. Burgio et al. (Burgio et al., 1996) also did not observe any increase in the distribution of etoposide, a P-gp substrate, into the CNS with the co-administration of cyclosporine (5 $mg \bullet kg^{-1}$, i.v.). Arboix et al.

did not see an increase in the distribution of vinblastine into the CNS with the co-administration of cyclosporine (200 mg•kg^{-1}, intraperitoneally (i.p.)). There are two reports which show an increase in the distribution of vinblastine and doxorubicin into the CNS with the co-administration of cyclosporine (200 mg•kg^{-1}, i.p.), however, the plasma concentrations of vinblastine and doxorubicin also increased significantly (Zhang et al., 2000b; Saito et al., 2001). In fact, the increase in the concentration of vinblastine and doxorubicin in the plasma was greater than the increase in brain concentrations, indicating that the increases in CNS concentrations are due to changes in elimination rather than inhibition of P-gp at the BBB. The distribution of rhodamine into the CNS was increased significantly with the co-administration of cyclosporine (10 mg•kg^{-1}), in addition to a constant infusion of cyclosporine (1 mg•kg^{-1}•hr^{-1}) (Wang et al., 1995b). Differences in the concentration of cyclosporine between the different studies could explain the discrepancy. The rhodamine study by Wang et al. (Wang et al., 1995a) used a loading and a maintenance dose of cyclosporine, whereas the other studies just used a single dose only. The results from these studies would suggest that cyclosporine does not inhibit P-gp at the BBB when the blood concentrations of cyclosporine are in the range of 2.70 to 4.91 μM.

Figure 43: Concentration-time profile of nelfinavir in plasma for a representative rat in the control, cyclosporine, and GF120918 treated animals. A constant infusion of nelfinavir (2.7 mg•hr^{-1}) was given for 4 hours after an i.v. bolus of (a) DMSO (control), (b) cyclosporine (20 mg•kg^{-1}), and (c) GF120918 (10 mg•kg^{-1}).

a. Control

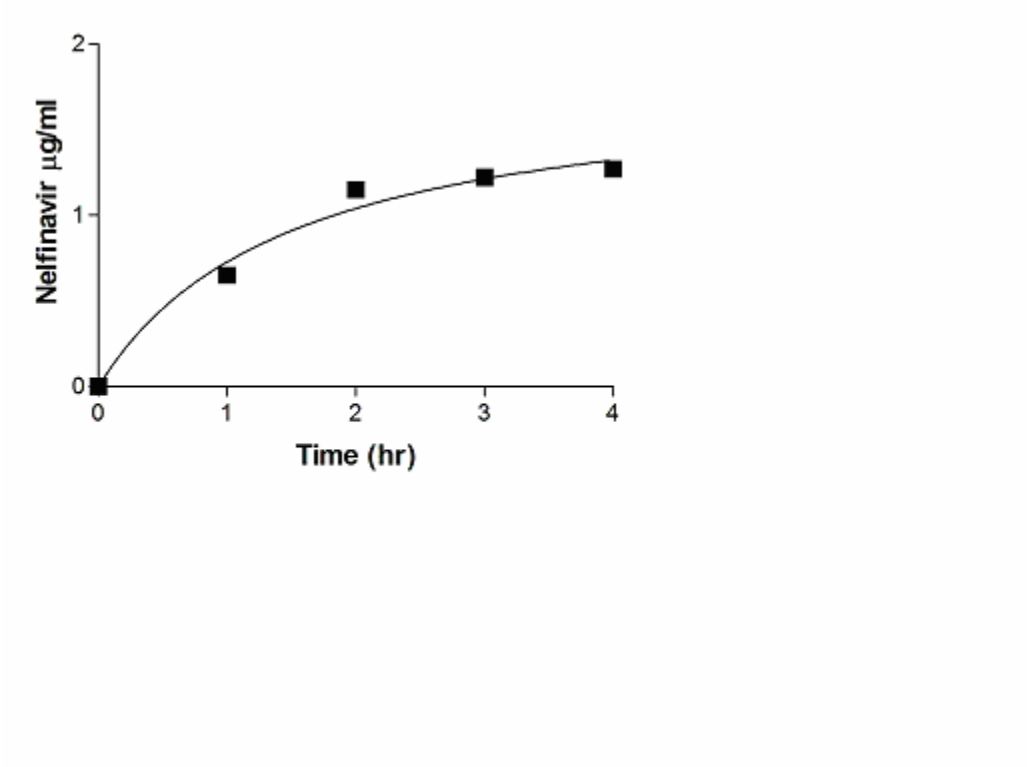

Figure 43: (Continued)

b. Cyclosporine

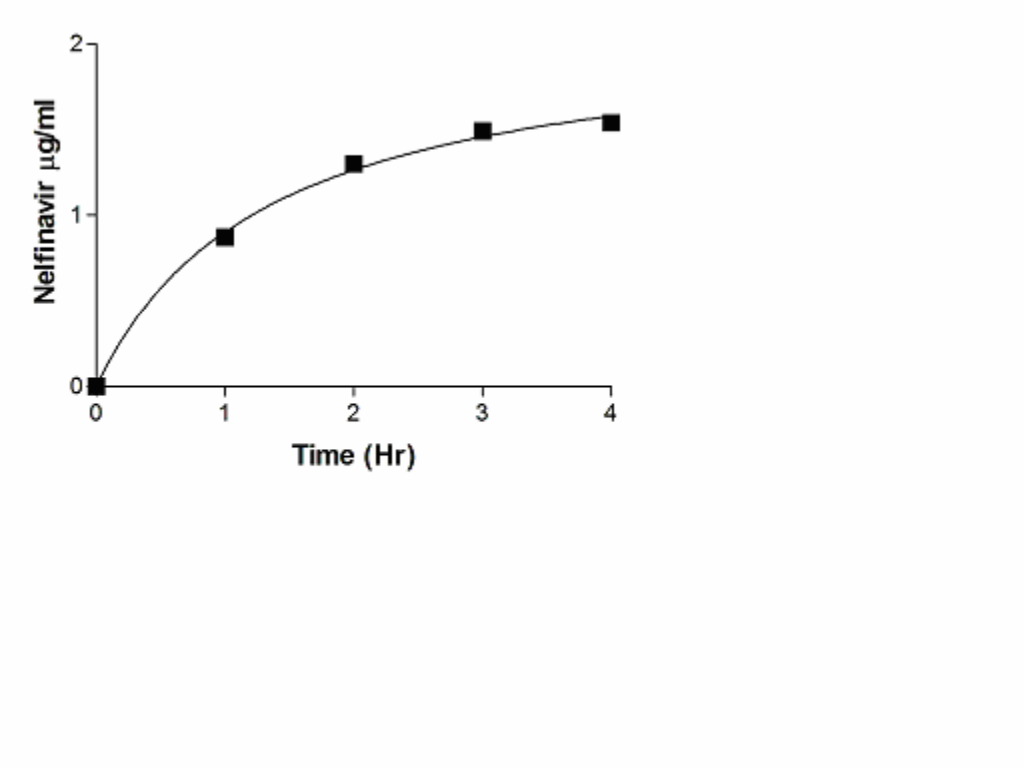

Figure 43: (Continued)

c. GF120918

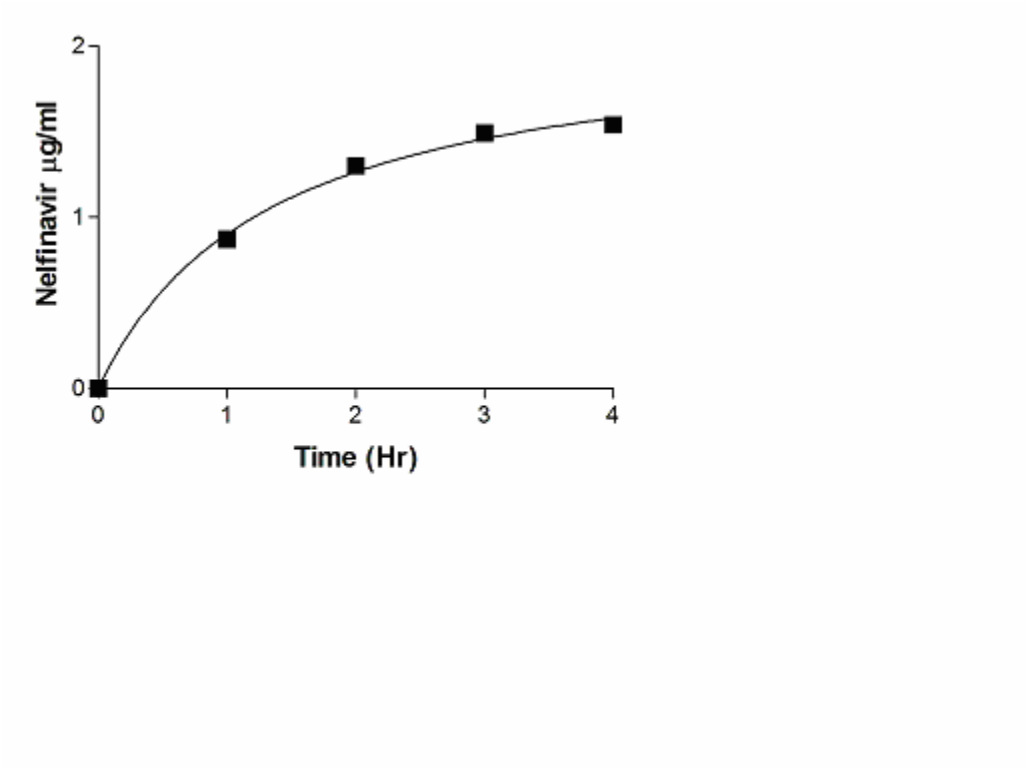

Figure 44: BBR of nelfinavir in the absence and presence of cyclosporine or GF10918. Nelfinavir was infused (2.7 mg•hr^{-1}) for 4 hours. The brain was removed after 4 hours. Results are shown as mean ±S.D. of 5 rats for each group.

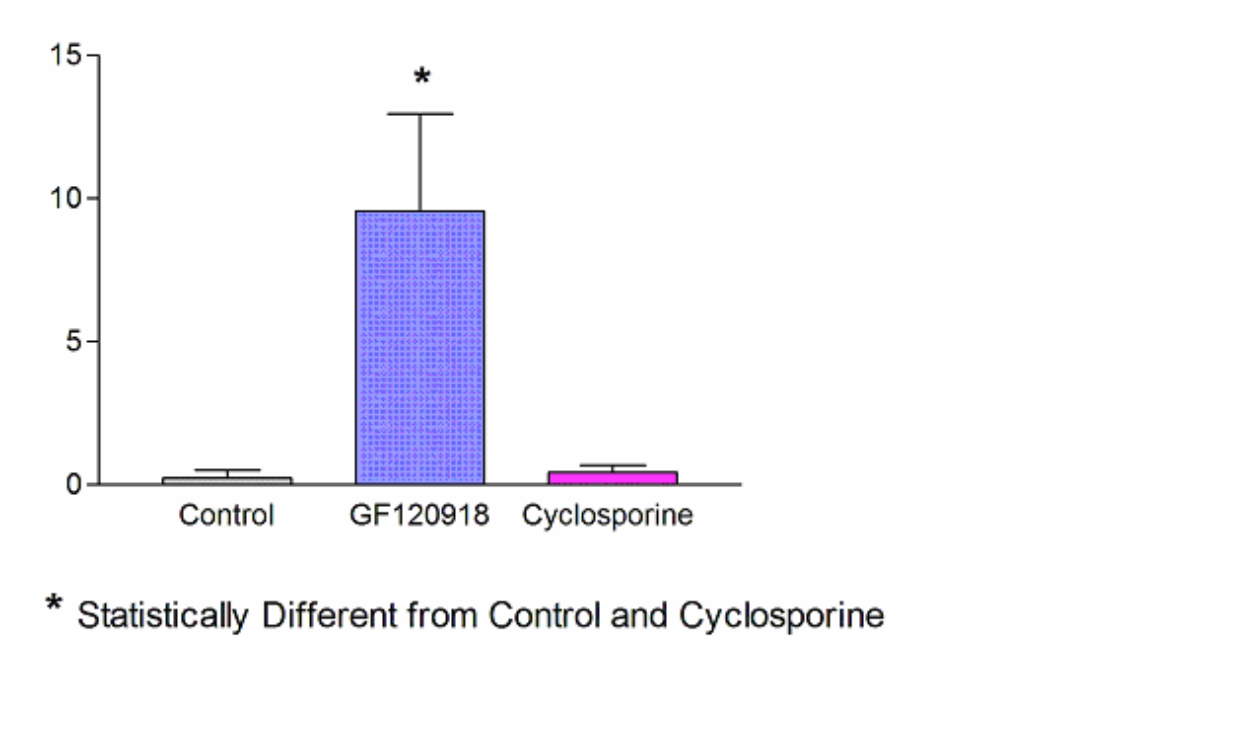

Table 7: Blood concentrations of cyclosporine and plasma concentrations of GF120918. The concentrations of GF120918 and cyclosporine at 30 minutes and 4 hours into the infusion of nelfinavir were determined. The results are shown as mean (n = 5) ± S.D..

	μM (Mean ± S.D.)	
	30 minutes μM	4 hours μM
GF120918	3.94 ± 1.12	1.64 ± 0.15
Cyclosporine	4.91 ± 0.43	2.70 ± 0.81

E. In Vivo Results for Midazolam

Midazolam was used as a model CYP3A substrate to determine the effects of GF120918 and cyclosporine on CYP3A metabolism in vivo. The systemic clearance of midazolam is similar to hepatic blood-flow and therefore its metabolism is most likely blood-flow rate limited (Kotegawa et al., 2002). Ketoconazole showed a greater effect on the oral clearance of midazolam compared to the systemic clearance, further suggesting that the elimination of midazolam is blood-flow rate limited. It has been shown that the liver is responsible for the majority of midazolam's oral clearance (Kotegawa et al., 2002) presumably by CYP3A metabolism.

1. Oral Clearance of Midazolam

The oral clearance of midazolam was used to determine the effects of cyclosporine and GF120918 on CYP3A metabolism in vivo. The plasma concentration-time profile of midazolam after a 15 mg•kg^{-1} oral gavage of midazolam is shown in Figure 45. The oral clearance and terminal half-life were determined to be 490 (336 to 644, 95% C.I.) ml•min^{-1}•kg^{-1} and 1.07 (0.91 to 1.24), 95% C.I.) hr, respectively. The oral clearance and terminal half-life of midazolam after an oral dose of midazolam (15 mg•kg^{-1}) has been reported to be 1054 ml•min^{-1}•kg^{-1} and 1.03 hr, respectively (Kotegawa et al., 2002). The terminal half-life of midazolam determined in these studies is similar to that of Kotegawa et al., however, the oral clearance in these studies is significantly lower. The oral clearances (mean ± S.D.) of midazolam for control, GF120918, and cyclosporine treated animals are shown in Figure 46. The oral clearance and terminal half-life of midazolam for the GF120918 treated animals were 509 ml•min^{-1}•kg^{-1} (354 to 664, 95% C.I.) and 1.14 (0.87 to 1.42, 95% C.I.) hr, respectively. GF120918 showed no significant effect on either parameter, which is consistent with the in vitro CYP3A4 results, where GF120918 (3.33 μM) showed no effect on metabolism. The concentrations of GF120918 at 0.5 and 4 hours post oral dose are shown in Table 8. The oral clearance and terminal half-life of midazolam for the cyclosporine treated animals were 69 (22.7 to 116, 95% C.I.) ml•min^{-1}•kg^{-1} and 1.32 (0.61 o 2.02, 95% C.I.) hr, respectively. Cyclosporine significantly decreased the oral clearance of midazolam, which is consistent with the inhibition of CYP3A4 in vitro. Cyclosporine has been

shown to inhibit the clearance of etoposide in rats, without inhibiting P-gp at the BBB (Burgio et al., 1996). The plasma concentrations of vinblastine and doxorubicin were also increased significantly with the co-administration of cyclosporine, further suggesting that cyclosporine can alter the metabolism of CYP3A substrates (Zhang et al., 2000b; Saito et al., 2001). The concentration of cyclosporine at 0.5 and 4 hours post oral dose are shown in Table 8.

Table 9 compares the in vitro and in vivo results for the inhibition of P-gp and CYP3A by GF120918. By comparing the in vitro Ki values for human P-gp and CYP3A4, it is apparent that GF120918 specifically inhibits P-gp over CYP3A4. This is consistent with the in vivo results using the rat model where GF120918 inhibited P-gp at the BBB, but had no effect of CYP3A metabolism. Table 10 compares the in vitro and in vivo results for the inhibition of P-gp and CYP3A by cyclosporine. The in vitro Ki values for human P-gp and CYP3A4 were not statistically different from one another. However, cyclosporine only inhibited CYP3A metabolism in vivo and not P-gp at the BBB. One explanation for this discrepancy is that the concentration of cyclosporine during the absorption phase of midazolam (between 0 to 30 minutes) was significantly higher than the measured concentration of cyclosporine at 30 minutes or 4 hours. Since the plasma concentration-time profile of cyclosporine has been shown to be biphasic after an i.v. bolus dose (Kawai et al., 1998), it is possible that the concentrations of cyclosporine at the initial time point (between 1 to 15 minutes) for the oral absorption of midazolam were significantly higher than the concentration of cyclosporine at 30 minutes. The results from these studies would indicate that GF120918 is a safer drug to administer for MDR modulation, since it does not appear to inhibit CYP3A4 and therefore should not affect CYP3A4 dependent metabolism of other drugs.

Figure 45: Concentration-time profile of midazolam in plasma. Concentration-time profile of midazolam in plasma for (a) control, (b) cyclosporine (20 mg•kg^{-1}), and (c) GF120918 (10 mg•kg^{-1}) treated animals. Rats were given an intragastric dose of midazolam (1.5 mg•kg^{-1}). Results are shown as mean ± S.D. of 5 rats for each group.

a. Control

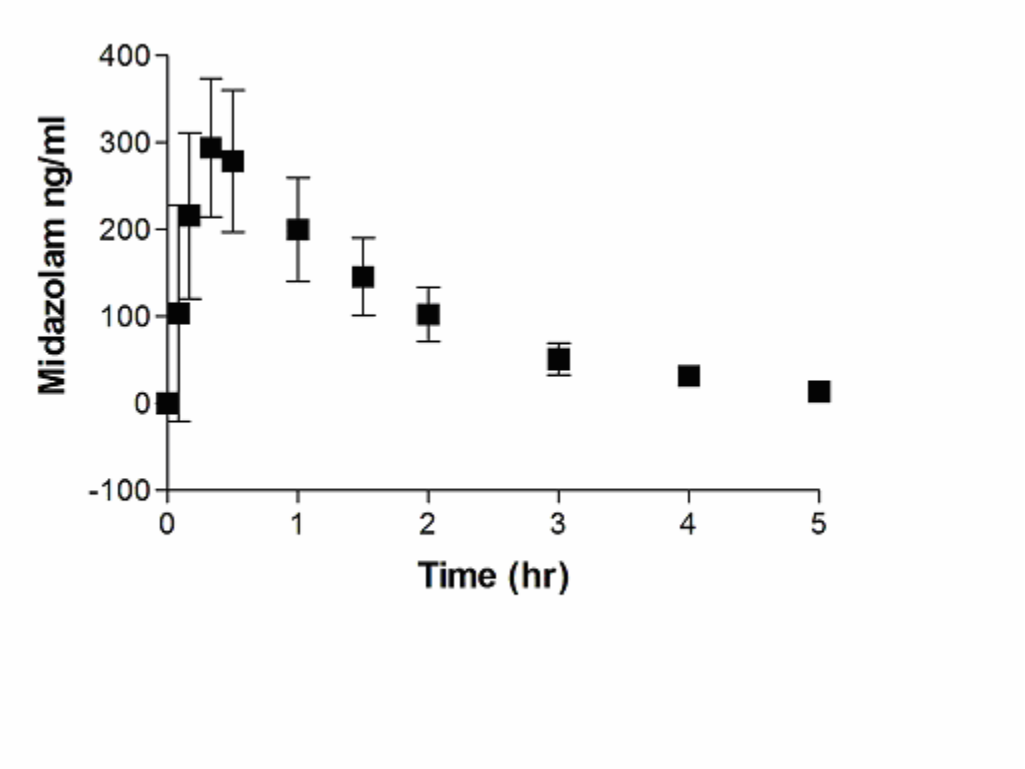

Figure 45: (Continued)

b. Cyclosporine

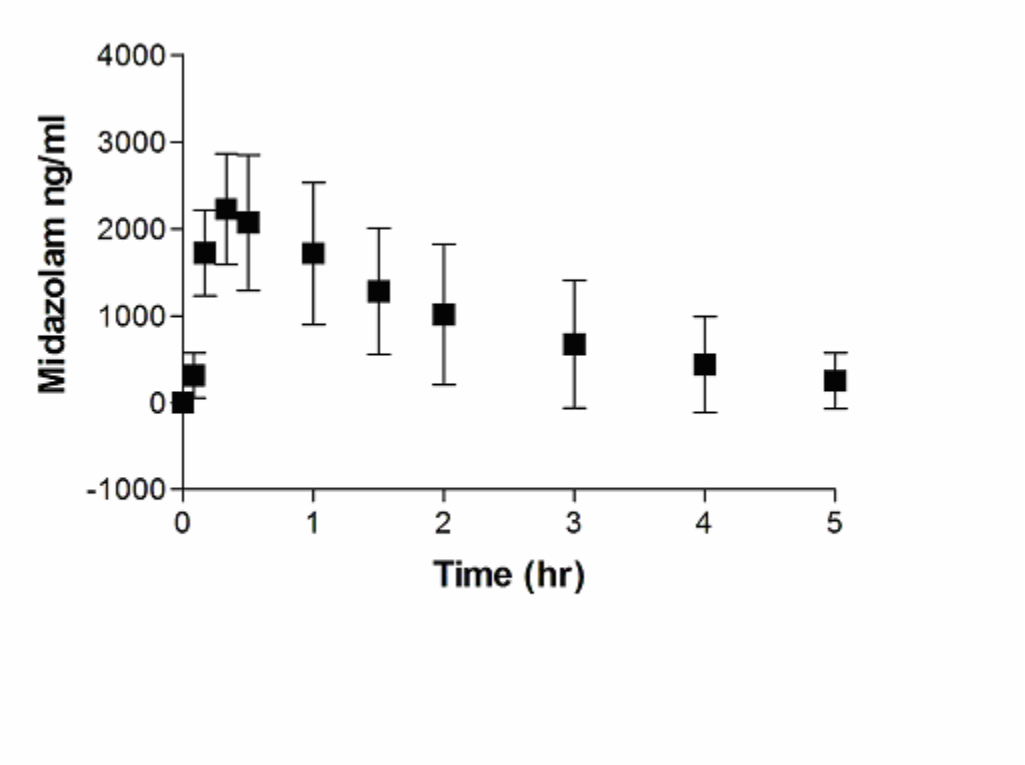

Figure 45: (Continued)

c. GF120918

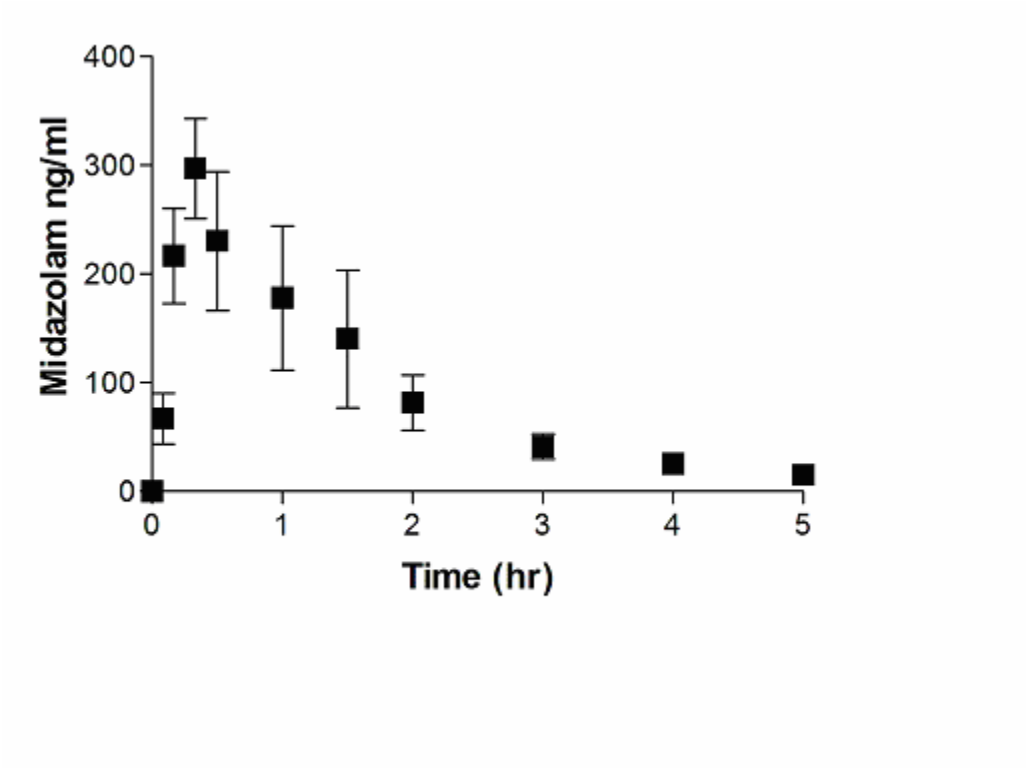

Figure 46: Oral clearance of midazolam after an intragastric dose (15 mg•kg-1). The oral clearance of midazolam was determined for control, GF120918 (10 mg•kg^{-1}), cyclosporine (20 mg•kg^{-1}) treated animals. Results are shown mean ± S.D. of 5 rats.

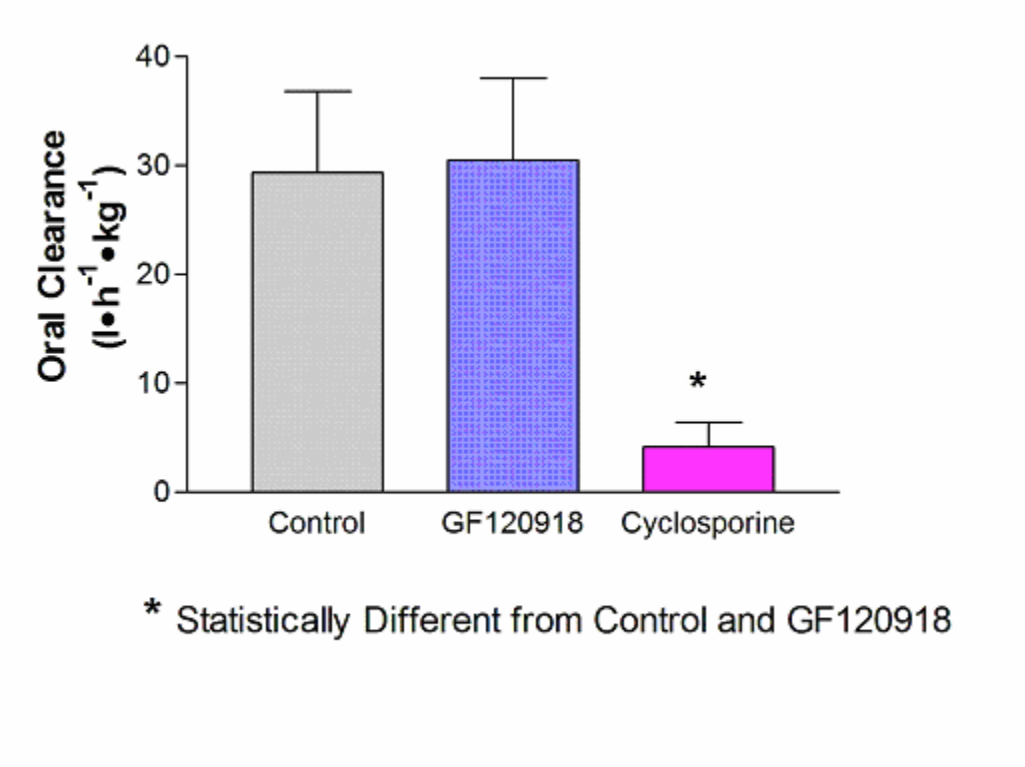

Table 8: Plasma and blood concentrations of GF120918 and cyclosporine, respectively. The concentrations of GF120918 and Cyclosporine at 30 minutes and 4 hours after an intragastric dose of midazolam (15 mg•kg^{-1}). Results are shown mean ± S.D. of 5 rats.

	30 minutes µM (S.D.)	4 hours µM (S.D.)
GF120918	4.00 ± 0.36	1.86 ± 0.11
Cyclosporine	4.06 ± 1.56	2.14 ± 1.00

Table 9: In vitro and in vivo inhibition of P-gp and CYP3A by GF120918.

	In Vitro (Human)	**In Vivo (Rat)**
P-gp	Ki = 85 nM	Inhibition of P-gp at BBB 1.64 to 3.94 μM
CYP3A	No Inhibition Observed up to 3.33 μM	No Inhibition of CYP3A Metabolism 1.86 to 4.00 μM

Table 10: In vitro and in vivo inhibition of P-gp and CYP3A by cyclosporine.

	In Vitro (Human)	**In Vivo (Rat)**
P-gp	Ki = 2.96 μM	No Inhibition of P-gp at BBB 2.70 to 4.91 μM
CYP3A	Ki = 1.64 μM	Inhibition of CYP3A Metabolism 2.14 to 4.06 μM

F. Expression of mdr1a and mrp1 at the BBB

1. Qualitative PCR

There are conflicting reports concerning the mRNA expression of mrp1 at the BBB. In order to further investigate this issue, capillary endothelial cells were isolated from rat brains and the mRNA expression of mdr1a and mrp1 was determined. One possible explanation for the conflicting reports is the contamination of isolated capillary endothelial cells by glial cells (e.g. astrocytes). Glial cells are also known to express drug transporters, including mrp1 (Ballerini et al., 2002). The mRNA expression of GFAP, a glial cell marker, was measured in the isolated endothelial cells to determine if there were glial cell contamination. The expression of PECAM was also measured as a marker of endothelial cells.

Brain capillary endothelial cells were isolated using density centrifugation. According to established methods, two fractions are produced from the centrifugation, a bottom fraction containing capillary endothelial cells and a top fraction containing glial cells, neurons, and fat. The mRNA from each fraction was isolated and converted to cDNA. Figure 47 shows the expression of PECAM and GFAP in the bottom fraction, top fraction, and in whole brains as determined using PCR (30 cycles). The bottom fraction (capillary endothelial cells) did not express GFAP at 30 cycles, suggesting that the isolated endothelial cells were not contaminated with glial cells. The bottom fraction did express PECAM, which is expected since it is an endothelial cell marker. The top fraction (capillary depleted fraction) expressed both GFAP and PECAM. The expression of PECAM in the top fraction would suggest that the isolation process did not recover all of the endothelial cells. This may help explain some of the discrepancy in the literature concerning the expression of drug transporters in the CNS. The expression of GFAP is consistent with the top fraction expressing glial cells. The whole brain homogenate contained both GFAP and PECAM, which is expected since both capillary endothelial cells and glial cells are found in the whole brain samples.

Figure 48 shows the expression of mdr1a and mrp1 in the two fractions and in whole brains. Mdr1a was expressed in both the top and bottom fraction. This is consistent with the expression of PECAM. Mrp1 was also expressed in the top and bottom fractions. Since the top fraction contains both endothelial cells and glial cells and the bottom fraction contains only

endothelial cells, this would indicate that mrp1 is located in capillary endothelial cells. However, the expression of GFAP changes at increasing number of cycles (Figure 49). At 25 and 30 cycles no GFAP is detected. However, at 40 and 50 cycles GFAP is detected in the bottom fraction, suggesting that there is some glial cell contamination. This also would help to explain some of the discrepancies in the literature concerning the location of mrp1. One way to overcome the difficulties of glial cell contamination is to determine the relative concentrations of PECAM, GFAP, mdr1a, and mrp1 and compare these expression profiles.

Figure 47: Expression of PECAM and GFAP in rat whole brain, capillary depleted, and capillary enriched homogenates. cDNA (0.1 µg/ml) from whole brain, capillary depleted, and capillary enriched homogenates was amplified using PCR (30 cycles). The products of the PCR were run on a 1.5 % agarose TBE gel.

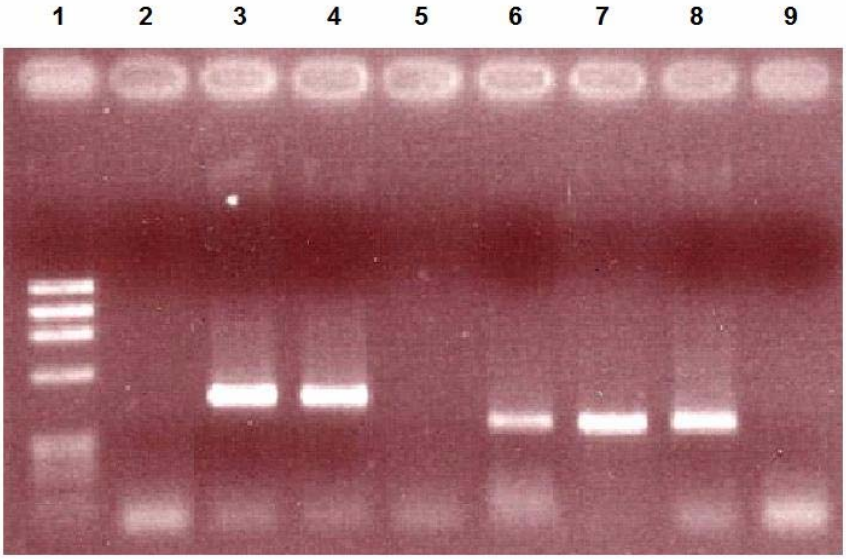

Lane	Source	Gene
1	ΦX174 RF DNA/*Hae III* Ladder	
2	Isolated Endothelial Cell Fraction	GFAP
3	Depleted Endothelial Cell Fraction	GFAP
4	Whole Brain	GFAP
5	Negative	GFAP
6	Isolated Endothelial Cell Fraction	PECAM
7	Depleted Endothelial Cell Fraction	PECAM
8	Whole Brain	PECAM
9	Negative	PECAM

Figure 48: Expression of mdr1a and mrp1 in rat whole brain, capillary depleted, and capillary enriched homogenates. cDNA (0.1 µg/ml) from whole brain, capillary depleted, and capillary enriched homogenates were amplified using PCR (30 cycles). The products of the PCR were run on a 1.5 % agarose TBE gel.

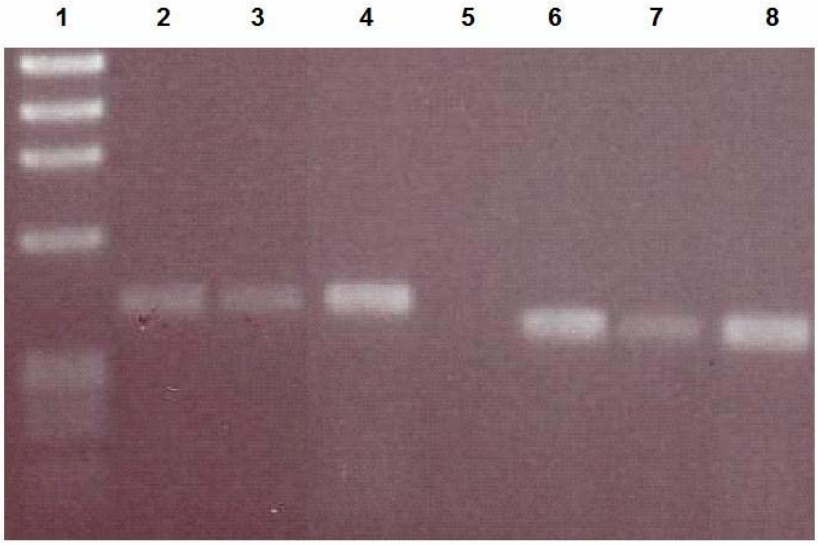

Lane	Source	Gene
1	ΦX174 RF DNA/*Hae III* Ladder	
2	Isolated Endothelial Cell Fraction	mdr1a
3	Depleted Endothelial Cell Fraction	mdr1a
4	Whole Brain	mdr1a
5	Negative	
6	Isolated Endothelial Cell Fraction	mrp1
7	Depleted Endothelial Cell Fraction	mrp1
8	Whole Brain	mrp1

Figure 49: Expression of β-actin and GFAP in capillary enriched homogenates. cDNA (0.1 µg/ml) from rat capillary enriched homogenates were amplified using PCR at 25, 30, 40, and 50 cycles. The products of the PCR were run on a 1.5 % agarose TBE gel.

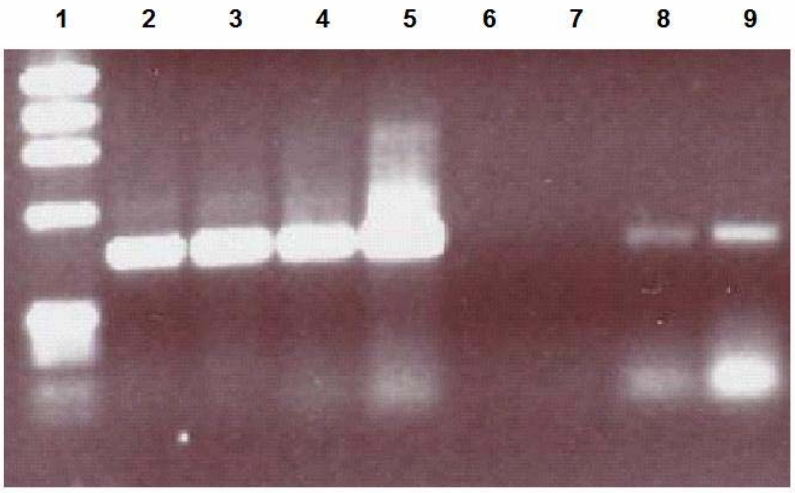

Lane	Number of Amplification Cycles	Gene
1	ΦX174 RF DNA/*Hae III* Ladder	
2	25	β-Actin
3	30	β-Actin
4	40	β-Actin
5	50	β-Actin
6	25	GFAP
7	30	GFAP
8	40	GFAP
9	50	GFAP

2. Quantitative PCR

Quantitative PCR was used to determine the relative expression of PECAM, GFAP, mdr1a, and mrp1. In addition, γ-glutamyl transferase activity was determined as a functional marker of the BBB. Since mdr1a is localized to the BBB, it was assumed that if mrp1 were localized to the BBB, then it too would be important in the distribution of HIV PIs into the CNS. The expression profile of PECAM, GFAP, mdr1a, mrp1, and γ-glutamyl transferase were compared to determine if mrp1 were localized to the BBB. Figure 50 shows the activity of γ-glutamyl transferase in the bottom fraction, top fraction, and rat whole brain. The activity was corrected for total protein levels using the Lowry method. All three fractions showed γ-glutamyl transferase activity. The activity in the top fraction and the whole brain was not significantly different ($p < 0.05$) from each other, suggesting that the percentage of endothelial cells is similar. This is consistent with the results from the qualitative PCR where PECAM was expressed in the top fraction and in whole brain. There was a statistically significant ($p < 0.05$) increase (8.7 fold) in the activity of γ-glutamyl transferase between the bottom fraction and the whole brain. This would indicate that there is an 8-fold enrichment in the amount of endothelial cells. This too is consistent with the qualitative PCR which showed no expression of GFAP but did express PECAM at 30 cycles.

Figure 50: γ-Glutamyl transferase activity in rat whole brain, capillary depleted, and capillary enriched homogenates. γ-Glutamyl transferase activity was corrected for total protein. Results are shown mean ± S.D. of 3.

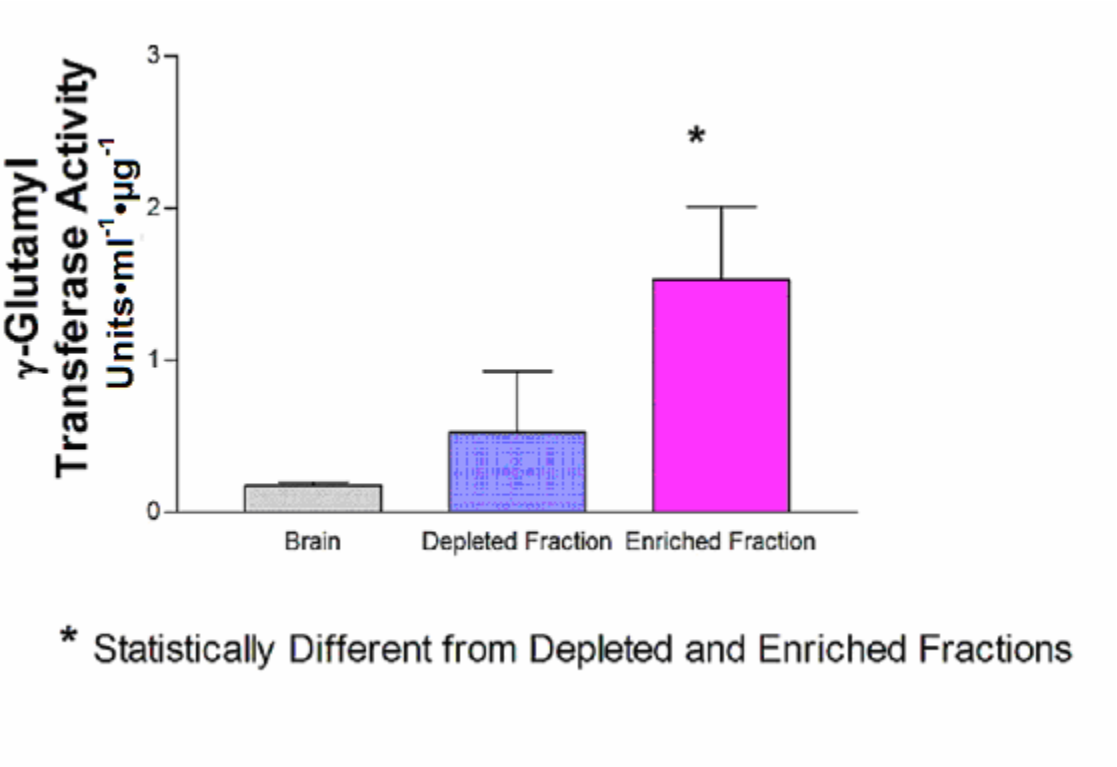

n = 3 for each group

The expression of PECAM, GFAP, mdr1a, and mrp1 were corrected using β-actin as a house keeping gene. Figure 51 (mean ± s.d.) shows the relative expression of PECAM in the bottom fraction, top fraction, and whole brain. The relative expression of PECAM for the whole brain and top fraction were not significantly different ($p > 0.05$) from each other. This is consistent with the γ-glutamyl transferase activity and confirms the observation that capillary endothelial cells are located in both fractions. There was a statistically significant ($p < 0.05$) increase (5.4 fold) in the relative expression of PECAM between the bottom fraction and whole brain. Again this is consistent with the γ-glutamyl transferase activity confirming an enrichment of capillary endothelial cells in the bottom fraction. The relative expression of GFAP is shown in Figure 52 (mean ± s.d.). There was no significant difference ($p = 0.15$) in the expression of GFAP in the top fraction, bottom fraction, or whole brain. This is consistent with the qualitative PCR where the expression of GFAP was observed at higher cycles (>30). However, it must be noted that the levels of GFAP in the isolated endothelial cells is similar to the levels in the top fraction and in whole brains. One possible explanation why higher PCR cycles were needed to observe the expression of GFAP in qualitative PCR versus quantitative PCR is that the primers used in the quantitative PCR were more efficient in amplifying GFAP as compared to the qualitative GFAP primers. Differences in primer efficiencies may also explain some of the differences observed in the literature concerning the expression of mrp1 at the BBB.

Figure 51: Relative expression of PECAM in rat whole brain, capillary depleted, and capillary enriched homogenates. cDNA (0.1 µg/ml) from whole brain, capillary depleted, and capillary enriched homogenates were amplified by PCR and quantified using SYBR green. PECAM expressions were corrected with β-actin. Results are shown mean ± S.D. of 3 rats.

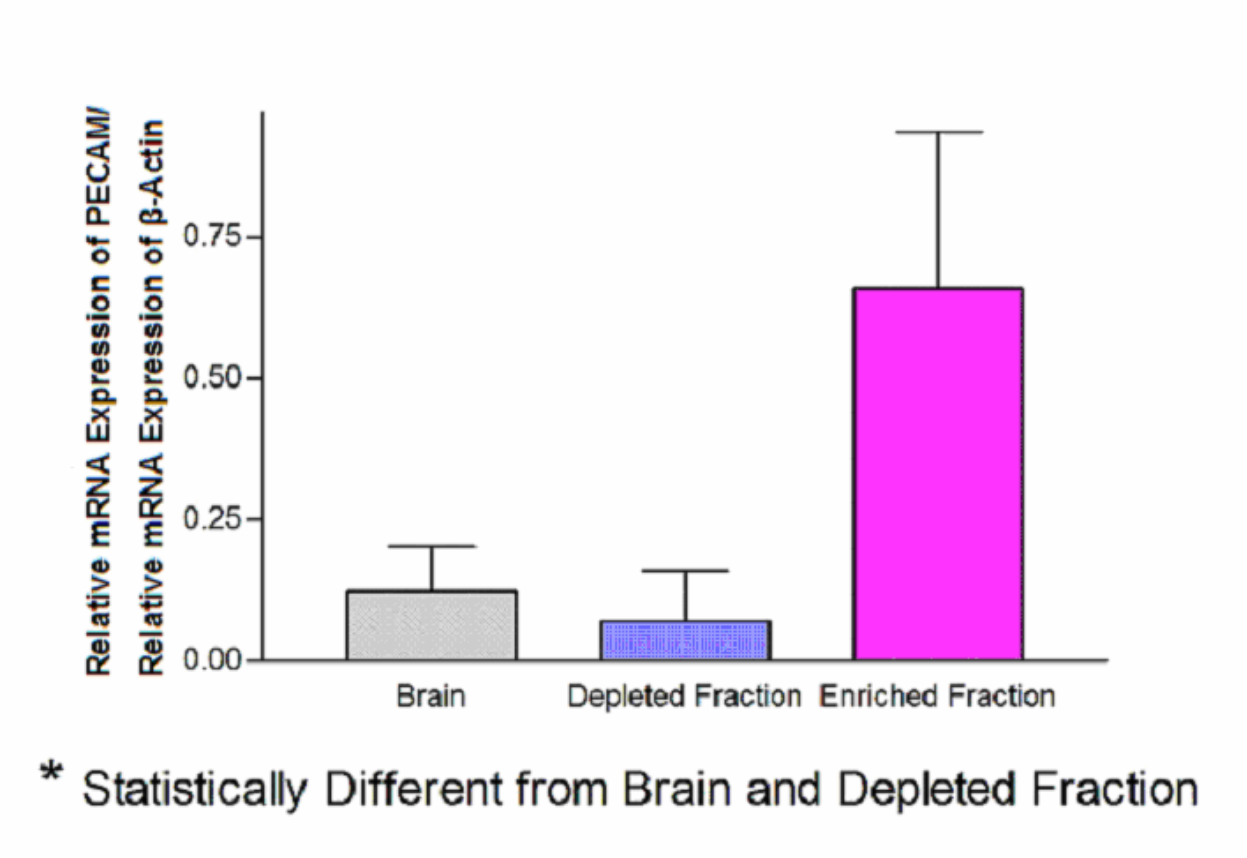

Figure 52: Relative expression of GFAP in rat whole brain, capillary depleted, and capillary enriched homogenates. cDNA (0.1 µg/ml) from whole brain, capillary depleted, and capillary enriched homogenates were amplified by PCR and quantified using SYBR green. GFAP expressions were corrected with β-actin. Results are shown mean ± S.D. of 3 rats.

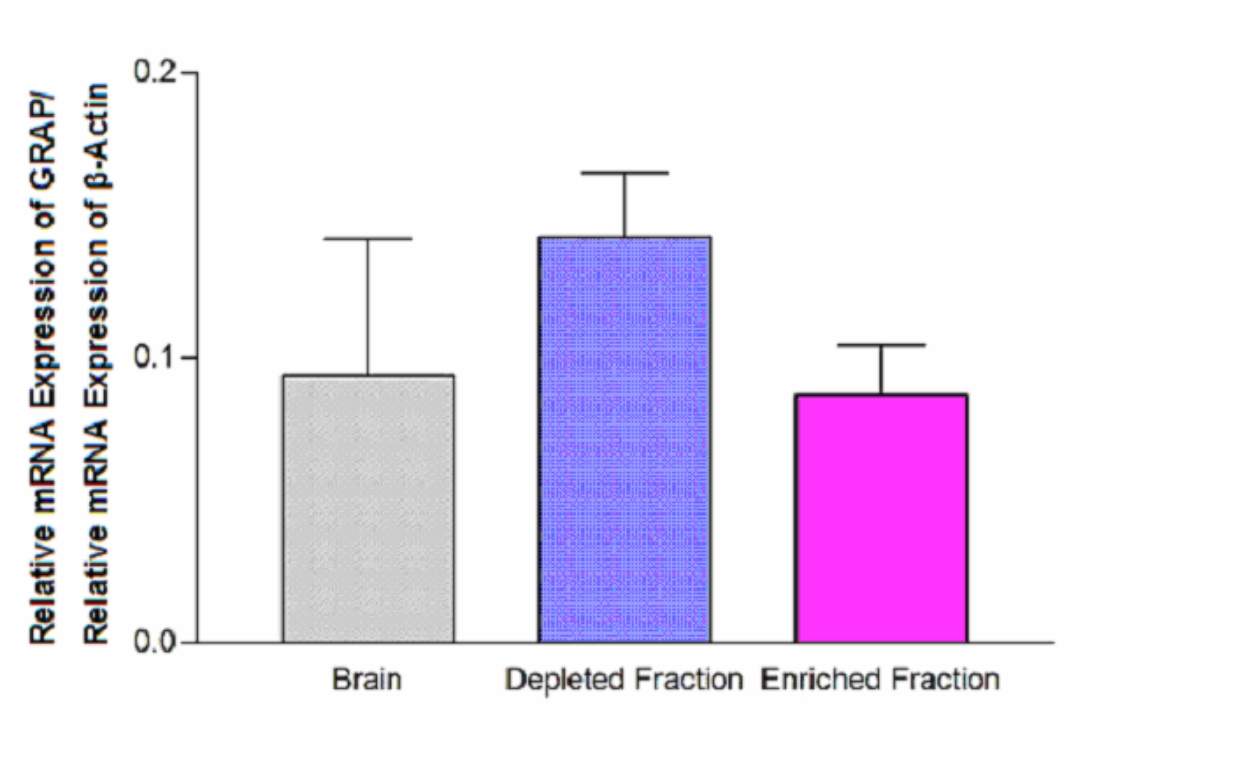

Figure 53 shows the relative expression of mdr1a. There was no significant difference ($p > 0.05$) between the top fraction and whole brain. There was a statistically significant ($p < 0.05$) increase (8.8 fold) in the mdr1a expression between the bottom fraction and the whole brain. This indicates that mdr1a is localized to the BBB which is consistent with other literature reports for mdr1a (Demeule et al., 2001). The relative expression of mrp1 (Figure 64) on the other hand did not show a statistically significant increase ($p = 0.82$) in expression in the bottom fraction. This would suggest that mrp1 is not localized to the BBB, however it should be noted that these experiments do not conclusively show the absence of mrp1 in endothelial cells. The parallel expression of GFAP and MRP1 was also observed in human brain tissue (Seetharaman et al., 1998a). From these studies it can be concluded that mrp1 is not localized to the BBB and therefore does not play a significant role in the distribution of HIV PIs into the CNS. Concurrent with these studies, a knockout mouse for mrp1 was developed and the CNS distribution of fluorescein, a model mrp1 substrate, was determined (Sun et al., 2001) in the knockout mouse. There was no significant difference in the CNS distribution of fluorescein between mrp1 knockout mice (mrp1 -/-) and wild-type mice (mrp+/+). These results are consistent with the findings in these studies.

Figure 53: Relative expression of mdr1a in rat whole brain, capillary depleted, and capillary enriched homogenates. cDNA (0.1 µg/ml) from whole brain, capillary depleted, and capillary enriched homogenates were amplified by PCR and quantified using SYBR green. Mdr1a expressions were corrected with β-actin. Results are shown mean ± S.D. of 3 rats.

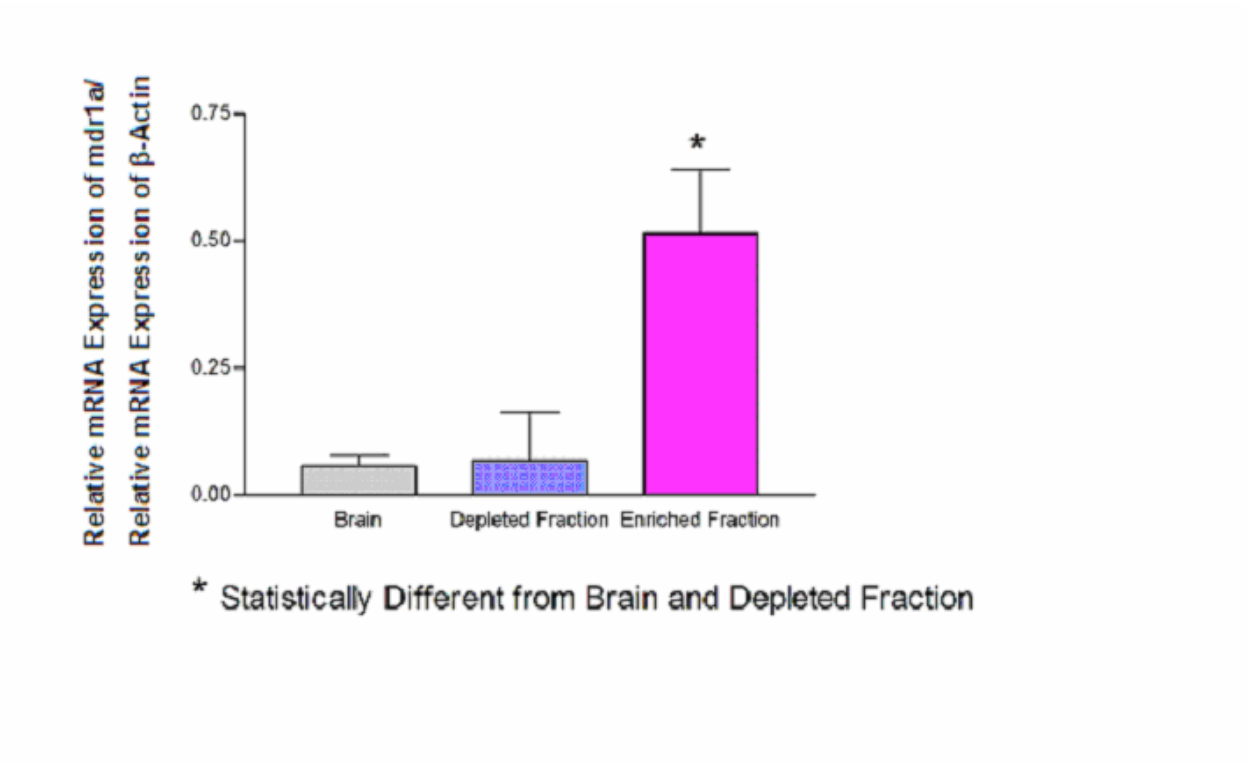

Figure 54: Relative expression of mrp1 in rat whole brain, capillary depleted, and capillary enriched homogenates. cDNA (0.1 µg/ml) from whole brain, capillary depleted, and capillary enriched homogenates were amplified by PCR and quantified using SYBR green. Mrp1 expressions were corrected with β-actin. Results are shown mean ± S.D. of 3.

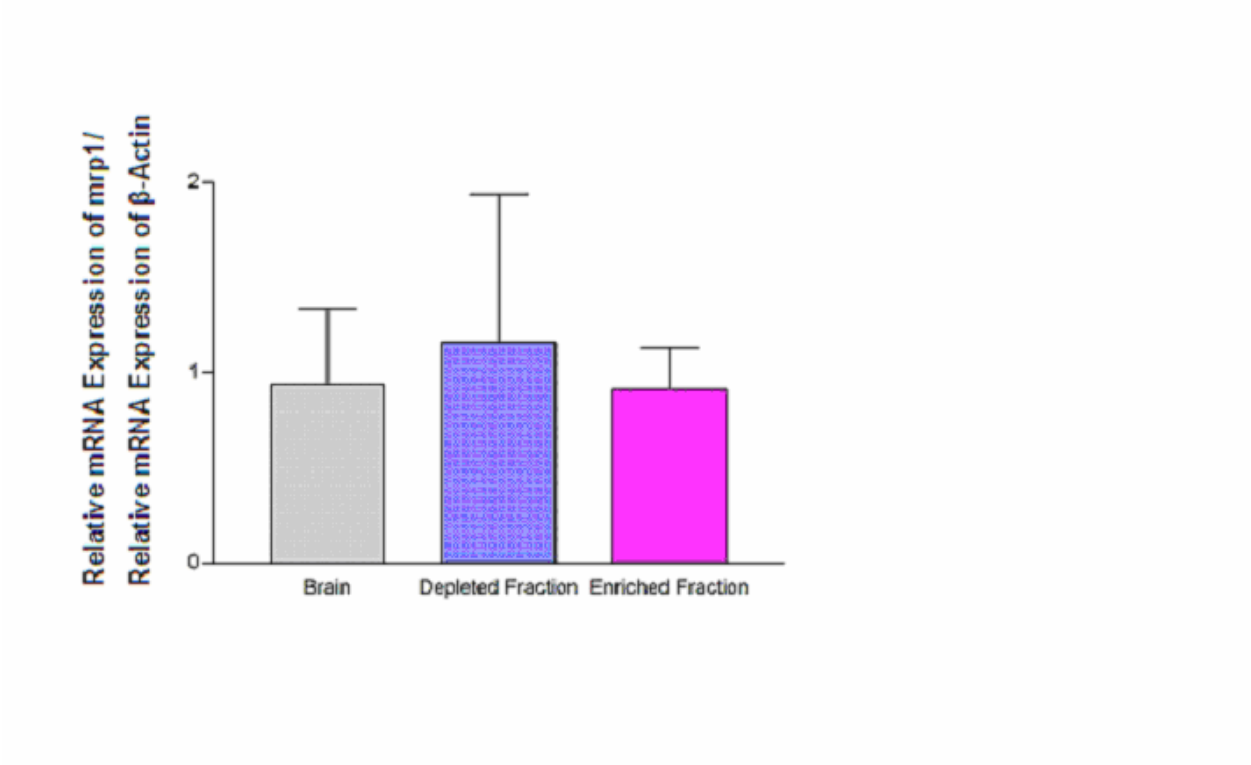

G. Distribution of Nelfinavir into Rat Milk

As mentioned previously, HIV reverse transcriptase inhibitors have been used to reduce the transmission of HIV from mother to child through breast milk. This leads one to postulate about the use of other antiretroviral drugs, including HIV protease inhibitors, to prevent the transmission of HIV from mother to child. Unfortunately, there is little information concerning the distribution of HIV protease inhibitors into breast milk. Therefore the distribution of nelfinavir into rat milk was determined as a first attempt to understand the distribution of HIV protease inhibitors into milk. Since nelfinavir is lipophilic, transcellular flux across the mammary epithelial cells should not be a barrier to its distribution. However, preliminary studies have shown the presence of mdr1b mRNA in rat mammary tissue. Therefore P-gp may play a role in the distribution of nelfinavir into milk. The protein expression of P-gp was determined in lactating rat mammary tissue. The effects of GF120918 on the distribution of nelfinavir into the CNS and milk were determined.

Figure 55 shows the western blot of rat mammary tissue and brain samples for P-gp using the C219 and JSB1 antibodies. The C219 is a mouse antibody against P-gp. However, C219 also reacts with MDR3, another ABC transporter. Therefore a second antibody, JSB1 was used to detect P-gp as well. JSB1 is a mouse antibody against hamster P-gp. It does not cross react with MDR3. The results of the western blot show the expression of P-gp in both rat mammary tissue and rat brains. This is consistent with the expression of mdr1b mRNA in rat mammary tissue and would suggest that P-gp may play a role in the distribution of HIV PIs into milk.

Figure 55: Western blot of P-gp in rat brain and mammary tissues using C219 (a) and JSB1 (b) antibody. Rat brain and mammary homogenates (40 µg total protein) were loaded onto a NuPAGE 4 to 12 % Bis-Tris gel and transferred to a PVDF membrane. Membranes were incubated with primary antibody (either C219 or JSB1, 250 ng/ml) and then incubated with a secondary antibody (1:25000 dilution) linked to alkaline phosphatase. Membranes were imaged using NBT/BCIP.

a. C219

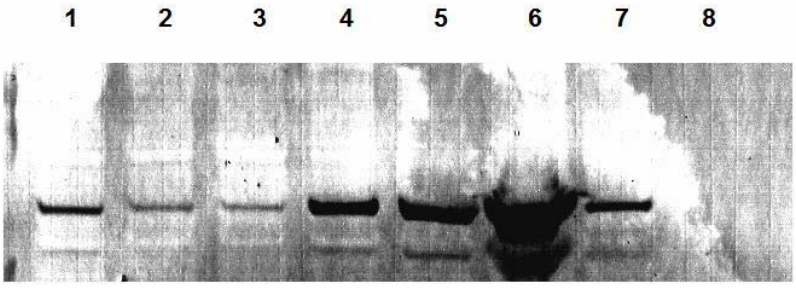

Lane	Sample
1	Brain #1
2	Brain #2
3	Brain #3
4	Mammary #1
5	Mammary #2
6	Mammary #3
7	Liver (Positive Control)
8	Negative Control

Figure 55: (Continued)

b. JSB1

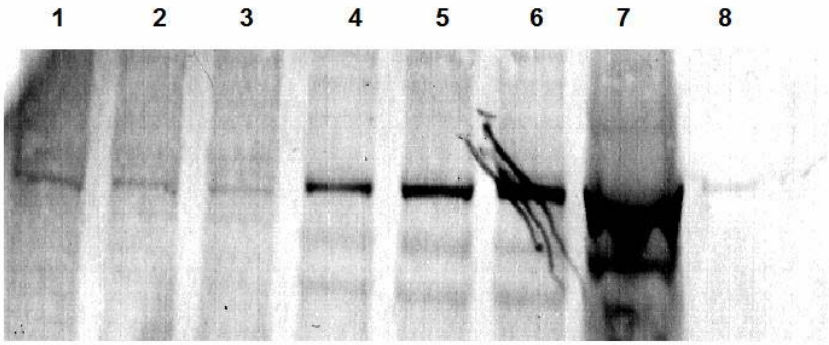

Lane	Sample
1	Brain #1
2	Brain #2
3	Brain #3
4	Mammary #1
5	Mammary #2
6	Mammary #3
7	Liver (Positive Control)
8	Negative Control

In order to determine the distribution of nelfinavir into milk,and if P-gp plays a significant role in the distribution of nelfinavir into milk, nelfinavir (2.7 mg•hr^{-1}) was infused into lactating rats for 8 hours. Using a cross-over design GF120918 or DMSO (vehicle) was given i.v. at 6 hours. Approximately 16 hours after the end of the first infusion the rat was given a second infusion of nelfinavir and was given the opposite treatment of GF120918 or DMSO as the previous day. The brain was removed from the rats at the end of the second infusion in order to determine the brain to plasma ratio. Plasma samples were collected during the infusion and a milk sample was taken after the 8 hour plasma sample. Figure 56 shows the concentration-time profile of nelfinavir for a representative rat in the GF120918 and control groups.

Figure 56: Concentration-time profile of nelfinavir in plasma from control (a) and GF120918 (b) treated rats. A constant infusion of nelfinavir (12 mg•kg^{-1}) was given for 8 hours. An i.v. dose of GF120918 or DMSO (vehicle) was given at 6 hours. Brain and milk samples were taken at 8 hours.

a. Control

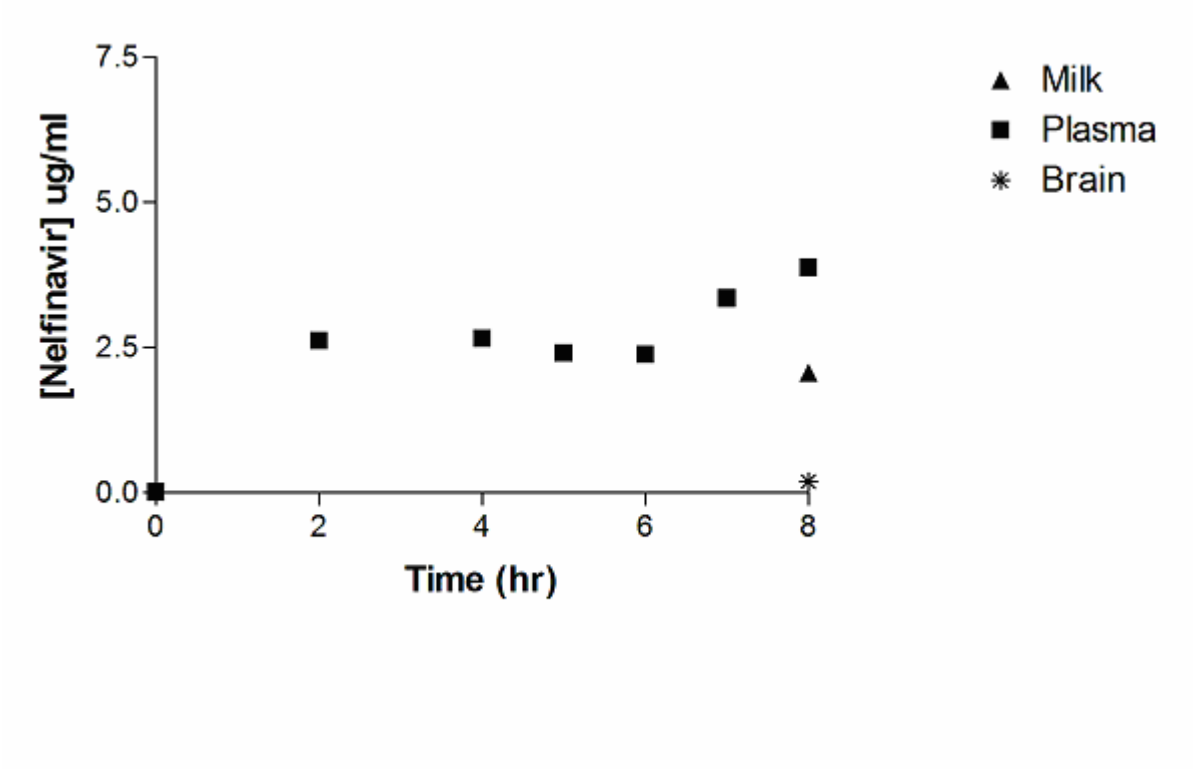

b. GF120918

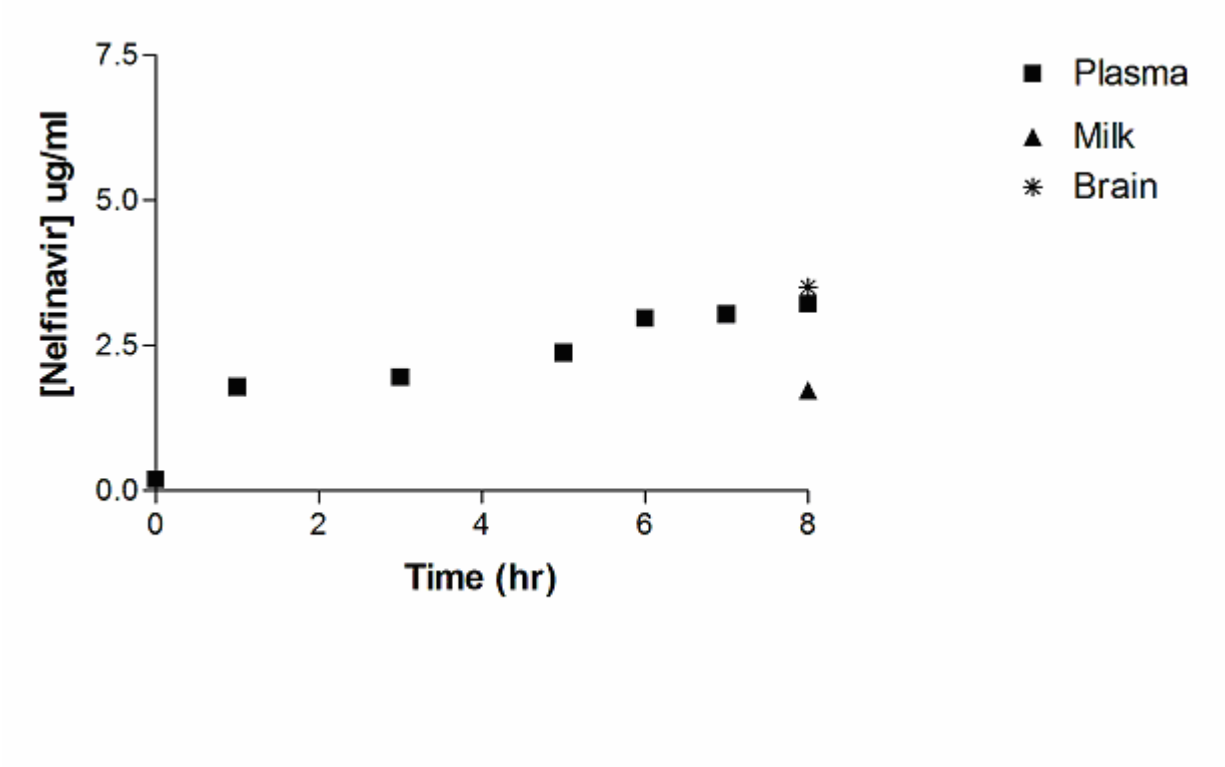

There was a high degree of variability in the plasma concentrations of nelfinavir as can be seen by the 8 hour plasma concentrations (Figure 57). There was no statistical difference ($p = 0.35$) between the control and GF120918 treated animals at 8 hours. Figure 58 shows the milk to plasma ratio of nelfinavir in the control and GF120918 treated animals. The average milk to plasma ratio of nelfinavir is 0.500 and 0.544 for the control and treated animals respectively. This indicates that nelfinavir does distribute into milk, but the concentrations are about half that of plasma concentrations. Nelfinavir is extensively bound to human plasma proteins, which may help to explain the lower concentration of nelfinavir in milk compared to plasma. There was no statistical difference (0.33) in the milk to plasma ratio of nelfinavir for GF120918 treated animals and control animals. There was a statistically significant difference ($p = 0.03$) in the brain to blood ratio of nelfinavir in the presence of GF120918 (Figure 59). This indicates that the concentrations of GF120918 should be enough to inhibit P-gp at the mammary epithelial barrier. These results suggest that P-gp does not play a significant role in the distribution of nelfinavir into milk, even though P-gp is expressed in rat mammary tissue.

Figure 57: Plasma concentrations of nelfinavir at 8 hours in rats. A constant infusion of nelfinavir (12 mg•kg^{-1}) was given for 8 hours. An i.v. bolus dose of GF120918 or DMSO (vehicle) was given at 6 hours. Results are shown as mean ± S.D. for 6 animals.

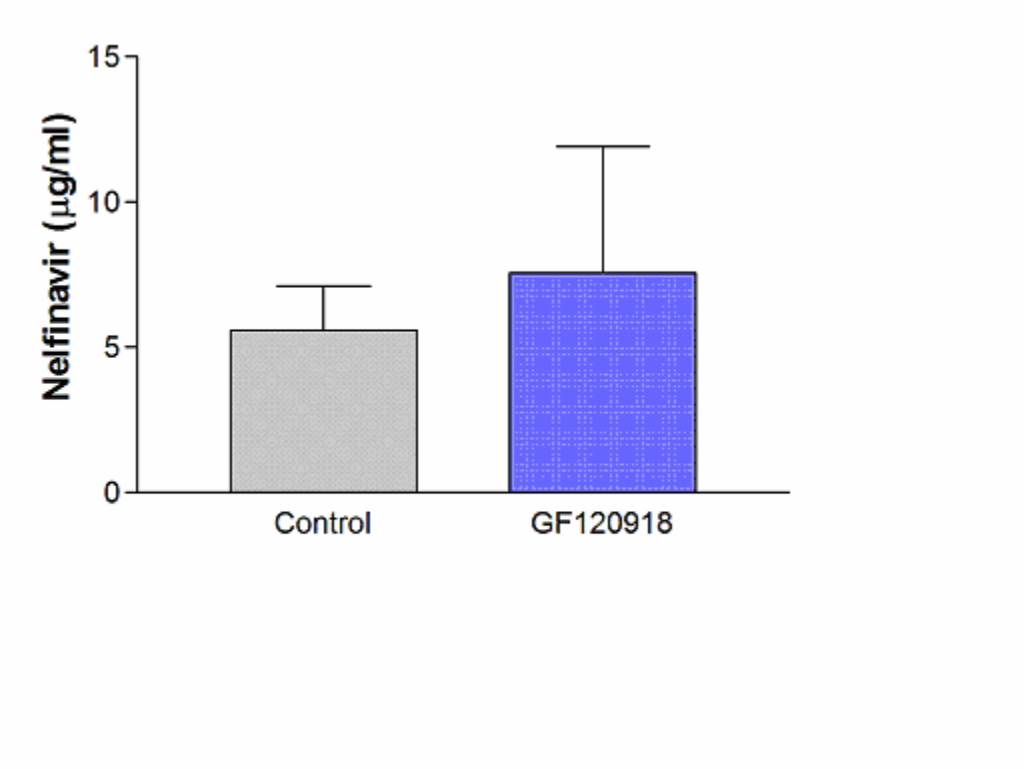

Figure 58: Milk to plasma ratio of nelfinavir at 8 hours in rats. A constant infusion of nelfinavir (12 mg•kg^{-1}) was given for 8 hours. An i.v. bolus dose of GF120918 or DMSO (vehicle) was given at 6 hours. Results are shown as mean ± S.D. for 6 animals.

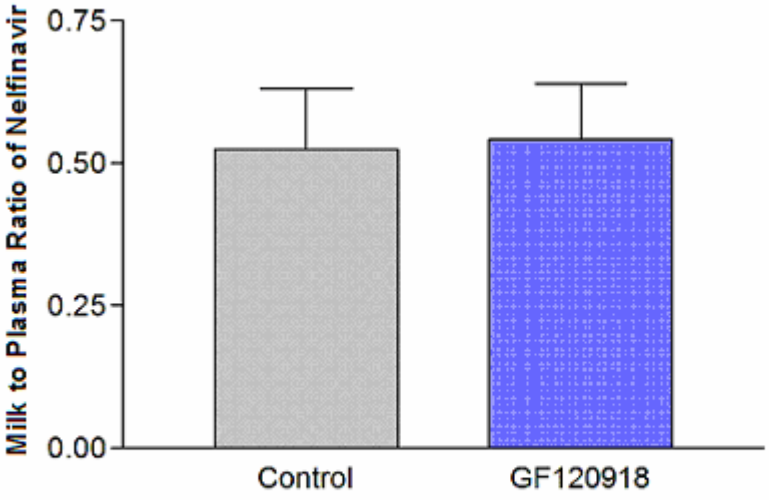

Figure 59: Brain to plasma ratio of nelfinavir at 8 hours in rats. A constant infusion of nelfinavir (12 mg•kg^{-1}) was given for 8 hours. An i.v. bolus dose of GF120918 or DMSO (vehicle) was given at 6 hours. Results are shown as mean ± S.D. for 3 animals.

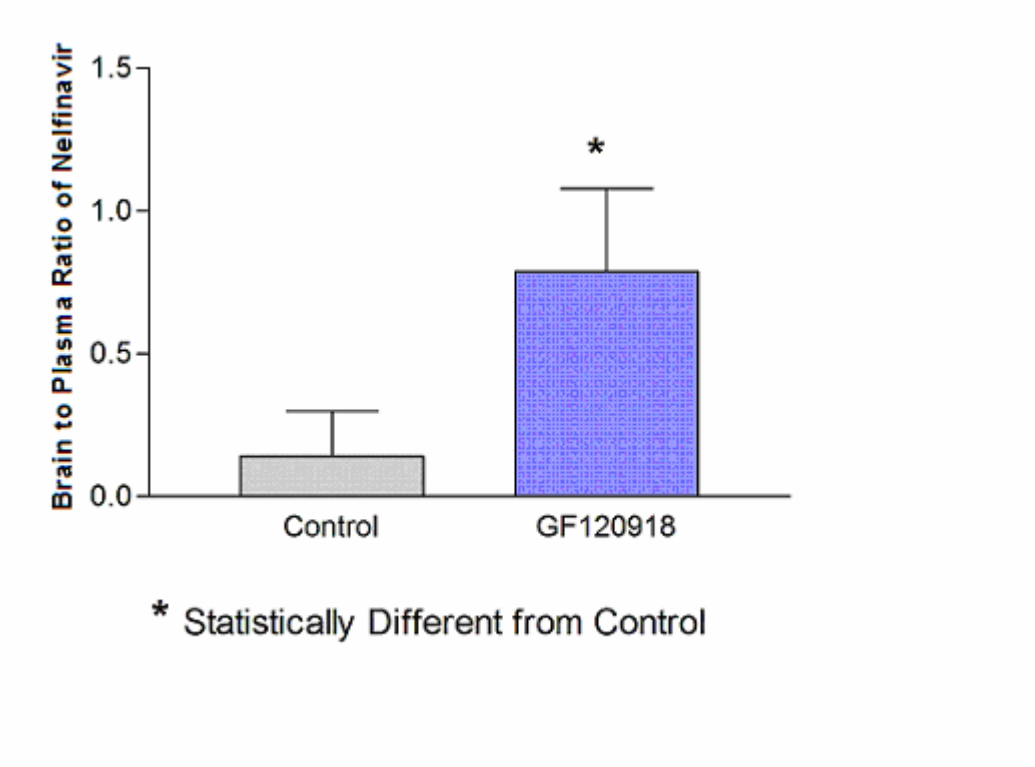

CHAPTER VI. CONCLUSIONS

This dissertation studied the distribution and modulation of HIV protease inhibitors into the CNS and milk of rats. MDR modulators have been shown to increase the distribution of HIV protease inhibitors into the CNS of rodents (Kim et al., 1998; Polli et al., 1999; Choo et al., 2000). HIV protease inhibitors are significantly bound to plasma binding proteins, including α-1-acid glycoprotein and albumin (Acosta et al., 2000; Acosta, 2002). Unfortunately, the previously mentioned studies did not discriminate between the effects of the MDR modulators on inhibiting P-gp at the BBB and the displacement of the HIV protease inhibitors from plasma binding proteins. As part of this dissertation, a third generation MDR modulator, GF120918, was administered to rats and caused an 8-fold increase in the unbound concentration of amprenavir, an HIV protease inhibitor, in the CNS. GF120918 showed no significant effect on the unbound blood concentrations of amprenavir, indicating that the increase in the CNS distribution of amprenavir is due to inhibition of P-gp at the BBB and not displacement of amprenavir from plasma binding proteins.

Clinically, MDR modulators have been shown to reduce the elimination of antineoplastic drugs (Lum et al., 1992; Raderer and Scheithauer, 1993; Lum and Gosland, 1995). One reason for the reduction in the elimination of these antineoplastic drugs is that many MDR modulators inhibit CYP3A metabolism (Wandel et al., 1999). This enzyme is responsible for metabolizing numerous xenobiotics including antineoplastic drugs and HIV protease inhibitors (Raderer and Scheithauer, 1993; Acosta, 2002). A principal goal of this dissertation was to determine the selectivity of GF120918 for inhibition of P-gp transport and CYP3A metabolism. In vitro, GF120918 showed no effect on CYP3A4 (human) metabolism, but did inhibit P-gp dependent transport (human), indicating that, at least in vitro, GF120918 is a selective inhibitor of P-gp transport over CYP3A4 metabolism. In rats, GF120918 inhibited P-gp at the BBB, but showed no effect of CYP3A metabolism. This is consistent with the in vitro results which show GF120918 to be a selective inhibitor of P-gp. Cyclosporine inhibited CYP3A4 (human) metabolism and P-gp (human) transport in vitro. The inhibition constants of cyclosporine for CYP3A4 and P-gp transport were not significantly different from one another, indicating that in vitro cyclosporine is not a selective inhibitor of P-gp. In rats, cyclosporine inhibited CYP3A metabolism, but showed no effect on P-gp transport at the BBB. The inconsistency between the

in vitro and in vivo results for cyclosporine may be due to interspecies differences in CYP3A or P-gp since human proteins were studied in vitro and comparisons made in vivo with the rat. Another reason for observing such a large effect of cyclosporine on CYP3A in vivo was that such inhibition would have been magnified by decreasing both the first pass effect and systemic clearance of midazolam.

HIV protease inhibitors are also transported by MRP1 (Jones et al., 2001a; van der Sandt et al., 2001; Williams et al., 2002), and therefore, another goal of the dissertation was to determine if mrp1 plays an important role in the distribution of HIV protease inhibitors into the CNS of rats. MRP1 is expressed in the CNS, but there are conflicting reports concerning the mRNA expression of MRP1 at the BBB (Huai-Yun et al., 1998; Regina et al., 1998; Seetharaman et al., 1998a; Decleves et al., 2000; Zhang et al., 2000a). Mrp1 is expressed in glial cells (Ballerini et al., 2002) and therefore it is possible that the initial reports which indicated that mrp1 is expressed at the BBB (Huai-Yun et al., 1998; Regina et al., 1998; Decleves et al., 2000; Zhang et al., 2000a), might have also been contaminated with glial cells. Mdr1a has been shown to be localized to the BBB (Seetharaman et al., 1998a) and therefore an assumption of this dissertation was that if mrp1 was also localized to the BBB, then it would be important in the distribution of HIV protease inhibitors into the CNS. In studies conducted as part of this dissertation, the activity of γ-glutamyl transferase and the mRNA expression of PECAM, markers of capillary endothelial cells (the BBB) and mRNA expression of GFAP, a marker of glial cells were measured in isolated capillary endothelial cells and whole rat brain homogenates. The expression profile of γ-glutamyl transferase, PECAM, and GFAP were compared to the mRNA expression of mdr1a and mrp1. The endothelial cell fraction isolated from rat brains contained glial cells. There was a >5 fold increase in the expression of γ-glutamyl transferase activity, PECAM mRNA, and mdr1a mRNA in the isolated endothelial cell fraction. This indicates that mdr1a is localized to the BBB, which is consistent with other literature reports (Seetharaman et al., 1998a). By contrast, there was no increase in the expression of mrp1 mRNA in the isolated endothelial cell fraction, which indicates that mrp1 is not localized to the BBB. Assuming that only transporters that are localized to the BBB play a significant role in the distribution of xenobiotics into the CNS, then mrp1 does not play a significant role in the distribution of HIV protease inhibitors into the CNS of rats.

Antiretroviral drugs have been used to reduce the transmission of the HIV virus from mother to child during breast feeding (Fowler and Newell, 2002). Another goal of the thesis was to determine the distribution of nelfinavir into rat milk as a first approach in understanding the extent to which HIV protease inhibitors can accumulate into milk. Current studies documented the presence of P-gp in lactating rat mammary tissue. Therefore a possible role of P-gp in the distribution of HIV protease inhibitors into rat milk was examined. The distribution of nelfinavir into rat milk was determined by measuring the milk to plasma ratio of nelfinavir after an 8 hour infusion. The milk to plasma ratio of nelfinavir was measured in the presence and absence of GF120918 in order to determine if P-gp plays a significant role in the distribution of HIV protease inhibitors into milk. GF120918 had no significant effect on the distribution of nelfinavir into rat milk and therefore it was concluded that P-gp does not play a significant role in the distribution of HIV protease inhibitors into rat milk. The concentration of nelfinavir in milk was approximately half that of the plasma concentration (milk to plasma ratio = 0.5). Potentially, the administration of nelfinavir and other HIV protease inhibitors could prevent the transmission of HIV from mother to child during breast feeding.

The research presented has shown that (1) GF120918 can significantly increase the distribution of HIV protease inhibitors into the CNS of rats by inhibiting P-gp at the BBB, (2) GF120918 can selectively inhibit P-gp transport without inhibiting CYP3A metabolism, both in vitro (human) and in vivo (rats), (3) mrp1 is not localized to the BBB of rats, and therefore does not play a significant role in the distribution of HIV protease inhibitors into the CNS, (4) the concentrations of nelfinavir in rat milk were approximately half that of plasma, and (5) P-gp does not play a significant role in the distribution of HIV protease inhibitors into rat milk.

APPENDICES

1. Quantitative PCR Results

    1. B-Actin

PCR Quantification

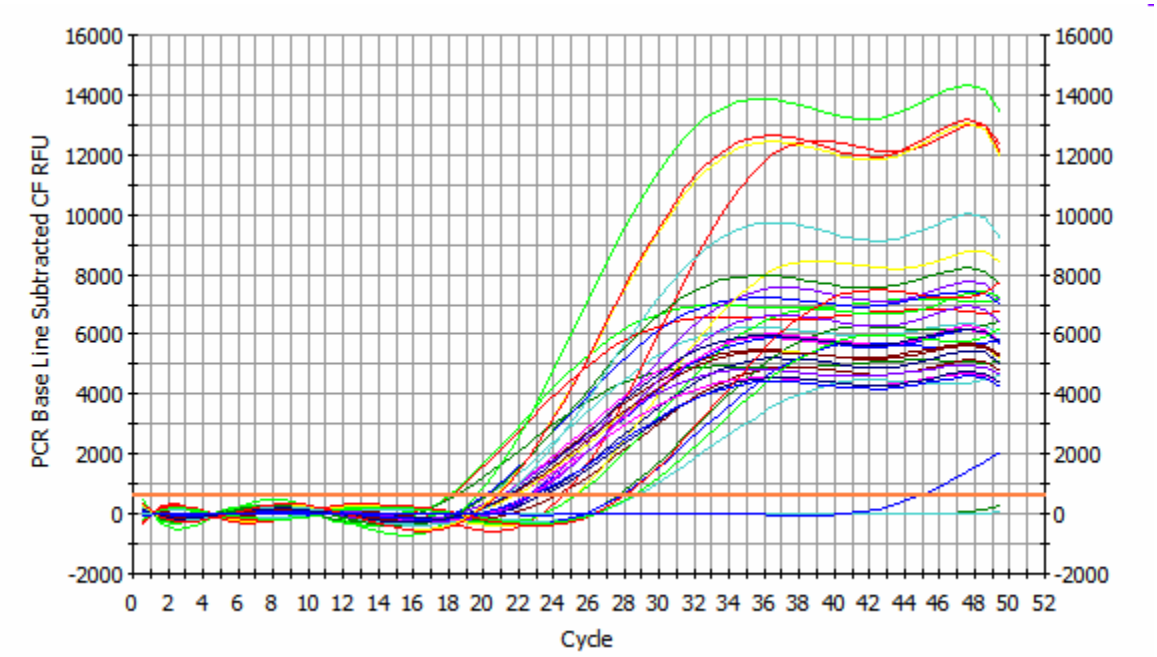

PCR Quantification Spreadsheet Data for FAM-490

Well	Identifier	Ct	Setpoint
A01	Standard Sample #1	18.1	
A02		18	Standard Sample #1
A03		18.4	Standard Sample #1
A04		20.2	Standard Sample #2
A05		20	Standard Sample #2
A06		20.9	Standard Sample #2
A07		24.2	Standard Sample #3
A08		23.2	Standard Sample #3
A09		22.5	Standard Sample #3
A10		25.1	Standard Sample #4
A11		24.5	Standard Sample #4
A12		25.3	Standard Sample #4
B01		27.6	Standard Sample #5
B02		28.7	Standard Sample #5
B03		27.8	Standard Sample #5
B04		21.7	Whole Brain #1
B05		21	Whole Brain #1
B07		20.9	Whole Brain #2
B08		21.7	Whole Brain #2
B10		19.6	Whole Brain #3

B11	20.2	Whole Brain #3
C01	22.5	Capillary Depleted Fraction #1
C02	22.6	Capillary Depleted Fraction #1
C04	23.4	Capillary Depleted Fraction #2
C05	22.8	Capillary Depleted Fraction #2
C07	28.1	Capillary Depleted Fraction #3
C08	28.5	Capillary Depleted Fraction #3
C10	21.2	Capillary Enriched Fraction #1
C11	22.8	Capillary Enriched Fraction #1
D01	21.5	Capillary Enriched Fraction #2
D02	21.3	Capillary Enriched Fraction #2
D04	20.7	Capillary Enriched Fraction #3
D05	20.8	Capillary Enriched Fraction #3
D07	N/A	Negative Control
D08	N/A	Negative Control
D09	44.9	Negative Control

Melt Curve

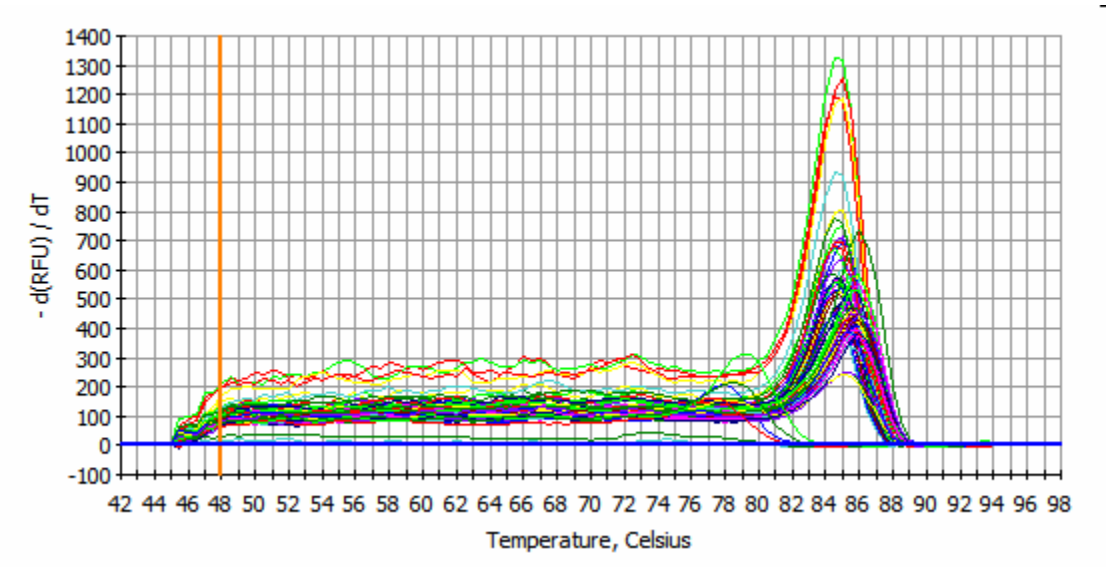

1.5% Agarose Gel Stained with Ethidium Bromide

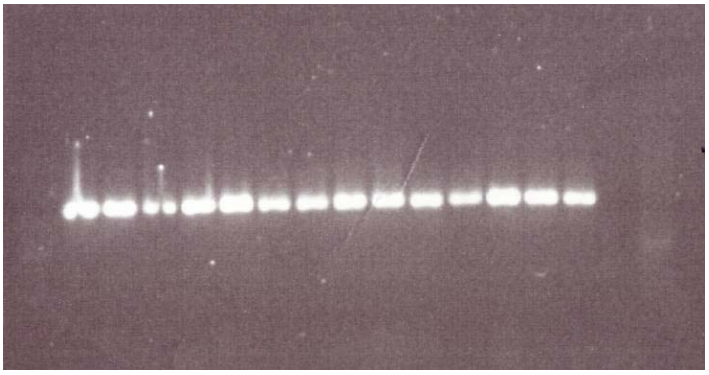

2. PECAM

PCR Quantification

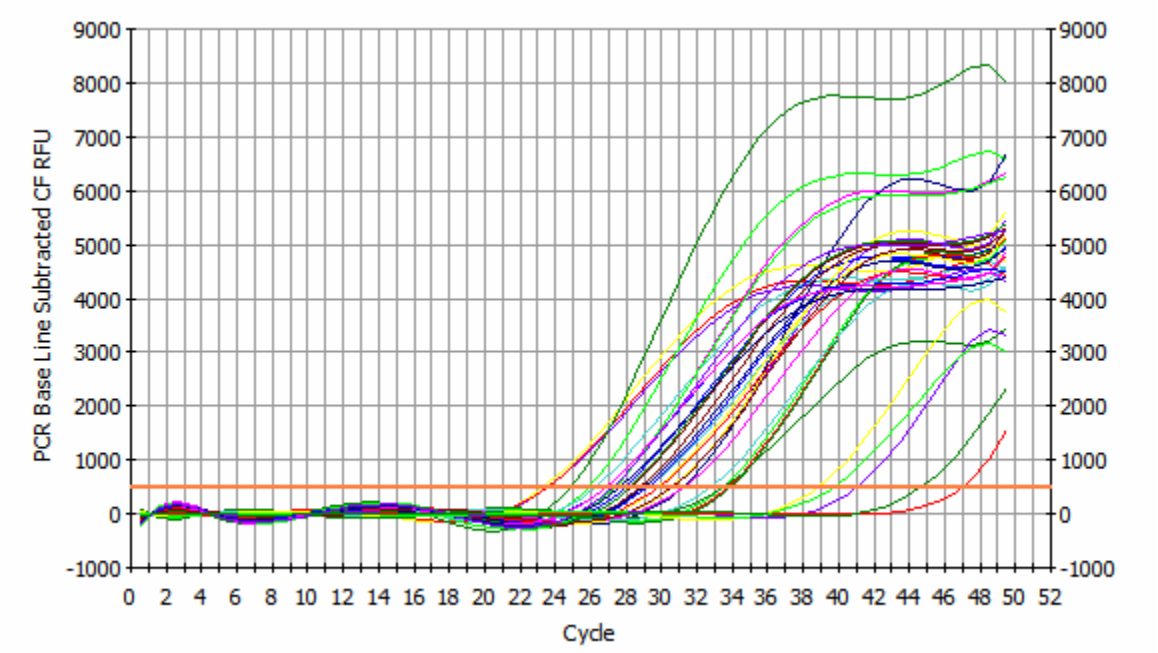

PCR Quantification Spreadsheet Data for FAM-490

Well	Identifier	Ct	Setpoint
E01		23.5	Standard #1
E02		23.2	Standard #1
E03		23.5	Standard #1
E04		25.8	Standard #2
E05		24.8	Standard #2
E06		26.1	Standard #2
E07		27.8	Standard #3
E08		27.2	Standard #3

E09	28.2	Standard #3
E10	31.1	Standard #4
E11	30.5	Standard #4
E12	30.5	Standard #4
F01	33.6	Standard #5
F02	33.4	Standard #5
F03	33.8	Standard #5
F04	29.2	Whole Brain #1
F05	29.1	Whole Brain #1
F07	28.7	Whole Brain #2
F08	28.9	Whole Brain #2
F10	29.7	Whole Brain #3
F11	29.7	Whole Brain #3
G01	33.3	Capillary Depleted Fraction #1
G02	32.7	Capillary Depleted Fraction #1
G04	31.1	Capillary Depleted Fraction #2
G05	30.5	Capillary Depleted Fraction #2
G07	41	Capillary Depleted Fraction #3
G08	38.7	Capillary Depleted Fraction #3
G10	27.2	Capillary Enriched Fraction #1
G11	28.1	Capillary Enriched Fraction #1
H01	26.7	Capillary Enriched Fraction #2
H02	26.7	Capillary Enriched Fraction #2
H04	27.5	Capillary Enriched Fraction #3
H05	27.1	Capillary Enriched Fraction #3
H08	39.6	Negative Control
H09	44.5	Negative Control

Melt Curve

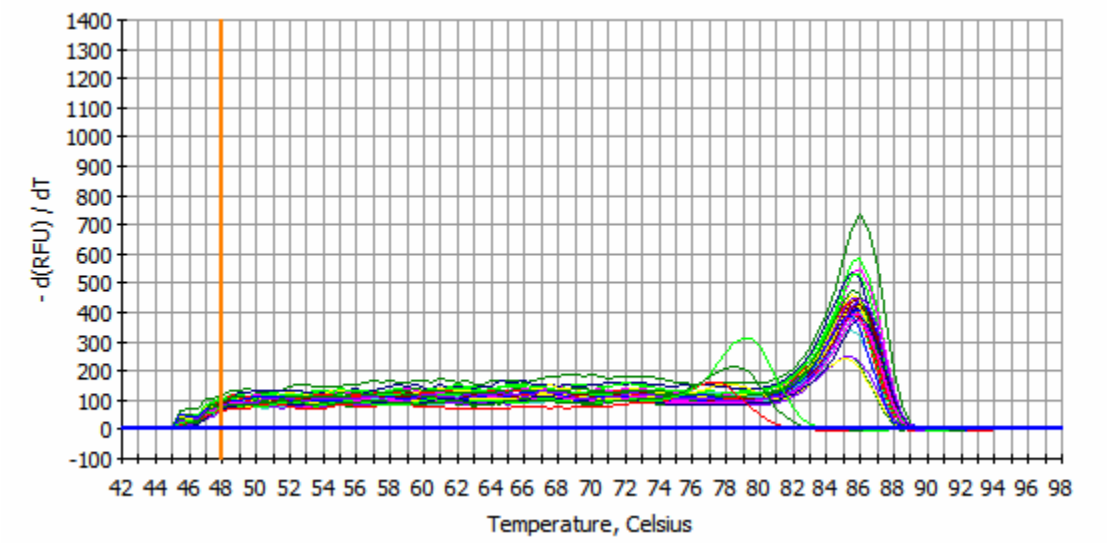

1.5% Agarose Gel Stained with Ethidium Bromide

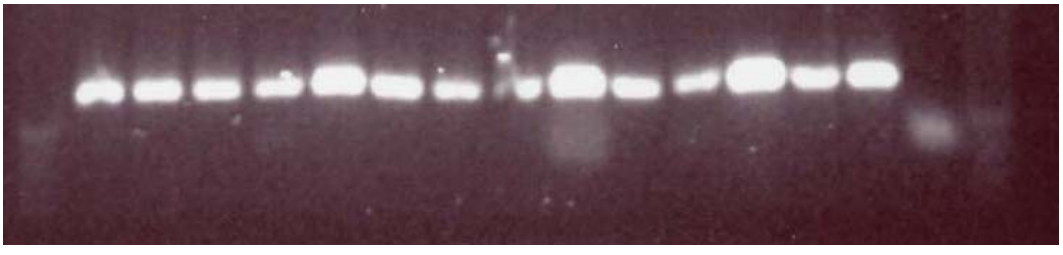

3. GFAP

PCR Quantification

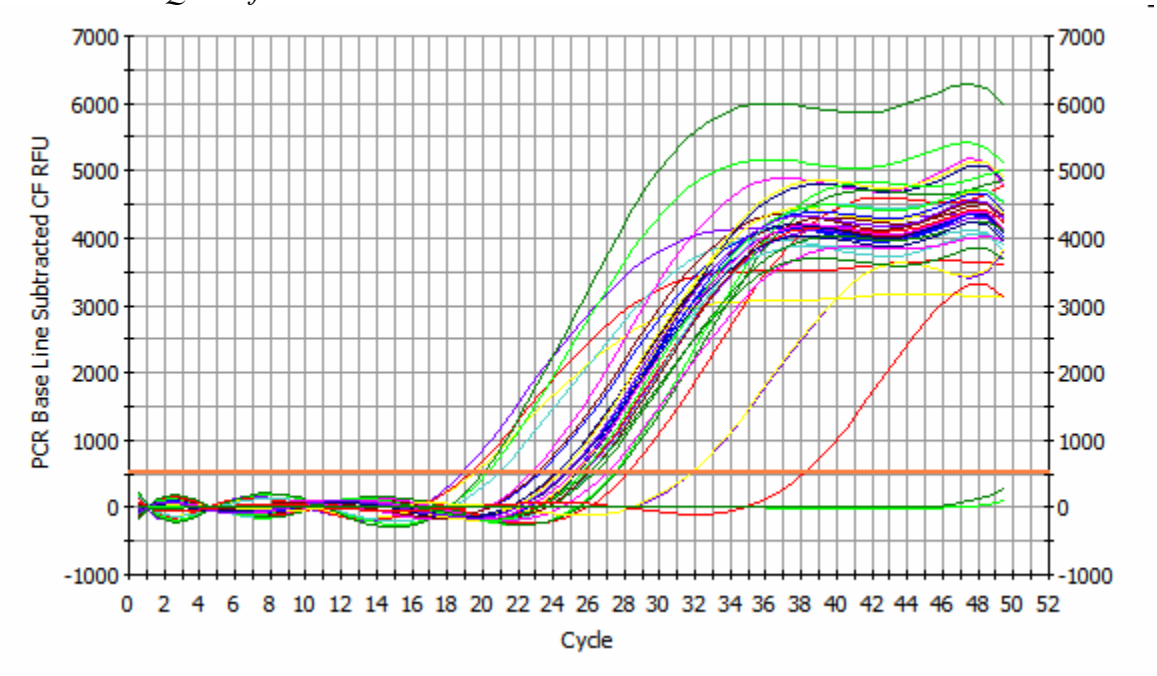

PCR Quantification Spreadsheet Data for FAM-490

Well	Identifier	Ct	Setpoint
E01		18.9	Standard #1
E02		19.6	Standard #1
E03		19.3	Standard #1
E04		20.3	Standard #2
E05		20	Standard #2
E06		20.9	Standard #2
E07		23.3	Standard #3
E08		22.8	Standard #3
E09		23.2	Standard #3
E10		25.4	Standard #4
E11		25.7	Standard #4
E12		25.3	Standard #4
F01		28.3	Standard #5
F02		27.4	Standard #5
F03		27.6	Standard #5
F04		24.8	Whole Brain #1
F05		24.8	Whole Brain #1
F07		24.3	Whole Brain #2
F08		24.2	Whole Brain #2
F10		24.5	Whole Brain #3
F11		25.6	Whole Brain #3
G01		26.3	Capillary Depleted Fraction #1
G02		26	Capillary Depleted Fraction #1
G04		27	Capillary Depleted Fraction #2
G05		26	Capillary Depleted Fraction #2
G07		31.9	Capillary Depleted Fraction #3
G08		31.8	Capillary Depleted Fraction #3

G10	25.6	Capillary Enriched Fraction #1
G11	26	Capillary Enriched Fraction #1
H01	25.2	Capillary Enriched Fraction #2
H02	25.2	Capillary Enriched Fraction #2
H04	24.8	Capillary Enriched Fraction #3
H05	24.7	Capillary Enriched Fraction #3
H08	N/A	Negative
H09	N/A	Negative

Melt Curve

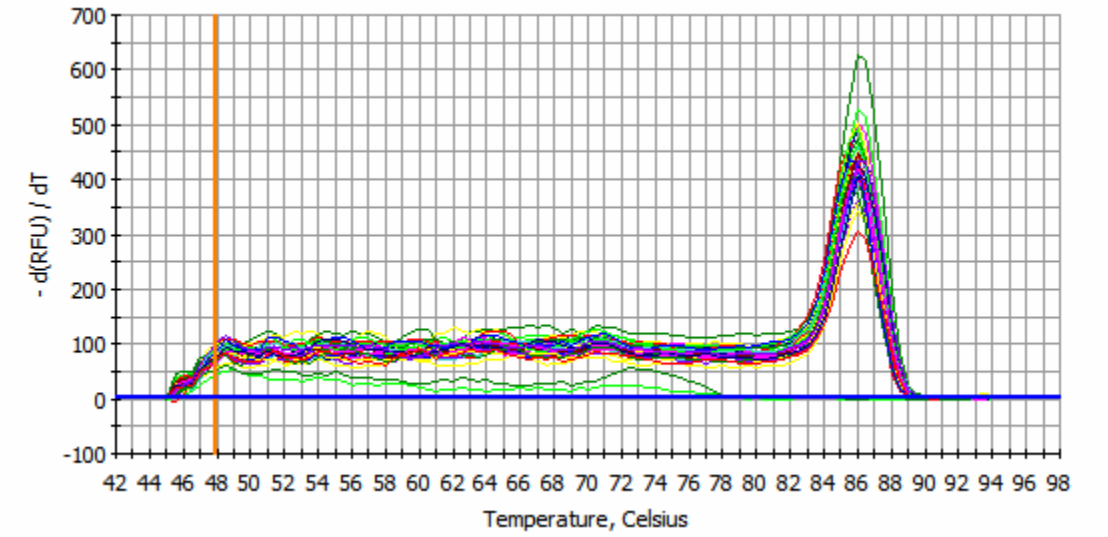

1.5% Agarose Gel Stained with Ethidium Bromide

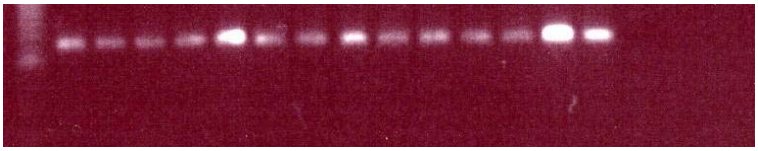

4. mdr1a

PCR Quantification

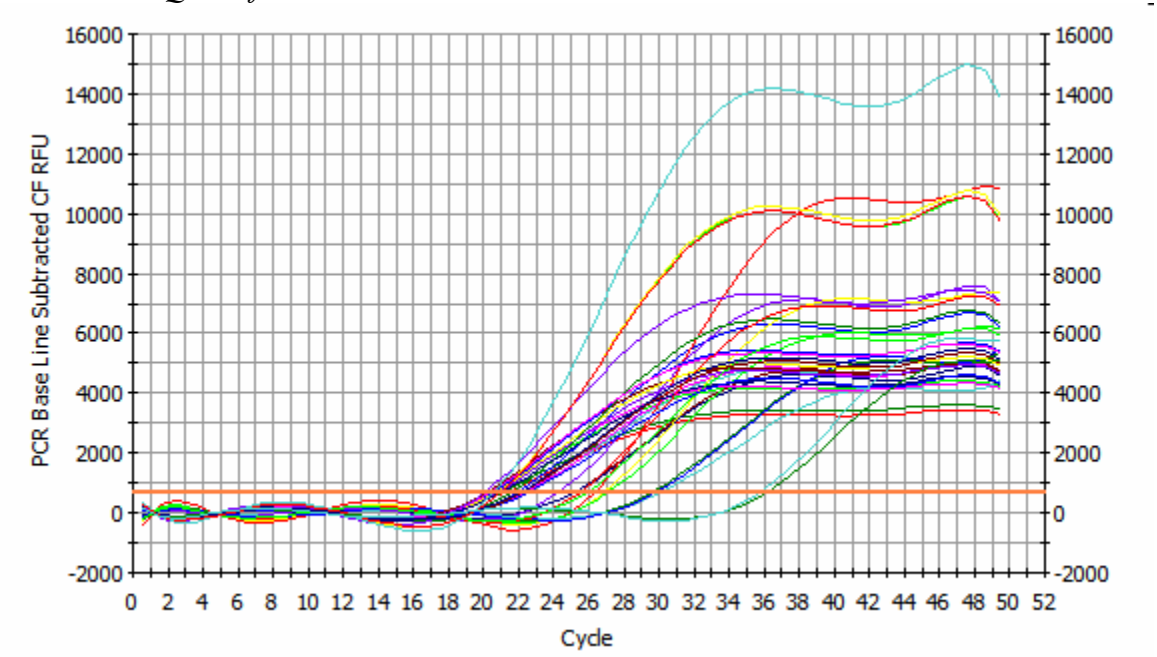

PCR Quantification Spreadsheet Data for FAM-490

Well	Identifier	Ct	Sample
			Liver as Standard Curve
A01		21.1	Standard Curve #1
A02		20.4	Standard Curve #1
A03		20.9	Standard Curve #1
A04		22.3	Standard Curve #2
A05		21.9	Standard Curve #2
A06		22.4	Standard Curve #2
A07		25.1	Standard Curve #3
A08		25.1	Standard Curve #3
A09		24.2	Standard Curve #3
A10		26.8	Standard Curve #4
A11		26.3	Standard Curve #4
A12		27.1	Standard Curve #4
B01		29.6	Standard Curve #5
B02		30	Standard Curve #5
B03		29.8	Standard Curve #5
B04		20.4	Brain #1
B05		20	Brain #1
B07		20.7	Brain #2
B08		20.6	Brain #2
B10		20.9	Brain #3
B11		21.5	Brain #3
C01		20.5	Capillary Depleted Fraction #1
C02		20.3	Capillary Depleted Fraction #1
C04		20.9	Capillary Depleted Fraction #2
C05		20	Capillary Depleted Fraction #2
C07		20.4	Capillary Depleted Fraction #3
C08		20.8	Capillary Depleted Fraction #3

C10	20.6	Capillary Enriched Fraction #1
C11	22.5	Capillary Enriched Fraction #1
D01	22.1	Capillary Enriched Fraction #2
D02	22	Capillary Enriched Fraction #2
D04	20.9	Capillary Enriched Fraction #3
D05	20.9	Capillary Enriched Fraction #3
D07	36.1	Negative
D08	35.7	Negative

Melt Curve

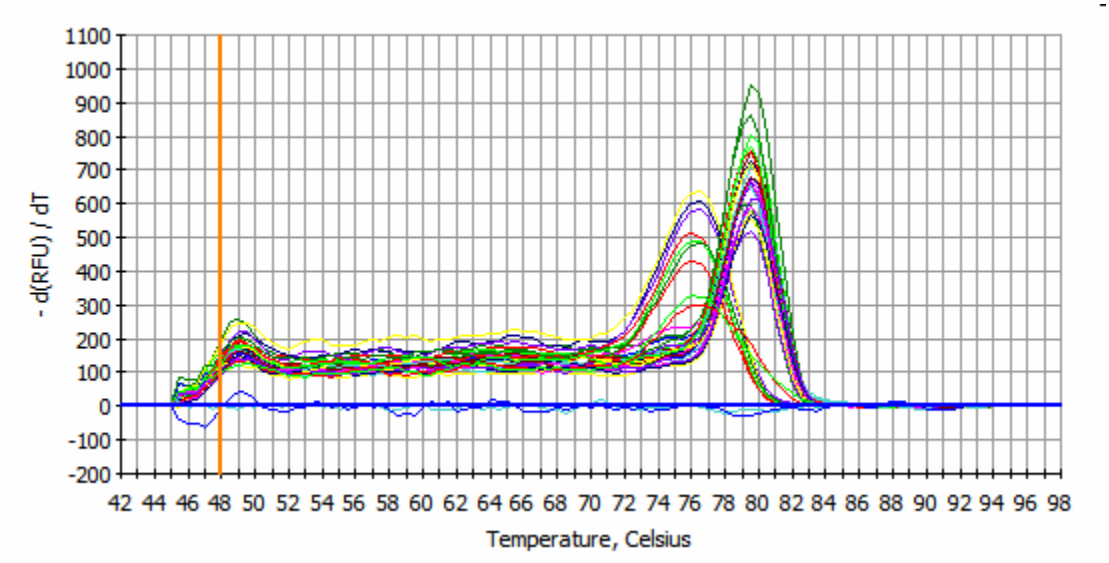

1.5% Agarose Gel Stained with Ethidium Bromide

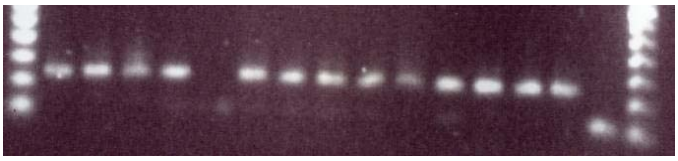

5. mrp1

PCR Quantification

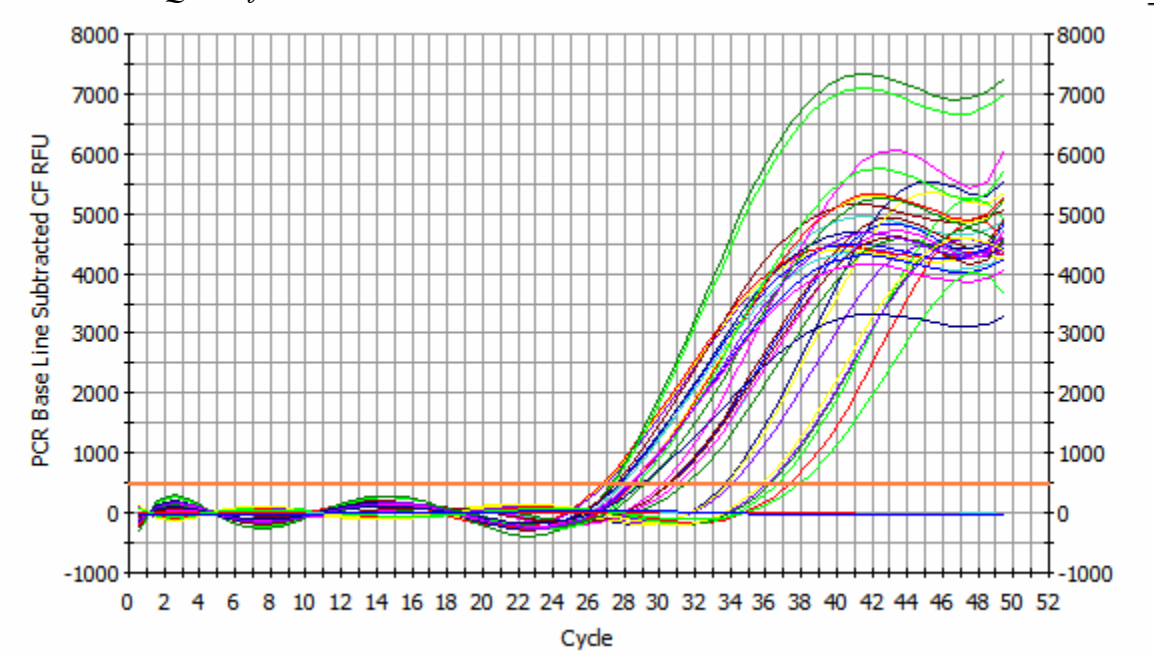

PCR Quantification Spreadsheet Data for FAM-490

Well	Identifier	Ct	Setpoint
			Brain as Standard Curve
E01		26.8	Standard Curve #1
E02		26.7	Standard Curve #1
E03		26.6	Standard Curve #1
E04		27.2	Standard Curve #2
E05		27.2	Standard Curve #2
E06		27.9	Standard Curve #2
E07		30.5	Standard Curve #3
E08		30	Standard Curve #3
E09		30.4	Standard Curve #3
E10		33.6	Standard Curve #4
E11		34	Standard Curve #4
E12		33.7	Standard Curve #4
F01		37.2	Standard Curve #5
F02		36.5	Standard Curve #5
F03		36.1	Standard Curve #5
F04		27.7	Whole Brain #1
F05		27.6	Whole Brain #1
F07		27.4	Whole Brain #2
F08		27.6	Whole Brain #2
F10		28.4	Whole Brain #3
F11		28.4	Whole Brain #3
G01		31.4	Capillary depleted Fraction #1
G02		30.8	Capillary depleted Fraction #1
G04		30.8	Capillary depleted Fraction #2
G05		30.5	Capillary depleted Fraction #2
G07		36	Capillary depleted Fraction #3
G08		35.7	Capillary depleted Fraction #3

G10	28.7	Capillary Enriched Fraction #1
G11	29.1	Capillary Enriched Fraction #1
H01	28.2	Capillary Enriched Fraction #2
H02	28.2	Capillary Enriched Fraction #2
H04	28.9	Capillary Enriched Fraction #3
H05	28.4	Capillary Enriched Fraction #3
H07	N/A	Negative
H10	N/A	Negative

Melt Curve

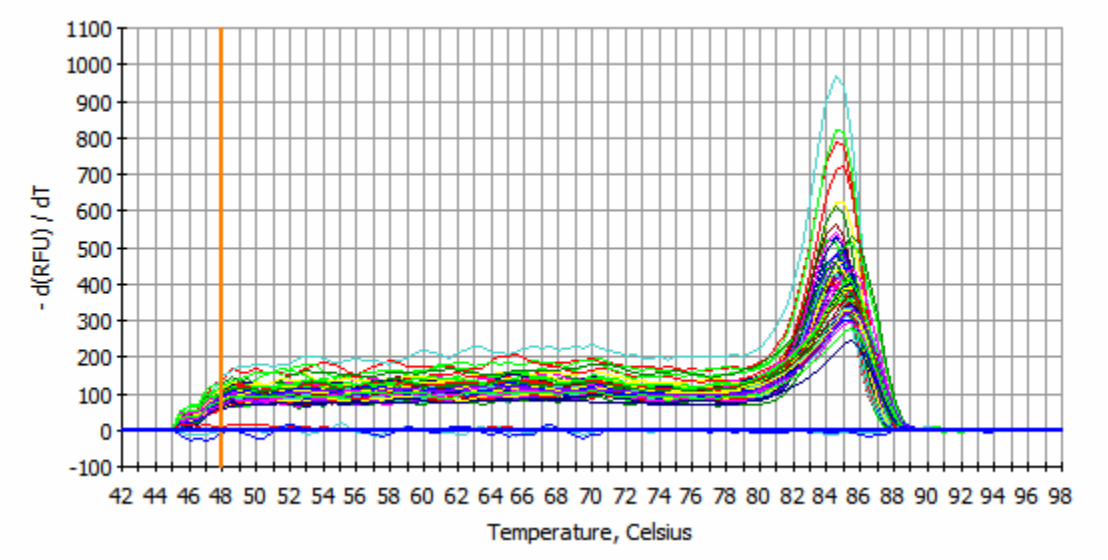

1.5% Agarose Gel Stained with Ethidium Bromide

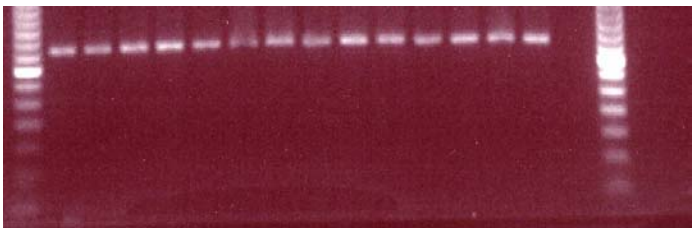

BIBLIOGRAPHY

Abbott NJ (2002) Astrocyte-endothelial interactions and blood-brain barrier permeability. *J Anat* **200:**629-638.

Abel SM and Back DJ (1993) Cortisol metabolism in vitro--III. Inhibition of microsomal 6 beta-hydroxylase and cytosolic 4-ene-reductase. *J Steroid Biochem Mol Biol* **46:**827-832.

Acosta EP (2002) Pharmacokinetic enhancement of protease inhibitors. *J Acquir Immune Defic Syndr* **29 Suppl 1:**S11-18.

Acosta EP, Kakuda TN, Brundage RC, Anderson PL and Fletcher CV (2000) Pharmacodynamics of human immunodeficiency virus type 1 protease inhibitors. *Clin Infect Dis* **30 Suppl 2:**S151-159.

Acosta EP, Page LM and Fletcher CV (1996) Clinical pharmacokinetics of zidovudine. An update. *Clin Pharmacokinet* **30:**251-262.

Albright AV, Soldan SS and Gonzalez-Scarano F (2003) Pathogenesis of human immunodeficiency virus-induced neurological disease. *J Neurovirol* **9:**222-227.

Alcorn J, Lu X, Moscow JA and McNamara PJ (2002) Transporter gene expression in lactating and nonlactating human mammary epithelial cells using real-time reverse transcription-polymerase chain reaction. *J Pharmacol Exp Ther* **303:**487-496.

Alcorn J and McNamara PJ (2002) Acyclovir, ganciclovir, and zidovudine transfer into rat milk. *Antimicrob Agents Chemother* **46:**1831-1836.

Ambudkar SV, Dey S, Hrycyna CA, Ramachandra M, Pastan I and Gottesman MM (1999) Biochemical, cellular, and pharmacological aspects of the multidrug transporter. *Annu Rev Pharmacol Toxicol* **39:**361-398.

Andrews J, Abd-Ellah MF, Randolph NL, Kenworthy KE, Carlile DJ, Friedberg T and Houston JB (2002) Comparative study of the metabolism of drug substrates by human cytochrome P450 3A4 expressed in bacterial, yeast and human lymphoblastoid cells. *Xenobiotica* **32:**937-947.

Asperen Jv, Mayer u, Tellingen Ov and Beijnen JH (1997) The functional role of P-Glycoprotein in the Blood-Brain Barrier. *Journal of Pharmaceutical Sciences* **86:**881-884.

Baede-van Dijk PA, Hugen PW, Verweij-van Wissen CP, Koopmans PP, Burger DM and Hekster YA (2001) Analysis of variation in plasma concentrations of nelfinavir and its active metabolite M8 in HIV-positive patients. *Aids* **15:**991-998.

Ballerini P, Di Iorio P, Ciccarelli R, Nargi E, D'Alimonte I, Traversa U, Rathbone MP and Caciagli F (2002) Glial cells express multiple ATP binding cassette proteins which are involved in ATP release. *Neuroreport* **13:**1789-1792.

Bartlett NL, Lum BL, Fisher GA, Brophy NA, Ehsan MN, Halsey J and Sikic BI (1994) Phase I trial of doxorubicin with cyclosporine as a modulator of multidrug resistance. *J Clin Oncol* **12:**835-842.

Bellamy WT (1996) P-glycoproteins and multidrug resistance. *Annu Rev Pharmacol Toxicol* **36:**161-183.

Berg SL, Tolcher A, O'Shaughnessy JA, Denicoff AM, Noone M, Ognibene FP, Cowan KH and Balis FM (1995) Effect of R-verapamil on the pharmacokinetics of paclitaxel in women with breast cancer. *J Clin Oncol* **13:**2039-2042.

Bickel U, Yoshikawa T and Pardridge WM (2001) Delivery of peptides and proteins through the blood-brain barrier. *Adv Drug Deliv Rev* **46:**247-279.

Bohme M, Buchler M, Muller M and Keppler D (1993) Differential inhibition by cyclosporins of primary-active ATP-dependent transporters in the hepatocyte canalicular membrane. *FEBS Lett* **333:**193-196.

Boote DJ, Dennis IF, Twentyman PR, Osborne RJ, Laburte C, Hensel S, Smyth JF, Brampton MH and Bleehen NM (1996) Phase I study of etoposide with SDZ PSC 833 as a modulator of multidrug resistance in patients with cancer. *J Clin Oncol* **14:**610-618.

Borst P and Elferink RO (2002) Mammalian ABC transporters in health and disease. *Annu Rev Biochem* **71:**537-592.

Borst P, Evers R, Kool M and Wijnholds J (2000) A family of drug transporters: the multidrug resistance-associated proteins. *J Natl Cancer Inst* **92:**1295-1302.

Borst P and Schinkel AH (1996) What have we learnt thus far from mice with disrupted P-glycoprotein genes? *Eur J Cancer* **32A:**985-990.

Briggs GG, Freeman rK and Yaffe SJ (1998) *Drugs in Pregnancy and Lactation*. Lippincott Williams & Wilkins, Philadelphia.

Burgio DE, Gosland MP and McNamara PJ (1996) Modulation effects of cyclosporine on etoposide pharmacokinetics and CNS distribution in the rat utilizing microdialysis. *Biochem Pharmacol* **51:**987-992.

Cherrington NJ, Hartley DP, Li N, Johnson DR and Klaassen CD (2002) Organ distribution of multidrug resistance proteins 1, 2, and 3 (Mrp1, 2, and 3) mRNA and hepatic induction of Mrp3 by constitutive androstane receptor activators in rats. *J Pharmacol Exp Ther* **300:**97-104.

Choo EF, Leake B, Wandel C, Imamura H, Wood AJ, Wilkinson GR and Kim RB (2000) Pharmacological inhibition of P-glycoprotein transport enhances the distribution of HIV-1 protease inhibitors into brain and testes [In Process Citation]. *Drug Metab Dispos* **28:**655-660.

Chun TW and Fauci AS (1999) Latent reservoirs of HIV: obstacles to the eradication of virus. *Proc Natl Acad Sci U S A* **96:**10958-10961.

Cummins CL, Jacobsen W and Benet LZ (2002) Unmasking the dynamic interplay between intestinal P-glycoprotein and CYP3A4. *J Pharmacol Exp Ther* **300:**1036-1045.

Cummins CL, Salphati L, Reid MJ and Benet LZ (2003) In vivo modulation of intestinal CYP3A metabolism by P-glycoprotein: studies using the rat single-pass intestinal perfusion model. *J Pharmacol Exp Ther* **305:**306-314.

Davies B and Morris T (1993) Physiological parameters in laboratory animals and humans. *Pharm Res* **10:**1093-1095.

De Boer AB, De Lange EL, Van der Sandt IC and Breimer DD (1998) Transporters and the blood-brain barrier (BBB). *Int J Clin Pharmacol Ther* **36:**14-15.

Dean M and Allikmets R (2001) Complete characterization of the human ABC gene family. *J Bioenerg Biomembr* **33:**475-479.

Dean M, Hamon Y and Chimini G (2001a) The human ATP-binding cassette (ABC) transporter superfamily. *J Lipid Res* **42:**1007-1017.

Dean M, Rzhetsky A and Allikmets R (2001b) The human ATP-binding cassette (ABC) transporter superfamily. *Genome Res* **11:**1156-1166.

Decleves X, Regina A, Laplanche JL, Roux F, Boval B, Launay JM and Scherrmann JM (2000) Functional expression of P-glycoprotein and multidrug resistance-associated protein (Mrp1) in primary cultures of rat astrocytes. *J Neurosci Res* **60:**594-601.

Demeule M, Jodoin J, Gingras D and Beliveau R (2000) P-glycoprotein is localized in caveolae in resistant cells and in brain capillaries. *FEBS Lett* **466:**219-224.
Demeule M, Labelle M, Regina A, Berthelet F and Beliveau R (2001) Isolation of endothelial cells from brain, lung, and kidney: expression of the multidrug resistance P-glycoprotein isoforms. *Biochem Biophys Res Commun* **281:**827-834.
Deuchars KL, Duthie M and Ling V (1992) Identification of distinct P-glycoprotein gene sequences in rat. *Biochim Biophys Acta* **1130:**157-165.
Edwards JE, Brouwer KR and McNamara PJ (2002) GF120918, a P-glycoprotein modulator, increases the concentration of unbound amprenavir in the central nervous system in rats. *Antimicrob Agents Chemother* **46:**2284-2286.
Fardel O, Lecureur V and Guillouzo A (1996) The P-glycoprotein multidrug transporter. *Gen Pharmacol* **27:**1283-1291.
Feng MR, Liebert M, Wedemeyer G, Grossman HB, Mancini WR, Williams M and Wagner JG (1991) Effect of verapamil on the uptake and efflux of etoposide (VP16) in both sensitive and resistant cancer cells. *Sel Cancer Ther* **7:**75-83.
Finzi D, Hermankova M, Pierson T, Carruth LM, Buck C, Chaisson RE, Quinn TC, Chadwick K, Margolick J, Brookmeyer R, Gallant J, Markowitz M, Ho DD, Richman DD and Siliciano RF (1997) Identification of a reservoir for HIV-1 in patients on highly active antiretroviral therapy. *Science* **278:**1295-1300.
Fleishaker JC, Desai N and McNamara PJ (1987) Factors affecting the milk-to-plasma drug concentration ratio in lactating women: physical interactions with protein and fat. *J Pharm Sci* **76:**189-193.
Flexner C (1998) HIV-protease inhibitors. *N Engl J Med* **338:**1281-1292.
Fogli S, Danesi R, Innocenti F, Di Paolo A, Bocci G, Barbara C and Del Tacca M (1999) An improved HPLC method for therapeutic drug monitoring of daunorubicin, idarubicin, doxorubicin, epirubicin, and their 13-dihydro metabolites in human plasma. *Ther Drug Monit* **21:**367-375.
Ford JM (1996) Experimental reversal of P-glycoprotein-mediated multidrug resistance by pharmacological chemosensitisers. *Eur J Cancer* **32A:**991-1001.
Fowler MG and Newell ML (2002) Breast-feeding and HIV-1 transmission in resource-limited settings. *J Acquir Immune Defic Syndr* **30:**230-239.
Garrigues A, Loiseau N, Delaforge M, Ferte J, Garrigos M, Andre F and Orlowski S (2002) Characterization of two pharmacophores on the multidrug transporter P-glycoprotein. *Mol Pharmacol* **62:**1288-1298.
Gerk PM, Kuhn RJ, Desai NS and McNamara PJ (2001) Active transport of nitrofurantoin into human milk. *Pharmacotherapy* **21:**669-675.
Ghosal A, Satoh H, Thomas PE, Bush E and Moore D (1996) Inhibition and kinetics of cytochrome P4503A activity in microsomes from rat, human, and cdna-expressed human cytochrome P450. *Drug Metab Dispos* **24:**940-947.
Gottesman MM and Pastan I (1993) Biochemistry of multidrug resistance mediated by the multidrug transporter. *Annu Rev Biochem* **62:**385-427.
Higashikawa F, Murakami T, Kaneda T and Takano M (1999) In-vivo and in-vitro metabolic clearance of midazolam, a cytochrome P450 3A substrate, by the liver under normal and increased enzyme activity in rats. *J Pharm Pharmacol* **51:**405-410.

Hooiveld GJ, Heegsma J, van Montfoort JE, Jansen PL, Meijer DK and Muller M (2002) Stereoselective transport of hydrophilic quaternary drugs by human MDR1 and rat Mdr1b P-glycoproteins. *Br J Pharmacol* **135:**1685-1694.

Huai-Yun H, Secrest DT, Mark KS, Carney D, Brandquist C, Elmquist WF and Miller DW (1998) Expression of multidrug resistance-associated protein (MRP) in brain microvessel endothelial cells. *Biochem Biophys Res Commun* **243:**816-820.

Huber JD, Egleton RD and Davis TP (2001) Molecular physiology and pathophysiology of tight junctions in the blood-brain barrier. *Trends Neurosci* **24:**719-725.

Huisman MT, Smit JW, Crommentuyn KM, Zelcer N, Wiltshire HR, Beijnen JH and Schinkel AH (2002) Multidrug resistance protein 2 (MRP2) transports HIV protease inhibitors, and transport can be enhanced by other drugs. *Aids* **16:**2295-2301.

Hutzler JM and Tracy TS (2002) Atypical kinetic profiles in drug metabolism reactions. *Drug Metab Dispos* **30:**355-362.

Hyafil F, Vergely C, Du Vignaud P and Grand-Perret T (1993) In vitro and in vivo reversal of multidrug resistance by GF120918, an acridonecarboxamide derivative. *Cancer Res* **53:**4595-4602.

Ishikawa T, Kuo MT, Furuta K and Suzuki M (2000) The human multidrug resistance-associated protein (MRP) gene family: from biological function to drug molecular design. *Clin Chem Lab Med* **38:**893-897.

Jedlitschky G, Leier I, Buchholz U, Barnouin K, Kurz G and Keppler D (1996) Transport of glutathione, glucuronate, and sulfate conjugates by the MRP gene-encoded conjugate export pump. *Cancer Res* **56:**988-994.

Jones K, Bray PG, Khoo SH, Davey RA, Meaden ER, Ward SA and Back DJ (2001a) P-Glycoprotein and transporter MRP1 reduce HIV protease inhibitor uptake in CD4 cells: potential for accelerated viral drug resistance? *Aids* **15:**1353-1358.

Jones K, Hoggard PG, Sales SD, Khoo S, Davey R and Back DJ (2001b) Differences in the intracellular accumulation of HIV protease inhibitors in vitro and the effect of active transport. *Aids* **15:**675-681.

Kaul M, Garden GA and Lipton SA (2001) Pathways to neuronal injury and apoptosis in HIV-associated dementia. *Nature* **410:**988-994.

Kawai R, Mathew D, Tanaka C and Rowland M (1998) Physiologically based pharmacokinetics of cyclosporine A: extension to tissue distribution kinetics in rats and scale-up to human. *J Pharmacol Exp Ther* **287:**457-468.

Kemper EM, Jansen B, Brouwer KR, Schellens JH, Beijnen JH and van Tellingen O (2001) Bioanalysis and preliminary pharmacokinetics of the acridonecarboxamide derivative GF120918 in plasma of mice and humans by ion-pairing reversed-phase high-performance liquid chromatography with fluorescence detection. *J Chromatogr B Biomed Sci Appl* **759:**135-143.

Kim RB, Fromm MF, Wandel C, Leake B, Wood AJ, Roden DM and Wilkinson GR (1998) The drug transporter P-glycoprotein limits oral absorption and brain entry of HIV-1 protease inhibitors. *J Clin Invest* **101:**289-294.

Kim RB, Wandel C, Leake B, Cvetkovic M, Fromm MF, Dempsey PJ, Roden MM, Belas F, Chaudhary AK, Roden DM, Wood AJ and Wilkinson GR (1999) Interrelationship between substrates and inhibitors of human CYP3A and P-glycoprotein. *Pharm Res* **16:**408-414.

Klepper J and Voit T (2002) Facilitated glucose transporter protein type 1 (GLUT1) deficiency syndrome: impaired glucose transport into brain-- a review. *Eur J Pediatr* **161:**295-304.
Kobayashi K, Urashima K, Shimada N and Chiba K (2002) Substrate specificity for rat cytochrome P450 (CYP) isoforms: screening with cDNA-expressed systems of the rat. *Biochem Pharmacol* **63:**889-896.
Kotegawa T, Laurijssens BE, Von Moltke LL, Cotreau MM, Perloff MD, Venkatakrishnan K, Warrington JS, Granda BW, Harmatz JS and Greenblatt DJ (2002) In vitro, pharmacokinetic, and pharmacodynamic interactions of ketoconazole and midazolam in the rat. *J Pharmacol Exp Ther* **302:**1228-1237.
Krishna R and Mayer LD (2000) Multidrug resistance (MDR) in cancer. Mechanisms, reversal using modulators of MDR and the role of MDR modulators in influencing the pharmacokinetics of anticancer drugs. *Eur J Pharm Sci* **11:**265-283.
Lambotte O, Deiva K and Tardieu M (2003) HIV-1 persistence, viral reservoir, and the central nervous system in the HAART era. *Brain Pathol* **13:**95-103.
Lee CG, Gottesman MM, Cardarelli CO, Ramachandra M, Jeang KT, Ambudkar SV, Pastan I and Dey S (1998) HIV-1 protease inhibitors are substrates for the MDR1 multidrug transporter. *Biochemistry* **37:**3594-3601.
Lemaire M and Tillement JP (1982) Role of lipoproteins and erythrocytes in the in vitro binding and distribution of cyclosporin A in the blood. *J Pharm Pharmacol* **34:**715-718.
Leslie EM, Deeley RG and Cole SP (2001) Toxicological relevance of the multidrug resistance protein 1, MRP1 (ABCC1) and related transporters. *Toxicology* **167:**3-23.
List AF, Kopecky KJ, Willman CL, Head DR, Persons DL, Slovak ML, Dorr R, Karanes C, Hynes HE, Doroshow JH, Shurafa M and Appelbaum FR (2001) Benefit of cyclosporine modulation of drug resistance in patients with poor-risk acute myeloid leukemia: a Southwest Oncology Group study. *Blood* **98:**3212-3220.
Loe DW, Deeley RG and Cole SP (1998) Characterization of vincristine transport by the M(r) 190,000 multidrug resistance protein (MRP): evidence for cotransport with reduced glutathione. *Cancer Res* **58:**5130-5136.
Loo TW, Bartlett MC and Clarke DM (2003) Substrate-induced conformational changes in the transmembrane segments of human P-glycoprotein. Direct evidence for the substrate-induced fit mechanism for drug binding. *J Biol Chem* **278:**13603-13606.
Loo TW and Clarke DM (2001) Defining the drug-binding site in the human multidrug resistance P-glycoprotein using a methanethiosulfonate analog of verapamil, MTS-verapamil. *J Biol Chem* **276:**14972-14979.
Lowry OH, Rosebrough NJ and . RJR (1951) Protein measurement with the folin phenol reagent. *J. Biol. Chem* **193:**265-275.
Lum BL and Gosland MP (1995) MDR expression in normal tissues. Pharmacologic implications for the clinical use of P-glycoprotein inhibitors. *Hematol Oncol Clin North Am* **9:**319-336.
Lum BL, Kaubisch S, Yahanda AM, Adler KM, Jew L, Ehsan MN, Brophy NA, Halsey J, Gosland MP and Sikic BI (1992) Alteration of etoposide pharmacokinetics and pharmacodynamics by cyclosporine in a phase I trial to modulate multidrug resistance. *J Clin Oncol* **10:**1635-1642.
Ma F and Lau CE (1996) Determination of midazolam and its metabolites in serum microsamples by high-performance liquid chromatography and its application to pharmacokinetics in rats. *J Chromatogr B Biomed Appl* **682:**109-113.

Martin C, Berridge G, Higgins CF, Mistry P, Charlton P and Callaghan R (2000) Communication between multiple drug binding sites on P-glycoprotein. *Mol Pharmacol* **58:**624-632.

McArthur JC, Haughey N, Gartner S, Conant K, Pardo C, Nath A and Sacktor N (2003) Human immunodeficiency virus-associated dementia: an evolving disease. *J Neurovirol* **9:**205-221.

Meaden ER, Hoggard PG, Newton P, Tjia JF, Aldam D, Cornforth D, Lloyd J, Williams I, Back DJ and Khoo SH (2002) P-glycoprotein and MRP1 expression and reduced ritonavir and saquinavir accumulation in HIV-infected individuals. *J Antimicrob Chemother* **50:**583-588.

Nolan ML, Greenberg AE and Fowler MG (2002) A review of clinical trials to prevent mother-to-child HIV-1 transmission in Africa and inform rational intervention strategies. *Aids* **16:**1991-1999.

Oo CY, Kuhn RJ, Desai N and McNamara PJ (1995) Active transport of cimetidine into human milk. *Clin Pharmacol Ther* **58:**548-555.

Pardridge WM (1998) *Introduction to the Blood-Brain Barrier: Methodology, Biology and Pathology*. Cambridge University Press, Cambridge.

Patki KC, Von Moltke LL and Greenblatt DJ (2003) In vitro metabolism of midazolam, triazolam, nifedipine, and testosterone by human liver microsomes and recombinant cytochromes p450: role of cyp3a4 and cyp3a5. *Drug Metab Dispos* **31:**938-944.

Perelson AS, Essunger P, Cao Y, Vesanen M, Hurley A, Saksela K, Markowitz M and Ho DD (1997) Decay characteristics of HIV-1-infected compartments during combination therapy [see comments]. *Nature* **387:**188-191.

Pierson T, McArthur J and Siliciano RF (2000) Reservoirs for HIV-1: mechanisms for viral persistence in the presence of antiviral immune responses and antiretroviral therapy. *Annu Rev Immunol* **18:**665-708.

Polli JW, Jarrett JL, Studenberg SD, Humphreys JE, Dennis SW, Brouwer KR and Woolley JL (1999) Role of P-glycoprotein on the CNS disposition of amprenavir (141W94), an HIV protease inhibitor. *Pharm Res* **16:**1206-1212.

Pomerantz RJ and Horn DL (2003) Twenty years of therapy for HIV-1 infection. *Nat Med* **9:**867-873.

Prat A, Biernacki K, Wosik K and Antel JP (2001) Glial cell influence on the human blood-brain barrier. *Glia* **36:**145-155.

Priebe W, Krawczyk M, Kuo MT, Yamane Y, Savaraj N and Ishikawa T (1998) Doxorubicin- and daunorubicin-glutathione conjugates, but not unconjugated drugs, competitively inhibit leukotriene C4 transport mediated by MRP/GS-X pump. *Biochem Biophys Res Commun* **247:**859-863.

Raderer M and Scheithauer W (1993) Clinical trials of agents that reverse multidrug resistance. A literature review. *Cancer* **72:**3553-3563.

Rana KZ and Dudley MN (1999) Human immunodeficiency virus protease inhibitors. *Pharmacotherapy* **19:**35-59.

Rao US (1995) Mutation of glycine 185 to valine alters the ATPase function of the human P-glycoprotein expressed in Sf9 cells. *J Biol Chem* **270:**6686-6690.

Regina A, Koman A, Piciotti M, El Hafny B, Center MS, Bergmann R, Couraud PO and Roux F (1998) Mrp1 multidrug resistance-associated protein and P-glycoprotein expression in rat brain microvessel endothelial cells. *J Neurochem* **71:**705-715.

Rieckmann P and Engelhardt B (2003) Building up the blood-brain barrier. *Nat Med* **9:**828-829.
Roepe PD (1992) Analysis of the steady-state and initial rate of doxorubicin efflux from a series of multidrug-resistant cells expressing different levels of P-glycoprotein. *Biochemistry* **31:**12555-12564.
Rousseau CM, Nduati RW, Richardson BA, Steele MS, John-Stewart GC, Mbori-Ngacha DA, Kreiss JK and Overbaugh J (2003) Longitudinal analysis of human immunodeficiency virus type 1 RNA in breast milk and of its relationship to infant infection and maternal disease. *J Infect Dis* **187:**741-747.
Ruiz L, van Lunzen J, Arno A, Stellbrink HJ, Schneider C, Rull M, Castella E, Ojanguren I, Richman DD, Clotet B, Tenner-Racz K and Racz P (1999) Protease inhibitor-containing regimens compared with nucleoside analogues alone in the suppression of persistent HIV-1 replication in lymphoid tissue. *Aids* **13:**F1-8.
Sacktor N (2002) The epidemiology of human immunodeficiency virus-associated neurological disease in the era of highly active antiretroviral therapy. *J Neurovirol* **8 Suppl 2:**115-121.
Saito T, Zhang ZJ, Tokuriki M, Ohtsubo T, Shibamori Y, Yamamoto T and Saito H (2001) Cyclosporin A inhibits the extrusion pump function of p-glycoprotein in the inner ear of mice treated with vinblastine and doxorubicin. *Brain Res* **901:**265-270.
Sarkadi B, Price EM, Boucher RC, Germann UA and Scarborough GA (1992) Expression of the human multidrug resistance cDNA in insect cells generates a high activity drug-stimulated membrane ATPase. *J Biol Chem* **267:**4854-4858.
Savolainen J, Edwards JE, Morgan ME, McNamara PJ and Anderson BD (2002) Effects of a P-glycoprotein inhibitor on brain and plasma concentrations of anti-human immunodeficiency virus drugs administered in combination in rats. *Drug Metab Dispos* **30:**479-482.
Schinkel AH (1998) Pharmacological insights from P-glycoprotein knockout mice. *Int J Clin Pharmacol Ther* **36:**9-13.
Schinkel AH, Smit JJ, van Tellingen O, Beijnen JH, Wagenaar E, van Deemter L, Mol CA, van der Valk MA, Robanus-Maandag EC, te Riele HP and et al. (1994) Disruption of the mouse mdr1a P-glycoprotein gene leads to a deficiency in the blood-brain barrier and to increased sensitivity to drugs. *Cell* **77:**491-502.
Seetharaman S, Barrand MA, Maskell L and Scheper RJ (1998a) Multidrug resistance-related transport proteins in isolated human brain microvessels and in cells cultured from these isolates. *J Neurochem* **70:**1151-1159.
Seetharaman S, Maskell L, Scheper RJ and Barrand MA (1998b) Changes in multidrug transporter protein expression in endothelial cells cultured from isolated human brain microvessels. *International Journal of clinical Pharmacology and Theraputics* **36:**81-83.
Serazin-Leroy V, Denis-Henriot D, Morot M, de Mazancourt P and Giudicelli Y (1998) Semi-quantitative RT-PCR for comparison of mRNAs in cells with different amounts of housekeeping gene transcripts. *Mol Cell Probes* **12:**283-291.
Sharom FJ (1997) The P-Glycoprotein Efflux Pump: How Does it Transport Drugs. *The Journal of Membrane Biology* **160:**161-175.
Shennan DB (1998) Mammary gland membrane transport systems. *J Mammary Gland Biol Neoplasia* **3:**247-258.
Sonza S and Crowe SM (2001) Reservoirs for HIV infection and their persistence in the face of undetectable viral load. *AIDS Patient Care STDS* **15:**511-518.

Srinivas RV, Middlemas D, Flynn P and Fridland A (1998) Human immunodeficiency virus protease inhibitors serve as substrates for multidrug transporter proteins MDR1 and MRP1 but retain antiviral efficacy in cell lines expressing these transporters. *Antimicrob Agents Chemother* **42:**3157-3162.

Sugiyama Y, Kusuhara H and Suzuki H (1999) Kinetic and biochemical analysis of carrier-mediated efflux of drugs through the blood-brain and blood-cerebrospinal fluid barriers: importance in the drug delivery to the brain. *J Controlled Release* **62:**179-186.

Sun H, Johnson DR, Finch RA, Sartorelli AC, Miller DW and Elmquist WF (2001) Transport of fluorescein in MDCKII-MRP1 transfected cells and mrp1-knockout mice. *Biochem Biophys Res Commun* **284:**863-869.

Swindells S, Zheng J and Gendelman HE (1999) HIV-associated dementia: new insights into disease pathogenesis and therapeutic interventions. *Aids Patient Care STDS* **13:**153-163.

Tanigawara Y (2000) Role of P-glycoprotein in drug disposition. *Ther Drug Monit* **22:**137-140.

Tolle-Sander S, Rautio J, Wring S, Polli JW and Polli JE (2003) Midazolam exhibits characteristics of a highly permeable P-glycoprotein substrate. *Pharm Res* **20:**757-764.

Triguero D, Buciak J and Pardridge WM (1990) Capillary depletion method for quantification of blood-brain barrier transport of circulating peptides and plasma proteins. *J Neurochem* **54:**1882-1888.

Tsuruo T, Iida H, Nojiri M, Tsukagoshi S and Sakurai Y (1983) Circumvention of vincristine and Adriamycin resistance in vitro and in vivo by calcium influx blockers. *Cancer Res* **43:**2905-2910.

van der Sandt IC, Blom-Roosemalen MC, de Boer AG and Breimer DD (2000) Specificity of doxorubicin versus rhodamine-123 in assessing P-glycoprotein functionality in the LLC-PK1, LLC-PK1:MDR1 and Caco-2 cell lines. *Eur J Pharm Sci* **11:**207-214.

van der Sandt IC, Vos CM, Nabulsi L, Blom-Roosemalen MC, Voorwinden HH, de Boer AG and Breimer DD (2001) Assessment of active transport of HIV protease inhibitors in various cell lines and the in vitro blood--brain barrier. *Aids* **15:**483-491.

Wallstab A, Koester M, Bohme M and Keppler D (1999) Selective inhibition of MDR1 P-glycoprotein-mediated transport by the acridone carboxamide derivative GG918. *Br J Cancer* **79:**1053-1060.

Wandel C, Kim RB, Kajiji S, Guengerich P, Wilkinson GR and Wood AJ (1999) P-glycoprotein and cytochrome P-450 3A inhibition: dissociation of inhibitory potencies. *Cancer Res* **59:**3944-3948.

Wang E, Lew K, Barecki M, Casciano CN, Clement RP and Johnson WW (2001) Quantitative distinctions of active site molecular recognition by P-glycoprotein and cytochrome P450 3A4. *Chem Res Toxicol* **14:**1596-1603.

Wang EJ, Casciano CN, Clement RP and Johnson WW (2000) Two transport binding sites of P-glycoprotein are unequal yet contingent: initial rate kinetic analysis by ATP hydrolysis demonstrates intersite dependence. *Biochim Biophys Acta* **1481:**63-74.

Wang Q, Yang H, Miller DW and Elmquist WF (1995a) Effect of the P-Glycoprotein inhibitor, cyclosporin A, on the distribution of rhodamine-123 to the brain: an in vivo microdialysis study in freely moving rats. *Biochemical and Biophysical Research Communications* **211:**719-726.

Wang Q, Yang H, Miller DW and Elmquist WF (1995b) Effect of the p-glycoprotein inhibitor, cyclosporin A, on the distribution of rhodamine-123 to the brain: an in vivo microdialysis study in freely moving rats. *Biochem Biophys Res Commun* **211:**719-726.

Williams GC, Liu A, Knipp G and Sinko PJ (2002) Direct evidence that saquinavir is transported by multidrug resistance-associated protein (MRP1) and canalicular multispecific organic anion transporter (MRP2). *Antimicrob Agents Chemother* **46:**3456-3462.

Wolburg H and Lippoldt A (2002) Tight junctions of the blood-brain barrier: development, composition and regulation. *Vascul Pharmacol* **38:**323-337.

Wong JK, Hezareh M, Gunthard HF, Havlir DV, Ignacio CC, Spina CA and Richman DD (1997) Recovery of replication-competent HIV despite prolonged suppression of plasma viremia. *Science* **278:**1291-1295.

Yasuda K, Lan LB, Sanglard D, Furuya K, Schuetz JD and Schuetz EG (2002) Interaction of cytochrome P450 3A inhibitors with P-glycoprotein. *J Pharmacol Exp Ther* **303:**323-332.

Zhang Y, Han H, Elmquist WF and Miller DW (2000a) Expression of various multidrug resistance-associated protein (MRP) homologues in brain microvessel endothelial cells. *Brain Res* **876:**148-153.

Zhang ZJ, Saito T, Kimura Y, Sugimoto C, Ohtsubo T and Saito H (2000b) Disruption of mdr1a p-glycoprotein gene results in dysfunction of blood-inner ear barrier in mice. *Brain Res* **852:**116-126.

Zong J and Pollack GM (2000) Morphine antinociception is enhanced in mdr1a gene-deficient mice. *Pharm Res* **17:**749-753.

VITA

Born March 22, 1970; Camden, NJ

Education

1997-2004 Doctor of Philosophy Candidate
Graduate Center for Toxicology
University of Kentucky, Lexington, KY

1991-1994 B.S. Major: Chemistry
James Madison University, Harrisonburg, VA

1989-1991 St. Andrew's Presbyterian College
Laurinburg, NC

Relevant Professional Experience

1997-Present Research Assistant

1994-1997 Teacher, Chemistry and Algebra
Sayre School, Lexington, KY

Responsibilities included instructing high school students in college preparatory and advanced placement chemistry, and algebra.

1992-1994 Undergraduate Research in Chemistry

The use of artificial neural networks to identify infrared spectrum as an alternative to computer database analysis.

Publications

Edwards JE, Rudy AC, Wermeling DP, Desai N, McNamara PJ.
Hydromorphone transfer into breast milk after intranasal administration.
Pharmacotherapy. 2003 Feb; 23(2):153-8.

Edwards JE, Brouwer KR, McNamara PJ.
GF120918, a P-glycoprotein modulator, increases the concentration of unbound amprenavir in the central nervous system in rats. Antimicrob Agents Chemother. 2002 Jul; 46(7):2284-6.

Savolainen J, Edwards JE, Morgan ME, McNamara PJ, Anderson BD.
Effects of a P-glycoprotein inhibitor on brain and plasma concentrations of anti-human immunodeficiency virus drugs administered in combination in rats.
Drug Metab Dispos. 2002 May;30(5):479-82.

Poster and Presentations

AAPS 2001 Annual Meeting

Jeffrey E. Edwards, Anita Rudy, Daniel Wermeling, Patrick J. McNamara.
The Distribution of Hydromorphone into Human Milk.
University of Kentucky, Lexington, KY.
AAPS Pharm Sci Vol. 3, No. 3 2001

Jeffrey E. Edwards, Jane Alcorn, Jouko Savolainen, Bradley D. Anderson, Patrick J. McNamara.
The Distribution of Nelfinavir into Rat Milk and Brain
University of Kentucky, Lexington, KY.
AAPS Pharm Sci Vol. 3, No. 3 2001

Society of Toxicology 1999 Annual Meeting

J. E. Edwards, K. Brouwer, P. J. McNamara
GF120918 Enchances the CNS Penetration of Amprenavir in Sprague-Dawley Rats
University of Kenucky, Lexington, KY

National Science Foundation 1993

Jeffrey E. Edwards, Frank Palocsay
The Use of Artificial Neural Network to Identify Infrared Red Spectrum
Old Dominion University, Norfolk, VA

Affiliation

American Association of Pharmaceutical Scientists
2107 Wilson Blvd, Suite 700, Arlington, VA 22201-3042